MOLECULAR GENETIC CHARACTERIZATION OF *XIPHOPHORUS MACULATUS* JP 163 B SKIN UPON EXPOSURE TO VARYING WAVELENGTHS OF LIGHT

by

Jordan Chang, B.S.

A thesis submitted to the Graduate Council of
Texas State University in partial fulfillment
of the requirements for the degree of
Master of Science
with a Major in Biochemistry
May 2016

Committee Members:

Ronald Walter, Committee Chair

Karen Lewis

Steven Whitten

FAIR USE AND AUTHOR'S PERMISSION STATEMENT

Fair Use

Duplication Permission

ACKNOWLEDGEMENTS

This work could not have been accomplished without the support and guidance I have received from my family, mentors, and colleagues. Although it would be impossible to name all who have helped, I would like to thank a few people in particular that have guided me through this journey.

Thank you Dr. Ron Walter for the guidance and support these past 2 years. The mentorship that you have provided has helped me grow as a student and as a scientist. I am truly grateful for all the opportunities and lessons you have given me. I will bring with me all that I have learned and continue down my path to becoming a scientist. I hope that one day I can show you that the time and support you have shown me were well spent. I would also like to thank the various current and former members of the Molecular Biosciences Research Group. In particular, I would like to thank Dr. Yuan Lu, Will and Mikki Boswell and Esther Lee for the help in and outside the lab; and graduate students Kaela Caballero and Angelica Riojas for their support and fellowship during my time here. To the *Xiphophorus* Genetic Stock Center Staff, thank you Markita Savage, Natalie Taylor, and Cristina Mendoza for the work you do. Without the assistance of everyone here, I would not have been able to accomplish all that I have.

Thank you to my committee members Drs. Karen Lewis and Steve Whitten for the academic input and mentorship during my time here. Your help has been most appreciated and invaluable.

Lastly, to my parents, family, and friends, thank you for your continuous love and patience. I could not have made it this far without your love and encouragement. Thank you.

TABLE OF CONTENTS

Page

LIST OF TABLES

Table **Page**

LIST OF FIGURES

Figure **Page**

I. INTRODUCTION

Melanocytes are melanin-producing cells that are found in the epidermal layer of the skin. These cells are responsible for melanin pigment in various tissues, such as skin, eye, and hair. Among the many types of skin cancer, the rapid proliferation of melanocytes, pathologically described as metastatic melanoma, is in need of better tools to improve prognosis (Jaywardana et al., 2012). It is commonly believed that melanoma is associated with prolonged exposure to sunlight (Armstrong and Kricker, 2001). Over the past 40 years, cases of melanoma have increased more than 6-fold in the United States, especially in young men (Reed et al., 2013). American Cancer Society statistics show melanoma as a leading cause of skin cancer deaths (74% of the estimated 13,650 skin cancer deaths) even though it only accounts for 1% of all documented cases of skin cancers (American Cancer Society, 2016). While much can be learned from studies using human melanoma cultured cell lines, the genetic etiology leading to melanoma must be studied within intact model organisms that display immune selectivity and the many genetic and organ specific factors that may contribute to melanomagenesis. Murine animal models are popular in melanoma studies (Herlyn and Fukunaga-Kalabis, 2010). However, human melanoma arises from melanocytes found in the basal layer of the epidermis while in mice, the melanocytes are confined to the hair follicles within the dermal layer of the skin (Ha et al., 2005; Chin, 1999). Furthermore, rodents have adapted to a nocturnal lifestyle and thus may have

subfunctionalized many of the human gene orthologues, shown to be involved in melanoma, to other uses.

Melanoma Models in *Xiphophorus*

A long-standing melanoma experimental model involves interspecies hybridization among *Xiphophorus* fish. Fish from the genus *Xiphophorus* have been used as a model organism for to study the genetics underlying carcinogenesis for over 90 years (Gordon, 1927; Kosswig, 1928; Walter and Kaziania, 2001; Meierjohann and Schartl, 2006). *Xiphophorus* consists of 26 known species that may be found in freshwater habitats along the Sierra Madre uplift from northern Mexico extending into Guatemala and Honduras in Central America (Kallman and Kazianis, 2006). Fish and human melanocytes, and subsequently melanoma, share similar characteristics originating from the embryonic neural crest and have similar histopathology (Vielkind et al., 1993). The transition from melanocytes to melanomas happens in two stages; after the initial radial growth, melanocytes may begin vertical growth, forming malignant tumors (Bandarchi et al., 2010). The similar growth characteristics between human and fish melanoma cells suggests that similar gene sets are involved in melanoma induction in both systems (Kazianis et al., 2001a). Comparison of the pathological structures of melanoma from humans and fish shows similar morphology and processes, such as pinocytotic activity and interdigitation of dendritic cell processes (Riehl et al., 1984; Gimenez-Conti et al., 2001). *Xiphophorus* interspecies hybrids have become the most widely utilized model to

study the genetics underlying UVB inducible melanomagenesis (Setlow et al., 1989; Setlow et al., 1993; Mitchell et al., 2001; Mitchell et al., 2009; Mitchell et al., 2010). The recent availability of the genome sequence assemblies for both *Xiphophorus* parents (i.e. *Xiphophorus maculatus* Jp 163 B and *X. couchianus*) of an interspecies backcross that produces progeny genetically susceptible to UVB induced melanoma, for the first time, allows each parental allele to be followed through the cross and greatly facilitates these genetic studies. Thus, researchers can assess allele specific gene expression in hybrid skin before and after the melanoma-inducing treatment and determine what sets the stage for melanoma development in susceptible animals.

A notable characteristic of *Xiphophorus* species are their many colors and polymorphic pigmentation patterns. Black pigmentation patterns in these fish are caused by two types of melanophores; micromelanophores and macromelanophores. Micromelanophores are commonly found in the dermal layer of tissue while macromelanophores are scattered throughout the dermis. In *Xiphophorus* melanoma, only the macromelanophores are the dominant cell type transformed, while micromelanophores appear incapable of forming melanoma (Gordon, 1941; Vielkind et al., 1971). Some species of *Xiphophorus* do not exhibit black pigmentation due to lack of macromelanophores (i.e. *X. couchianus* and *X. hellerii*). Others, such as *X. maculatus*, show black spotted patterns along the dorsal fin (termed "*Sd*", spot dorsal) and on the side or flank of the animal ("*Sp*", spot side) (Nairn et al., 1996b; Walter and Kazianis, 2001; Kallman and Kazianis, 2006). Two strains from *Xiphophorus maculatus* that are commonly

used in tumor studies are *X. maculatus* Jp 163 A, carrying the *Sd* pigment pattern and *X. maculatus* Jp 163 B, carrying the *Sp* pattern (Figures 1-1 and 1-2).

Classic Gordon-Kosswig Cross

In 1927, Gordon and Haussler in the United States and Kosswig in Germany published independent results of the [*X. maculatus* Jp 163 A (x) *X. hellerii*] (x) *X. hellerii* interspecies hybrid backcross (now termed the G-K cross) showing that 25% of the backcross progeny develop invasive melanoma. In the G-K model, *X. maculatus* Jp 163 A expressing the *Sd* pigmentation pattern are first crossed with *X. hellerii*, which do not possess macromelanophore spot patterns. The resulting F_1 hybrids show heavy pigmentation in the dorsal fin, but not invasive melanoma. However, when the F_1 hybrids are backcrossed with *X. hellerii*, 25% of the BC_1 offspring develop melanoma, ultimately leading to necrosis of the dorsal fin, invasion into the musculature, and ultimately death of the fish (Figure 1-1) (Gordon, 1927; Kosswig, 1928). This cross marked the beginning of investigation into the genetics of melanoma and in later studies provided the first evidence that cancer could be an inherited disease involving positive gene activators (now called oncogenes) and loss of gene suppressors (now called tumor suppressors) (Breider, 1952; Meierjohann et al., 2004). Current research studies utilizing *Xiphophorus* are aimed at elucidating the genetics underlying melanoma susceptibility, induction, and tumor progression.

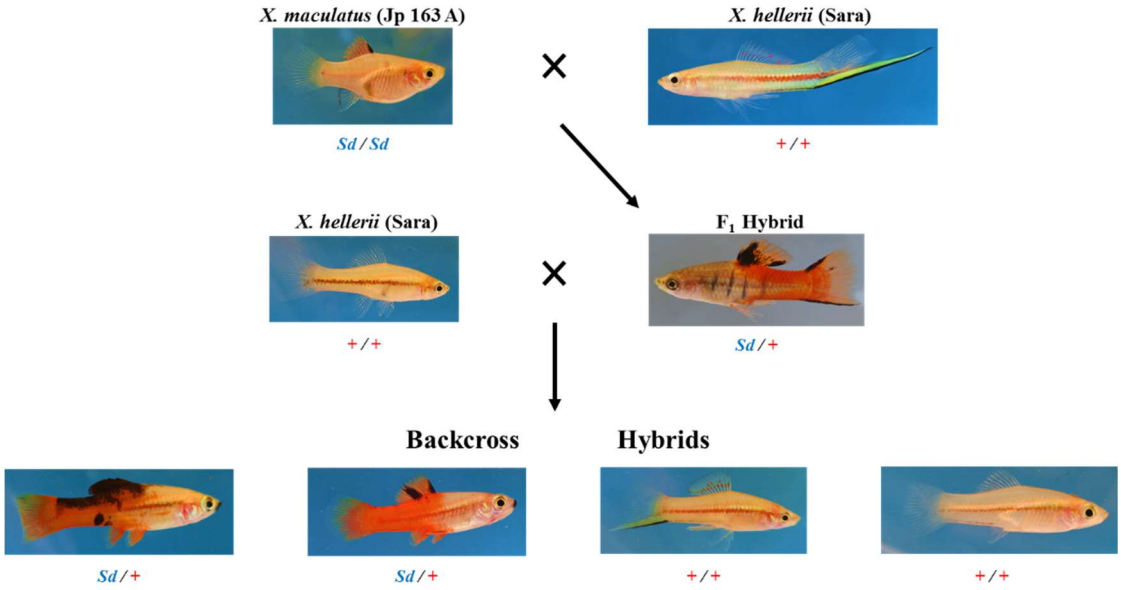

Figure 1-1. Gordon-Kosswig melanoma cross. Representation of the Gordon-Kosswig cross with *X. maculatus* Jp 163 A, exhibiting spot dorsal (*Sd*), and *X. hellerii*. *Sd* phenotype is observed in the resulting F_1 hybrid. Progeny of F_1 backcross with *X. hellerii* results in 50% unpigmented with no *Sd* allele, 25% exhibiting *Sd* phenotype similar to F_1 hybrid, and 25% with heavy pigmentations that develop spontaneous melanoma. Heavy pigmentation observed in backcross hybrids are thought to be the loss of *Sd* regulator, termed the *Diff* gene.

Inducible Melanoma Cross

While the G-K cross is an example of a spontaneous melanoma model, where progeny develop melanoma due to the cross itself, other *Xiphophorus* interspecies crosses have been documented wherein backcross progeny (BC_1) only develop melanoma after a tumor-inducing treatment, such as exposure to alkylating agents or UVB (Setlow et al., 1989; Nairn et al., 1996a; Kazianis et al., 2001; Walter and Kazianis, 2001). One example of a commonly used UVB-inducible melanoma model uses *X. maculatus* and *X. couchianus*. *X. maculatus*

Jp 163 B fish that exhibit the *Sp* pigment pattern are crossed with *X. couchianus*, which has no macromelanophore pattern. F_1 hybrids are then backcrossed to *X. couchianus* and exposed to UVB (6.2 kJ/m^2) six days after birth for five successive days (Setlow et al., 1989; Mitchell et al., 2010). The resulting pigmented backcross hybrid fish (termed *Sp-couch*) develop severe expansion of the melanophore pigmentation, appearing almost black from the gills to the tail (Figure 1-2) (Walter and Kazianis, 2001; Mitchell et al., 2009). Overexpression of macromelanophores pattern and treatment of young hybrids with UVB triggers active proliferation of melanocytes in about 30% of the pigmented BC_1 hybrids, eventually leading to melanoma (Walter and Kazianis, 2001). The precise genetic alleles inherited and/or shifts in genetic profiles induced by the UVB that lead to melanoma progression are the subject of ongoing research investigations.

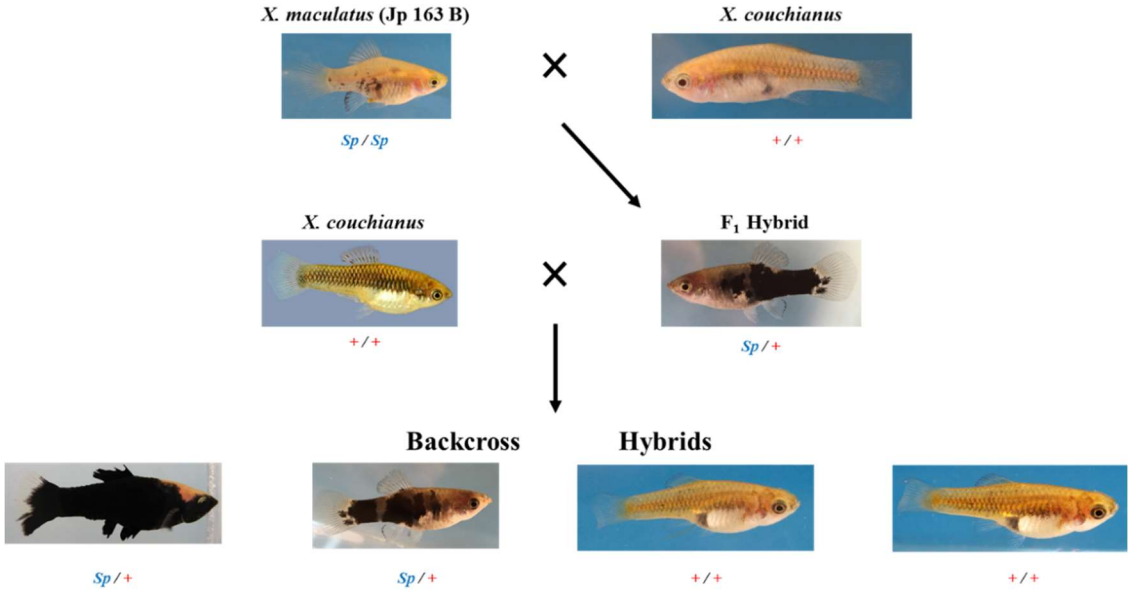

Figure 1-2. Inducible tumor cross. Representation of the *Sp-couch* cross with *X. maculatus* Jp 163 B, exhibiting side spot (*Sp*), and *X. couchianus*. The resulting F_1 hybrid exhibited pigmentation from dorsal fin to tail. Backcross of F_1 hybrid to *X. couchianus* exposed to UVB or MNU showed 50% nonpigmented progeny with no *Sp* allele, 25% exhibited fin to tail pigmentation similar to the F_1 hybrid, and 25% severe macromelanophore pigmentation leading to melanoma.

UV and Visible Light Properties

Effects of Ultraviolet Light

UVB is a narrow range of the much broader electromagnetic spectrum. Light is emitted as electromagnetic radiation measured in wavelengths. The frequency of wavelengths determines its color and properties, such as energy and penetration. The effects of UV light in vertebrate animals has been extensively studied due to the direct DNA damage induced by UV wavelengths. Within the UV spectrum, UV light is separated into three regions: UVC (100-280 nm), UVB (280-315 nm), and UVA (315-380 nm). UVC is absorbed by the earth's stratospheric ozone and does not reach the earth's surface (McKenzie et al*.,* 2003). However, UVB and UVA may penetrate through ozone and reach the skin of vertebrate animals. Only UVB has the energy to directly cause DNA damage, but due to its short wavelength, has limited penetration into skin layers (Figure 1-3) (Malloy et al., 1997; Tzung and Rünger, 1998; Maverakis et al*.,* 2010). Conversely, UVA can penetrate several dermal layers and may cause cellular damage via photooxidation and concomitant production of free radicals (Wood et al*.,* 2006). When melanin absorbs UVA light, metastable reactive melanin radicals form and release reactive oxygen species (ROS) that may directly interact with DNA, causing oxidative base damage (Wood et al*.,* 2006). There has been speculation that free radicals caused by UVA radiation may serve to produce mutations leading to melanoma induction (Garland et al, 1993; Moan et al., 1999; Wang et al., 2001; Wood et al., 2006; Maverakis et al., 2010).

However, other published data suggest that UVA light itself is insufficient to induce melanoma in susceptible *Xiphophorus* hybrids (Mitchell et al., 2010).

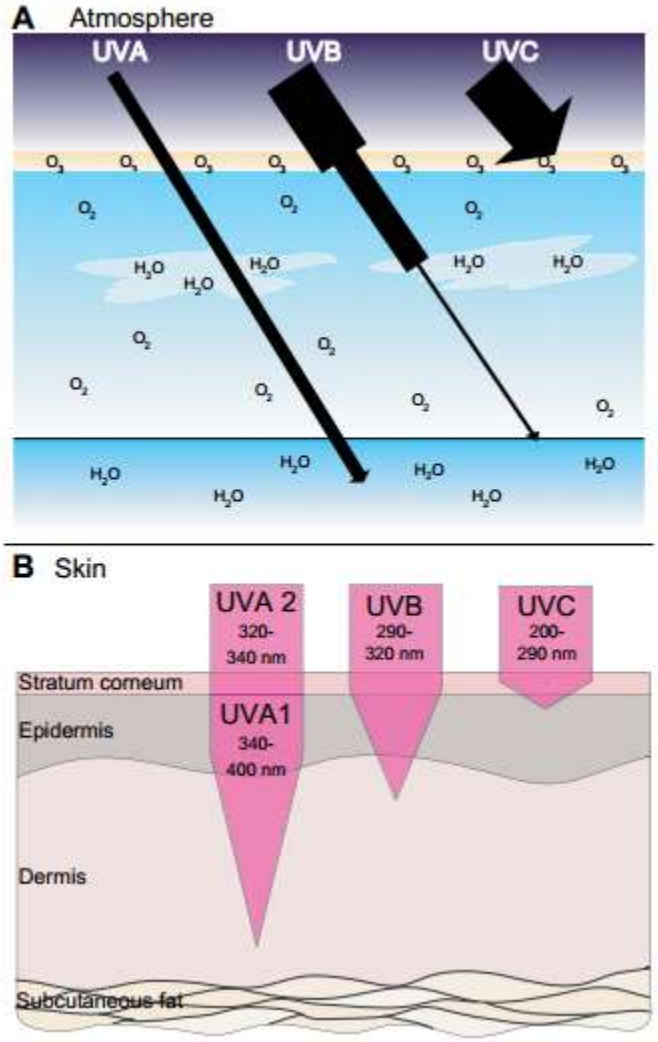

Figure 1-3. Penetration of UV light through (a) atmosphere and (b) skin. UVC light is filtered by the ozone and shows least penetration through the skin. UVB and UVA light both readily penetrate through the ozone layer. UVB is able to penetrate to the epidermal layer while UVA is observed to penetrate through the dermal layer of the skin. (Maverakis et al., 2010)

DNA Damage and Photorepair of UV-Induced Lesions

UVB has been shown to penetrate the upper epidermal layers of *Xiphophorus* skin and produce both cyclobutane pyrimidine dimers (CPDs) and 6-4 pyrimidine-pyrimidine photoproducts (6-4PD) (Meador et al., 2000; Mitchell et al., 2001, Mitchell et al., 2009). UV induced DNA damage causes kinks within the DNA strands that increase the flexibility of the DNA backbone. Thymine and cystosine residues around the site of UV absorption can form bonds with neighboring nucleotides, leading to the production of CPD and 6-4PD (Setlow and Carrier, 1964; Pfeifer et al., 2005; Rastogi et al., 2010). Severe damage in the DNA caused by UV light can trigger cell cycle arrest and apoptosis (Lo et al., 2005). Conversely, cells may recruit repair enzymes, such as photolyase, to repair damaged DNA (Meador et al., 2000).

Photolyases are light-dependent enzymes that specifically act to repair CPD and 6-4PD damage in the DNA. Interestingly, CPD and 6-4 photolyase gene expression is induced mostly by visible blue light (Mitani et al., 1996). Repair of DNA damage by photolyase requires absorption of visible light to trigger electron release for DNA repair. Photolyase enzymes contain a flavin adenine dinucleotide (FAD) cofactor and a light absorbing chromatophore. As light is absorbed, a tryptophan residue within the active site of photolyase photoreduces the FADH cofactor (Li et al., 1991). Activated photolyase is then able to transfer the excited electron to the repair site by splitting the dimer bond (Li et al., 2010).

Visible Light Spectrum

Besides the activation of photolyase, other cellular biomolecules respond to visible light (380-750 nm). For example, melanophore sensitivity to light peaks around 400–420 nm. Melanin within melanophores act as a photoreceptor that triggers melanosome aggregation. Melanosome movement is highly regulated via cAMP, which is inhibited by the activation of phosphodiesterase. As light is absorbed by phosphodiesterase, the enzyme becomes activated, lowering the concentration of cAMP in the cell (Wakamatsu et al*.,* 1980). Melatonin is another molecule that is dependent on light and regulates circadian rhythm patterns. Hormones, such as cortisol, respond to irregular circadian patterns, affecting metabolism, the immune system, and blood sugar levels (Brüning et al., 2015). These data suggest that many and varied biomolecules may respond differently in each tissue depending on the absorption levels of specific wavelengths of light.

As previously mentioned, wavelength and frequency of emitted light determines the properties, such as energy and penetration. Shorter wavelengths of light (i.e. blue light) have less penetration through tissue compared to longer wavelengths (i.e. red light) (Figure 1-4) (Foder et al., 2011). Thus, absorbance of certain wavelengths of light by the known array of reactive biomolecules may be varied, depending on the depth of penetration into tissue and the relative levels of the many receptor molecule structures. While some biomolecules have been identified as light responsive, the mechanism by which light induces gene expression has not been well studied and is largely unknown, and particularly within internal organs and tissues.

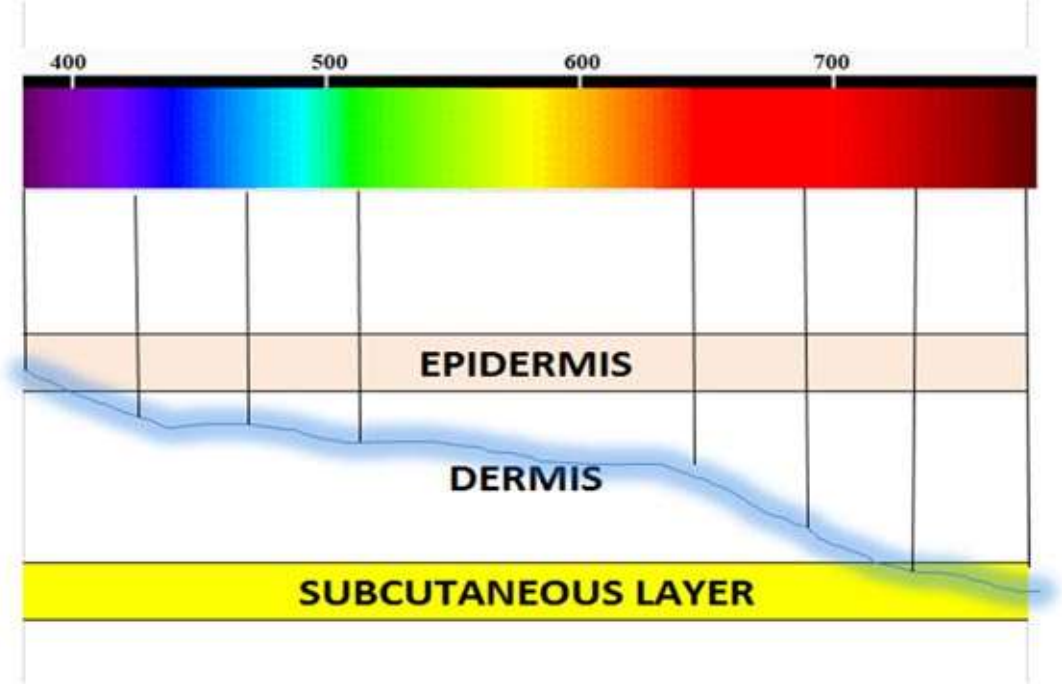

Figure 1-4. Diagram representation of penetration of visible light through skin tissue. Shorter wavelengths of light have less penetration through skin tissue compared to longer wavelengths of light. Large fraction of wavelengths in the visible light region penetrates through to the dermal layer of skin.

Source: http://theralightinc.com/how-light-penetrates-the-skin/

In considering light effects on gene expression, the amount of energy within each specific wavelength needs mention since the energy is inversely proportional to wavelength. For example, if the power remains constant at all wavelengths, the shorter wavelengths of light radiate more energy than longer wavelengths. Solarczyk et al. (2012) demonstrated that low intensity visible light in the blue region is able to induce a sub-lethal level of DNA breaks in HeLa cell culture. It was further suggested that direct DNA damage from the blue region visible light was unlikely, but rather the energy transduced led to photon

excitation within water, inflicting damage on DNA. This raises the question of whether it is absorption of energy or depth of penetration, or a combination, that leads to induction of gene expression.

UV vs. Fluorescent Light Effects on Gene Expression

UV Induced Gene Expression

Previous research conducted with *X. maculatus* Jp 163 B fish showed gene expression changes in skin after exposure to narrow-band UVB light (principally 311 nm) (Yang et al, 2014). Fish were exposed to varying doses of UVB light (8 kJ/m^2, 16 kJ/m^2, and 32 kJ/m^2) and skin was harvested for RNA sequencing analyses (RNA-seq). The results of these experiments indicate more than 200 genes in fish skin become differentially expressed when exposed to UV light at 16 kJ/m^2 (Yang et al., 2014). Among the classes of genes differentially up-regulated were immune response, metabolic processing, and cytoskeletal remodeling with doses as little as 8 kJ/m^2. The up-regulation of these clusters suggest fish skin exposed to UVB light elicited an inflammatory response. Furthermore, up-regulation of genes leading to cytoskeletal remodeling suggested that restructuring of the epidermis occurred in response to UV light (Yang et al., 2014).

Fluorescent Light Induced Gene Expression

In a separate RNA-seq study of a dose response using “cool white” fluorescent light (4,100K), changes in gene expression were documented in *X.*

maculatus Jp 163 B skin (Walter et al., 2015). Compared to UVB exposures, exposure of *X. maculatus* Jp 163 B to 4,100K fluorescent light resulted in a similar number of genes modulated as observed in the UVB study (i.e., 272 genes). However, the genes modulated by fluorescent or UVB exposure were quite different. Among the fluorescent differentially modulated genes were 115 genes showing suppression of cell cycle progression and DNA replication/repair. It was suggested this response to 4,100K "cool-white" bulbs might play a role in cell cycle arrest due to forced entry into a circadian light phase (Walter et al*.,* 2015). These surprising results suggest that energy emissions from different light sources, and perhaps select wavebands within these sources, may have currently unexplored effects on the molecular genetic profiles of expressed genes in fish skin, and perhaps other organs (brain, liver, etc.) as well.

Artificial Light Spectra

Sunlight encompasses a wide range of light wavelengths, with visible light (380-780 nm) being the most intense due to ozone and atmospheric filtering. The spectral distribution of sunlight shows increasing intensity up to the 400-500 nm regions where the intensity then remains constant (Condit and Grum, 1964). While sunlight maintains its intensity at every wavelength, UV and fluorescent lamps exhibit several disproportionate peaks of intensity at specific wavelengths. Figure 1-5 exhibits spectral distributions of two different types of fluorescent lights previously used in the lab (4,100K [termed "fluorescent light"] and 10,000K [termed "coral light"]) (Walter et al., 2015; unpublished data; respectively). The

differences observed at peaks of intensity suggests skin may be absorbing greater amounts of energy at certain wavelengths, and perhaps producing various and currently unknown genetic responses to varying wavelength peaks and valleys.

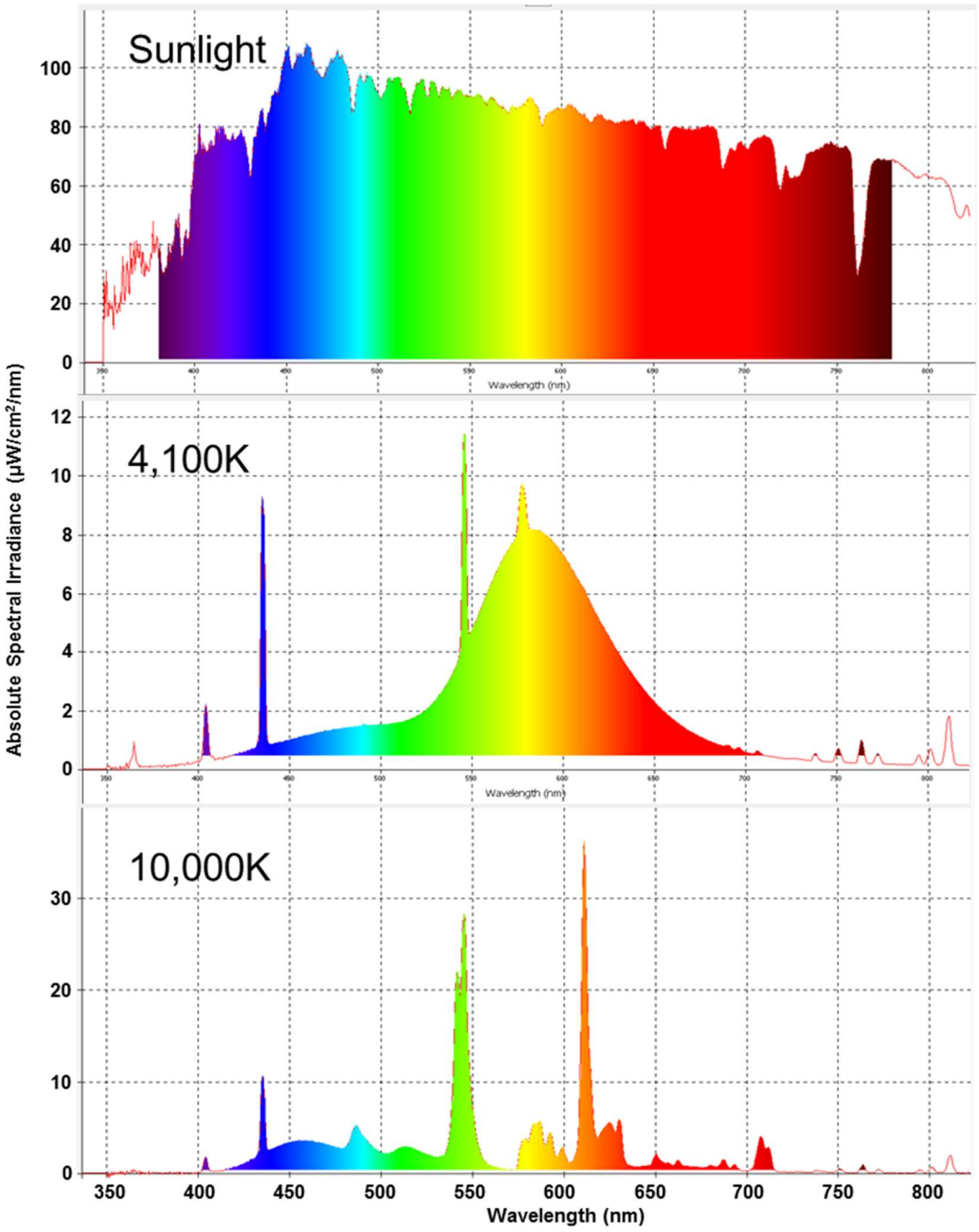

Figure 1-5. Spectral distribution of natural sunlight, 4,100K and 10,000K fluorescent light. Fluorescent lights were previously used in past research in the lab (Walter et al., 2015; unpublished data). Y-axis represents absolute spectral irradiance (µW/cm^2/nm) and X-axis represents wavelengths ranging from 350 to 800 nm. Distribution of irradiance across all wavelengths are not uniform, containing peak intensities at certain wavelengths.

Source: William Boswell

Although fluorescent light appears to cause a substantial amount of differential gene expression, little is known about the relationship between specific wavelengths of light and the regulation of gene sets within the skin of intact animals. To address this question, RNA isolated from skin of *Xiphophorus maculatus* Jp 163 B fish that are exposed to various wavelengths of light were assessed for modulation of global gene expression patterns using high throughput sequencing coupled with bioinformatic analyses. In these experiments, we attempted to identify narrow wavelength regions along spectral ranges from 300 to 600 nm that are responsible for modulation of specific sets of genes. This experimental design was employed in male and female *Xiphophorus* fish to compare responses due to sex for the same light stimulus. Herein we report results of global gene expression profiles and shifts in gene expression after exposure to monochromatic xenon light in 50 nm wide wavelength ranges across the spectrum from 300 nm to 600 nm in both male and female *X. maculatus* Jp 163 B.

II. METHODS AND MATERIALS

Research Animals

Xiphophorus maculatus Jp 163 B were provided by the *Xiphophorus* Genetic Stock Center (XGSC; Texas State University, San Marcos, TX; http://www.xiphophorus.txstate.edu). Fish were maintained in 5 to 20 gallon freshwater aquaria and fed twice daily with newly hatched brine shrimp (*Artemia*) nauplii and beef liver paste (Gordon, 1943b). All *X. maculatus* (male: pedigree 105 B and 105 F; female: pedigree 106 F and 106 D) were mature adult between the 9 to 10 months old and are of the 105^{th} and 106^{th} generation of XGSC inbreeding (IACUC #: IACUC2015107711).

Specific Wavelength Exposure

X. maculatus Jp 163 B were exposed to 50 nm wavelength regions of light (e.g. 300-350, 350-400, 400-450, 450-500, 500-550, and 550-600 nm). Specific wavelength exposure was carried out using a TLS-300X Series Tunable Light Source (Newport Corporation, Irvine, CA, USA) containing an Ushio 300 W Xenon Short Arc Lamp Model 6258. Emitted light was passed through an attached Cornerstone 130 Monochromator (Newport Corporation, Irvine, CA, USA) to define specific wavelengths. A custom-designed exposure chamber contained a center cuvette holder and 2 adjustable wooden blocks at each side. Two fiber-optic light cables were anchored to the wooden blocks that connected to the Cornerstone Monochromator to direct specified wavelengths to each side

of the cuvette (Figure 2-1). The xenon light source was burned in 15 min prior to all exposure treatments. Power output of each light source was measured at specific wavelengths using a Newport 1918-R power meter (Newport Corporation, Irvine, CA, USA). The dose of all exposures was determined to be 10 kJ/m^2, equivalent to the dose from a 40 min exposure to fluorescent light (Walter et al., 2015). The spectral distribution of the xenon light source was measured at full spectrum (0 nm) and at 400 nm using an Ocean Optics STS 350-800 nm microspectrometer (Ocean Optics Inc., Dundedin, FL, USA) and OceanView software v1.5 (http://oceanoptics.com/product/oceanview/). This ensures the wavelength set is the wavelength emitted through the fiber-optic cables. The microspectrometer was calibrated to a known standard using Ocean Optics Halogen Calibrated Light Source HL-3P-CAL (Ocean Optics Inc., Dundedin, FL, USA). To span all wavelengths within each 50 nm region, the monochromator was set to scan and repeat (*i.e.* loop) through the wavelengths of each region (1 nm/sec for 50 sec) for the duration of the light exposure using Asoftech Automation (http://www.asoftech.com/).

All animals were placed in the dark overnight for 12 hrs prior to experimental exposures in individual 125 mL flasks filled with 100 mL of filtered aquaria water. Each fish was placed in a 4 cm × 1 cm × 4.5 cm UV-transparent quartz cuvette filled with 14 mL of filtered aquaria water centered between the 2 fiber-optic cables. A cardboard box was utilized to cover the exposure chamber to eliminate ambient light. Following exposure, fish were removed from the cuvette, rinsed with filtered aquaria water, placed back into a 125 mL flask filled

with 100 mL of filtered aquaria water, and placed in the dark for 6 hours to allow for gene expression prior to sacrifice and tissue dissection.

At dissection, fish were sacrificed by cranial pith after anesthesia in ice and flash frozen in an ethanol dry ice bath. Skin was dissected into 1.5 mL microcentrifuge tubes filled with 300 μL TRI reagent (Sigma-Aldrich, St. Louis, MO; Product #: 93289) and immediately used for RNA isolation. Other organs (*e.g.* brain, eyes, liver, and whole fish) were dissected into RNAlater solution (Ambion Inc., Austin, TX, USA; Product #: AM7021) overnight, aspirated, and frozen at -80°C.

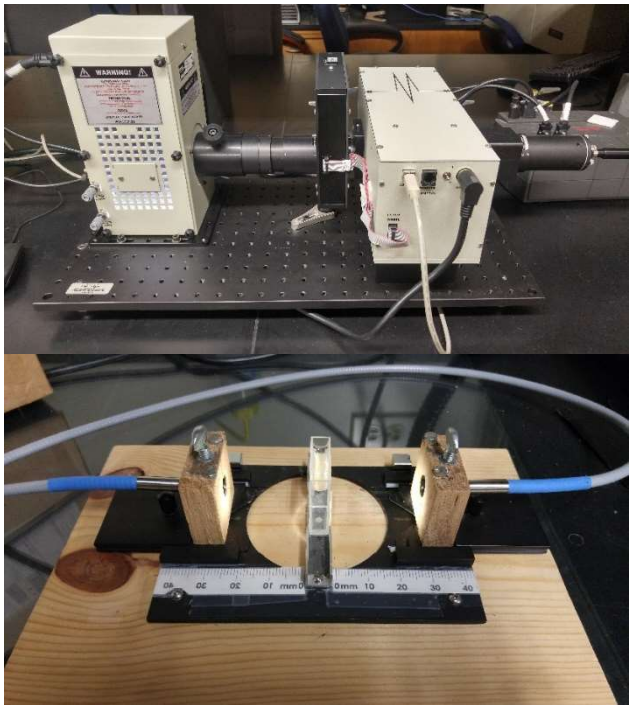

Figure 2-1. Monochromator exposure equipment. Image of the monochromator (top) and custom designed exposure chamber (bottom) used for light exposures. Light from the xenon lamp passes through the monochromator to select for specific wavelengths. One fish is placed into the quartz cuvette centered between 2 fiber optic cables to allow for exposure on both sides of the fish. Exposure protocol is repeated 3 times for 3 biological replicates.

Source: Jordan Chang

RNA Isolation

RNA isolation was performed following the Qiagen RNeasy RNA isolation protocol (Qiagen, Valencia, CA, USA). Flash frozen skin samples were macerated manually with a pestle tool and homogenized using a hand held homogenizer. Following homogenization, 300 μL TRI reagent was added to the samples followed by incubation for 5 min at room temperature. Chloroform extraction was performed by adding 120 μL chloroform to each sample and vigorously shaken for 15 sec. Samples were centrifuged (16,000 × g rcf for 5 min at 4°C) and the aqueous layer was transferred to a new 1.5 mL microcentrifuge tube. A second TRI reagent-chloroform extraction was performed using 300 μL TRI reagent and 60 μL chloroform on the recovered aqueous phase.

Isolated nucleic acids were precipitated with 500 μL ethanol in diethylpyrocarbonate (DEPC) treated water. The samples were then transferred to a Qiagen RNeasy mini spin column and on-column DNase treatment was performed for 15 min at 25°C to eliminate any residual DNA. RNA samples were then washed and eluted in 100 μL RNase-free water. RNA was quantified using Qubit 2.0 fluorometer (Life Technologies, Grand Island, NY, USA). To assess the RNA quality, an RNA integrity (RIN) score was determined using an Agilent 2100 Bioanalyzer (Agilent Technologies, Sana Clara, CA, USA). Samples with RIN scores above 8 were used for high-throughput Illumina sequencing.

RNA Sequencing

Two biological replicates of *X. maculatus* Jp 163 B skin samples were independently sequenced by Illumina High-Throughput sequencing using the Illumina TruSeq mRNA Library Prep Kit on the HiSeq 2000 platform (male: 75 bps and female: 125 bps, paired-end [PE] reads) at Beckman Coulter Genomics (Beckman Coulter, Inc., South Plainfield, NJ, USA) for each 50 nm exposure. Raw reads were trimmed and filtered using a custom Perl script (Garcia et al., 2012) and subsequently truncated by similarity to library adaptor sequences using a custom Perl script (Garcia et al., 2012). Low scoring reads were removed, preserving the longest remaining fragments (Yang et al., 2014). Overlapping PE reads were merged using FLASH (Magoč and Salzberg, 2011). FastQC was then used to assess the quality of the filtered reads to identify potential deficiencies within the data for each sample (http://www.bioinformatics.babraham.ac.uk/projects/fastqc/). Detailed statistics on raw and filtered reads for males and females are shown in Table 2-1 and 2-2, respectively.

Table 2-1. Read depth and RNA-Seq statistics for wavelength specific exposures in male skin. Biological duplicates are differentiated by “A” and “B”. M = million; X = average number of times each transcript is expected to be sequenced and mapped to the reference transcriptome. All values were generated using SAMtools flagstat (Li et al., 2009).

Male Exposure Sample	Reads Mapped (M)	Reads Unmapped (M)	% Mapped	Coverage (X)
0 - A	37.7	30.9	55.0%	60.6
0 - B	33.9	26.5	56.1%	54.6
300-350 - A	28.4	22.5	55.8%	47.2
300-350 - B	26.2	21.2	55.3%	43.8
350-400 - A	31.8	24.9	56.1%	52.5
350-400 - B	26.2	20.9	55.6%	44.0
400-450 - A	27.4	21.8	55.6%	46.5
400-450 - B	28.2	22.6	55.5%	47.5
450-500 - A	34.1	25.4	57.4%	44.9
450-500 - B	34.1	25.9	56.8%	57.4
500-550 - A	29.8	34.5	46.3%	39.9
500-550 - B	34.7	26.6	54.2%	56.0
550-600 - A	29.3	22.4	56.7%	47.1
550-600 - B	84.1	60.4	58.2%	93.4

Table 2-2. Read depth and RNA-Seq statistics for wavelength specific exposures in female skin. Biological duplicates are differentiated by “A” and “B”. M = million; X = average number of times each transcript is expected to be sequenced and mapped to the reference transcriptome. All values were generated using SAMtools flagstat (Li et al., 2009).

Female Exposure Sample	Reads Mapped (M)	Reads Unmapped (M)	% Mapped	Coverage (X)
0 - A	22.7	19.6	53.7%	56.6
0 - B	22.0	19.6	52.8%	56.3
0 - C	20.9	18.0	53.8%	52.7
0 - D	19.3	17.3	52.8%	47.8
300-350 - A	19.2	19.6	49.5%	50.8
300-350 - B	23.9	20.5	53.9%	60.7
350-400 - A	21.8	17.5	55.4%	51.9
350-400 - B	22.8	20.0	53.2%	58.5
400-450 - A	24.7	23.0	51.8%	59.1
400-450 - B	23.9	22.1	52.0%	58.0
450-500 - A	23.2	18.9	55.1%	57.0
450-500 - B	24.5	20.1	54.9%	58.6
500-550 - A	25.9	20.8	55.5%	64.5
500-550 - B	24.2	19.6	55.2%	57.6
550-600 - A	23.3	19.4	54.7%	57.0
550-600 - B	22.9	19.3	54.3%	55.4

Computational Analysis

All filtered reads were mapped to the *X. maculatus* reference transcriptome using GSNAP (Wu and Nacu, 2010) and were annotated using BioMart (Ensembl v83). Reads were mapped to two different *X. maculatus* transcriptome, “trimmed” and “enhanced”. The “enhanced” transcriptome contains all known transcripts produced in *X. maculatus* (20,512 transcripts), while the “trimmed” transcriptome only contains transcripts homologous with the *X. couchianus* (20,219 transcripts). This allows for direct species comparisons between different *Xiphophorus* species and determination of allele specific expression in *Xiphophorus* hybrids. Shown in Table 2-3 are comparisons between the number of differentially expressed (DE) genes in male *Xiphophorus* skin in response to various wavelength regions. Both gene sets (e.g. mapped to enhanced vs. trimmed) exhibited similar number of modulations across all wavelength regions. For the purpose of this analyses, we opted to use the trimmed transcriptome to allow for future cross species comparisons.

Table 2-3. Mapping to “trimmed” vs “enhanced” transcriptome. Comparison of the number of DE genes in male *Xiphophorus maculatus* skin at each wavelength region mapping to the “trimmed” versus the “enhanced” referenced transcriptome. Gene lists were generated using R-Bioconductor package EdgeR by comparison of two exposed samples to eight control samples (See Chapter 3).

	Trimmed				Enhanced		
	Total Genes	**Genes Up**	**Genes Down**		**Total Genes**	**Genes Up**	**Genes Down**
300-350	13	13	0		15	15	0
350-400	194	123	71		205	123	82
400-450	44	42	2		43	42	1
450-500	147	125	22		146	124	22
500-550	566	359	207		587	397	190
550-600	274	86	188		270	91	179

The percentage of reads mapped and unmapped to the trimmed transcriptome as well as the coverage depth were calculated using SAMtools flagstat (Li et al., 2009). Differential gene expression was determined using the R-Bioconductor package DESeq and EdgeR with a fold change cut off ± 2 (*p*-adj ≤ 0.05) by comparing normalized reads of exposed skin samples to control skin samples. Control samples represent unexposed fish that were place in the dark overnight and remained in the dark upon dissection. Ten male and 12 female *X. maculatus* Jp 163 B control samples were pooled from previous experiments conducted in the laboratory. Eight control samples were randomly chosen for both sex and was utilized for differential gene expression.

While both RNA-Seq methods are similar (Tarazona et al., 2011; Kvam et al., 2012), EdgeR produced greater number of differentially expressed (DE) genes across all wavelength regions. Furthermore, majority of the DE genes

observed from DESeq (70-100%) were encompassed within the EdgeR gene list (Table 2-4). To obtain a broader representation of the data, we opted the use of EdgeR for future analyses.

Table 2-4. DESeq vs EdgeR differential expression methods. Comparison of the number of differentially expressed genes using two separate RNA-Seq methods: DESeq and EdgeR. The number of shared genes as well as the percent shared are shown.

	# DE Genes (DESeq)	# DE Genes (EdgeR)	Number DE Genes Shared	% of DESeq Shared
300-350	11	13	8	73%
350-400	88	194	82	93%
400-450	3	44	3	100%
450-500	25	147	25	100%
500-550	276	566	270	98%
550-600	52	274	52	100%

Differentially expressed genes from each wavelength region were compared using Venny 2.1 (http://bioinfogp.cnb.csic.es/tools/venny/) to identify shared and unique genes between each region. Additionally, male and female *X. maculatus* comparisons were made using Venny 2.1 to identify differentially expressed genes shared between both sex. Human homolog gene identifications of *X. maculatus* genes were determined using BioMart to allow for functional analysis. ConsensusPathDB (http://cpdb.molgen.mpg.de/CPDB) was employed to visualize potential pathways and genetic associations at each wavelength region (Z-score = 30). These networks include predicted genes generated by ConcensusPathDB (CPDB; Max Planck Institute for Molecular Genetics). Genes

appearing in networks were manually characterized using GeneCards (http://www.genecards.org/) and gene ontology. Heat maps were generated using R package gplots (Warnes et al., 2012) and a custom script to display differential expression of genes shown in the networks.

A separate functionalization tool was employed on the same data set to gain a broader representation of the gene sets. Functional analysis of genes was performed with Ingenuity Pathway Analysis (IPA) software (http://www.ingenuity.com/products/ipa). IPA generates functional categories, pathways, and predict upstream regulators by referencing to established literature performed in human, mouse, and rat studies. Z-scores are accompanied with each gene cluster to determine activation or inhibition of a particular pathway. Z-scores are calculated based on an algorithm, scoring genes ±1 in agreement or disagreement with the literature. Furthermore, the score for each gene is weighted depending on the number of literature that supports the prediction (Krämer et al., 2013). Pathway and functional categories with a false discovery rate (FDR) ≤ 0.05 were considered significant.

NanoString

Aliquots of the same *X. maculatus* Jp 163 B skin samples used in RNA-Seq were used in a NanoString nCounter assay (NanoString Technologies, Inc., Seattle, WA, USA). The nCounter assay was performed at the Baylor College of Medicine Microarray Core Facility (Houston, TX, USA) using 500 ng (7 µL) RNA per sample. Hybridization protocols were strictly followed according to

manufacturer's instructions (Geiss et al., 2008). Hybridized samples were incubated overnight at 65°C with custom target probes in the NanoString Prep Station and immediately evaluated with the NanoString nCounter based on unique color coded signals. Data analyses were performed by lane normalization using a set of standard NanoString probes followed by sample normalization using a set of 10 housekeeping genes. Counts were generated by nCounter Digital Analyzer. Fold changes were calculated on normalized counts and plotted using Microsoft Excel. The two biological samples were averaged and standard deviations calculated. Seventeen genes (Table 2-5) were selected for NanoString gene expression analysis, 10 of which were housekeeping genes.

Table 2-5. Target of 17 genes custom designed probes used in NanoString nCounter assay. Seven genes were test targets and 10 genes were housekeeping controls. Listed are the 7 target genes.

Gene Name	Ensembl ID	Target Sequence (5' – 3')
ybx2	ENSXMAT00000015815	GTTCATCAGACTGCCATCAAGAAGAACAATCCTAGAAA GTTTCTCCGAAGTGTTGGAGATGGGGAAGTCGTAGAG TTTGACGTAATTGAAGCAACTAAAG
clock	ENSXMAT00000017010	CCCAGCAGGGCCAGACTCAGACCATCAGCATTTCTCA GCAGCAGGAGCAGCAGCAGCAGATTCAGGTGCAGAA CCAGGTTTCCGCGCTGCAGGCAGGTCA
dnah7	ENSXMAT00000007381	GATCCATCATCGACGTCAATCTGCCCAAGTTCCTGGC CCAAGATCTGCAGCTTTTTGAGGGTATCACCTCCGATC TCTTCCCGGGTGTGATGCTCCCGGA
klhl38b	ENSXMAT00000008690	TTTTGAGACACTTATTGGTTGGATCCGTCATGATCCCG TCTCCAGGCGGGGGACCATAAGCAGCCTTTTCAAAAA GGTCCGTCTTCGACATTTACACCCT
per2	ENSXMAT00000016248	TATACCCTTTAATTGGACATCAAGCACCACCGGTGCCA GTGTATCAGGTAGATTCTGGGGGTGTCCCAATGCAAG CGCAGCCATTTGATCAGACTGCTTT
ppp1r27	ENSXMAT00000018069	AGGTCCCTTGAGAATCACAGTCGTCCGAAAGCCGCTG CAAGTTCTTCGGCGGTGAACGGAGAAAGCCGCATCAG TCCAGGTTCCTGGTTTTTGAGCTGCC
tgm8	ENSXMAT00000009163	TGGTCAAGCGTGATGGTTCCATGGTAAACATTGAAACG GACTCTATCAAAATCGGGCAAAACATTTCAACCAAGTC AGTCGGCACCAACGACAGGATGAA

Table 2-5 Continued. Target of the 17 genes custom designed probes used in NanoString nCounter assay. Seven genes were test targets and 10 genes were housekeeping controls (asterisks).

Gene Name	Ensembl ID	Target Sequence (5' – 3')
*TPM4**	ENSXMAT00000000653	ATCCTGAATGACAGACTCAAGGAGGCGGAAACCC GTGCAGAATTTGCAGAAAGGACGGTGTCAAAGCTT GAAAAGACCATAGACGACCTAGAAGAGAACC
*fam102bb**	ENSXMAT00000000552	GTGATGAAGCATTAGCGCTGCGATGACAGGATGA CCTTGATCACACTTTAAACAAATGGTTTGCGTTGGT TTCTCAATTCCCACAGCAAACACAACGCCC
*flt4**	ENSXMAT00000009755	ACGCAACGCCAGCGTTTCCGTCATCTATAAGTGCT CTGCTGAAAACAAAGTGGGCAAAGATGAGTTCCCT ATCTACTTTTATGTGACCACCATTCCTGAA
*ints9**	ENSXMAT00000010762	TCTTTACAGAGCCAGATTTCTCCTACCTGGATGCC CTGGCTCCGTACCAGCCGCTAGCCATGAAATGTGT TTACTGTCCTATTGACACCAGGCTCAACTT
*lcp2a**	ENSXMAT00000007048	CACCGGCGGACGCATCGGAACCGCCAAGATCCAA ACCTCCGGTTCTTCCTCCTCCCACCTCCTCCGTCA GCAGGAGTAACTCCTCTGCCAGAGTAGCGCC
*pcp4a**	ENSXMAT00000016883	GACAAGGATCCGGGCCTGCTGCTGGCAACAACAA GACCTCTGGGGGAAAAGGTCCAGAAGAGTCCAAG GGAGAGATCCCAGAGGATTTTGACATTGATAT
*si dkey-1c7.1**	ENSXMAT00000012666	CAGTGATCACCTCTAGCAACACACAAAATGGACGA ATCAAACTCTCTGATGACAGGAAGTCAAGAATATT CACAGTGACCATTTCCAGTCTGACCCTGAA
*sort1a**	ENSXMAT00000003489	GCCATTTCTTCCCTGCGGGGCGTCTACTTGACCAG CATACTCACAGAAGACGGTAACATAGAGACAGTGA TCACGTATGACCAAGGAGCCAAGTGGCAGC
*tmem204**	ENSXMAT00000019159	GCTGCTGCTGTTACTACTGATGTGTTTTACCAGCT GACAAAACGTAGTTAATAATGTTAGAGATAAAGTTT GGAGCAGACATGATGGTAGTGGTGGGCAC
*wdr37**	ENSXMAT00000004652	GAACGGGAGTTTGAGAATCTGTACATTGAAAACCT TGAATTGCGCCGGGAAATCGACTCTCTCAACGAGC GTCTGACTGGAGACGGACAGGCCATCGAGG

Quantitative Real Time PCR

Quantitative real time PCR (qRT-PCR) was performed as previously described (Walter et al., 2014). RNA isolated from three independent biological replicates for each wavelength region exposure was transcribed to cDNA using a High Capacity cDNA reverse transcription kit (Applied Bioscience, Carlsbad, CA, USA) following the manufacturer's instructions. Reverse transcription was

performed by adding 1.5 µg RNA, 100 mM dNTPs, 10X RT random primers, RNase inhibitor, and MultiScribe Reverse Transcriptase in a 20 µL reaction employing standard thermocycler conditions (25°C for 10 min, 37°C for 120 min and 85°C for 5 min). Negative controls were synthesized using 0.5 µg RNA and without the reverse transcriptase. Each sample was diluted to a final volume of 500 µL with 0.1% DEPC treated water and stored in -80°C. Synthesized cDNA was utilized in qRT-PCR SYBR Green-based detection methods on Applied Biosystem 7500Fast systems (Applied Bioscience, Carlbad, CA, USA).

PCR primers were designed using Genious (Biomatters Ltd., Auckland, New Zealand) bioinformatics software. All primer sets designed had 40-60% GC content and a T_m between 60-62°C with less than 1°C difference within each primer set in 3.0 mM K, 50 mM Na, and 0.8 mM dNTPs. Primer lengths were limited to 18-26 bp in length with amplicons limited to 80-150 bp across at least one exon junction. The efficiency of all primers was tested in *X. maculatus* skin in triplicate 20 µL reactions in a standard serial dilution of 25, 2.5, 0.25, 0.025 ng cDNA with 0.5 µM of each primer and 10 µL SYBR Green ready mix (Applied Bioscience, Carlsbad, CA, USA). Each reaction was subjected to 40 cycles at 95°C for 20 sec, 95°C for 15 sec, and 60°C for 30 sec, before being subjected to melting curve analysis. 18S RNA was selected as the transcript for normalization of all samples. Primers with 70-120% efficiency were chosen for relative gene expression analysis.

Three biological replicates with four technical replicates of each samples were plated for expression analysis. To remain consistent with RNA-Seq and

NanoString, two of the biological replicates were selected to calculate fold change expression relative to unexposed skin samples. The threshold cycle (C_T) for each test target and 18S rRNA control was determined by the 7500Fast System SDS 2.0.6. The average 18S control C_T was subtracted from the average target C_T for each biological replicate independently to give a ΔC_T value. mRNA expressions relative to the 18S RNA endogenous control were calculated by applying $2^{-\Delta CT}$. Calculated values represent the mRNA expression level for each target tested relative to the 18S RNA control. Fold change for each sample was determined relative to the respective unexposed sample and standard deviations were calculated with the average of 3 technical replicates for each biological replicate. Primers selected for differential expression analysis are shown in Table 2-6.

Table 2-6. Forward and reverse qRT-PCR primer sequences. Primer sequences for 5 genes tested using qRT-PCR validation of a select subset of significant differentially expressed genes.

Gene Name	Ensembl ID	Forward Primer Sequence	Reverse Primer Sequence
tgm8	ENSXMAT00000009163	CAGTGCTGGGTGTATGCTG	CTTGTTGGTGTCGTGAGCC
klhl38b	ENSXMAT00000008690	TTCATCTTCGTCCTGGGTGG	CGGCTTCCCATTGGTTGAAC
dnah7	ENSXMAT00000007381	GCTTACCTGGGAGCCTTCAC	GAGGAACACGGGATCTCC
atm	ENSXMAT00000017002	CCTGGAGCATCTTGTCTTGAC	CTCCGAGACGACACACTCTC
per1b	ENSXMAT00000015376	TGCTCTCAAATACGCCCTGC	CAGCCATGACACTCCTCCAC

III. GENETIC RESPONSE OF MALE *XIPHOPOHORUS* SKIN TO VARYING WAVELENGTHS OF LIGHT

Introduction

Life evolved under the full spectrum of the sun and thus it is likely to have become attuned to the use of all energy wavelengths in diurnal cycling of gene expression and metabolic processing. Although sunlight is necessary for some beneficial biological processes, such as regulation of circadian rhythm (Cermakian et al., 2002) and vitamin D production (Lucock et al., 2014), it can also have adverse effects, such as skin cancer and photoaging (Berneburg et al., 2000; Diepgen and Mahler, 2002). Studies of biological consequences of exposure of *Xiphophorus* fishes to different regions within the UV spectrum (e.g. UVB or 290-320 nm and UVA or 320-400 nm) have documented induced DNA damage through a variety of mechanisms (Mitchell et al., 2001; Mitchell et al., 2009). As detailed in chapter one, UVB exposure may produce direct DNA damage (e.g. cyclobutane pyrimidine dimers and 6-4 photoproducts; Tzung and Rünger, 1998; You et al., 2001), whereas UVA exposure is thought to generate reactive oxygen species (ROS) via absorption of light energy by cellular photosensitizers (Kielbassa et al., 1997; Wood et al., 2006; Swalwell et al., 2012). The differences in the mechanisms for DNA damage and its repair suggest different gene sets may have evolved to respond to specific wavelengths of light. With the advancement of genetic sequencing technology (i.e., RNA-Seq) and bioinformatics, scientists are able to observe changes in global gene

expression patterns induced after external stimuli, such as light. Recently, the molecular genetic effects of UVB and fluorescent light (FL) exposure have been characterized in *Xiphophorus* skin (Yang et al., 2014; Walter et al., 2015). Results from these studies suggest both light sources induced some of the same gene sets (e.g., circadian), but also showed major and unique differences in the genetic result of UV (e.g., inflammatory response) or FL (e.g., suppression of cell cycle progression) exposure. These interesting studies forward the question; have sets of genes evolved to respond to specific wavelengths? However, the global molecular genetic responses of skin (or other organs) in live animals after exposure to specific wavelengths of light have not yet been studied.

Among its many effects, light plays a crucial role in regulating the cellular circadian clock. The circadian system has been shown to have a major impact on behavior, physiology, and gene expression based on the light-dark cycling of the sun (Kleitman, 1949; Reppert and Weaver, 2002; Hastings et al., 2007). Interaction of transcription factors CLOCK and BMAL1 serve as core circadian regulators of this system (Gekakis et al., 1998). Subsequent transcription and translation of period (*per1*, *per2*, and *per3*), cryptochrome (*cry1* and *cry2*), and timeless proteins during the light phase inhibit the CLOCK/BMAL1 complex in the dark phase, creating a negative regulatory loop (Gekakis et al., 1998; Sangoram et al, 1998; Griffin et al., 1999). There is clear evidence suggesting circadian cycles play a role in DNA repair and control of the cell cycle (Granda et al., 2005; Gery et al., 2006; Kondratov and Antoch, 2007; Kang et al., 2009; Kang et al., 2010). However, the specific light wavelengths needed for circadian regulation

and what other transcriptional effects might be triggered by each wavelength are unknown. Examination of these light-responsive genes will validate the effects of light on the circadian system in *Xiphophorus* fish.

To initiate a better understanding of the global genetic effects in response to varying wavelengths of light, male *Xiphophorus maculatus* Jp 163 B were exposed to six specific 50 nm waveband regions between 300-600 nm. RNA-Seq and subsequent bioinformatics mining were employed to document the transcriptional response following exposure to one of the six waveband regions. We observed two 50 nm wavebands exhibit increased levels of transcriptional response (350-400 and 500-550 nm) compared to all other waveband regions. Light exposure in these two wavebands appears to induce circadian and cellular stress responses as well as various other signaling pathways.

Results

Determination of the Effects of Water on Light

To determine whether the cuvette or water would shift the wavelength and energy emitted from the xenon source, light spectra were measured through the cuvette with and without filtered aquaria water (Figure 3-1). Both spectrums were nearly identical, indicating neither the quartz cuvette nor water altered the wavelength reaching the fish skin. Furthermore, the energy transmitted through the cuvette was only altered by about 3 $\mu W/cm^2/nm$ when measured through water, indicating the volume of water used in the 1 cm path did not absorb a significant amount of energy.

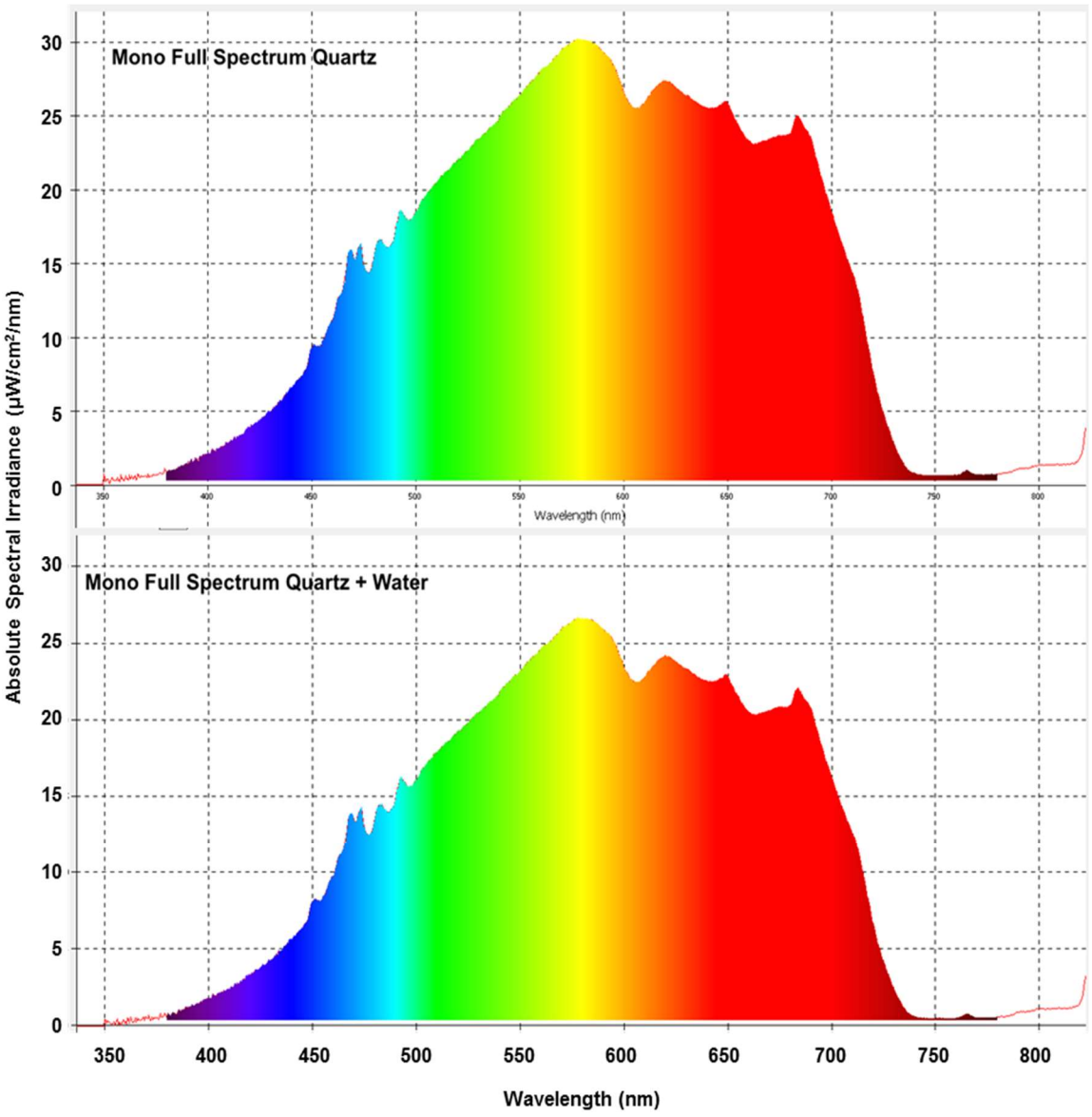

Figure 3-1. Spectral distribution of the monochromator through the quartz cuvette with and without water. Measurements were taken at full spectrum (set to 0 nm on the monochromator). Graphed is the absolute spectral irradiance (µW/cm^2/nm; y-axis) versus the wavelength of light (x-axis). Little difference is observed between the 2 graphs, suggesting the amount of water had little effect on energy reaching the fish skin.

Source: William Boswell

Distribution of Differentially Expressed Genes in Response to Varying Wavebands

Using EdgeR and the established 8 control samples, assessment of gene expression across six 50 nm wavebands from 300 nm to 600 nm exhibits 2 regions with increased number of DE genes. These regions are 350-400 nm with 194 DE genes and 500-550 nm with 566 DE genes. Overall, DE genes in both of these waveband regions exhibited up-modulation to a greater extent than down-modulation (Figure 3-2). Among the 194 DE genes in the 350-400 nm region, 63% (123 genes) were up-modulated and 37% (71 genes) were down-modulated. At the 500-550 nm region, 63% (359 genes) were up-modulated and 37% (207 genes) were down-modulated (Figure 3-2). In contrast to these two wavelength regions, considerably fewer genes were modulated following exposure to 400-450 and 450-500 nm light (44 and 147 genes, respectively).

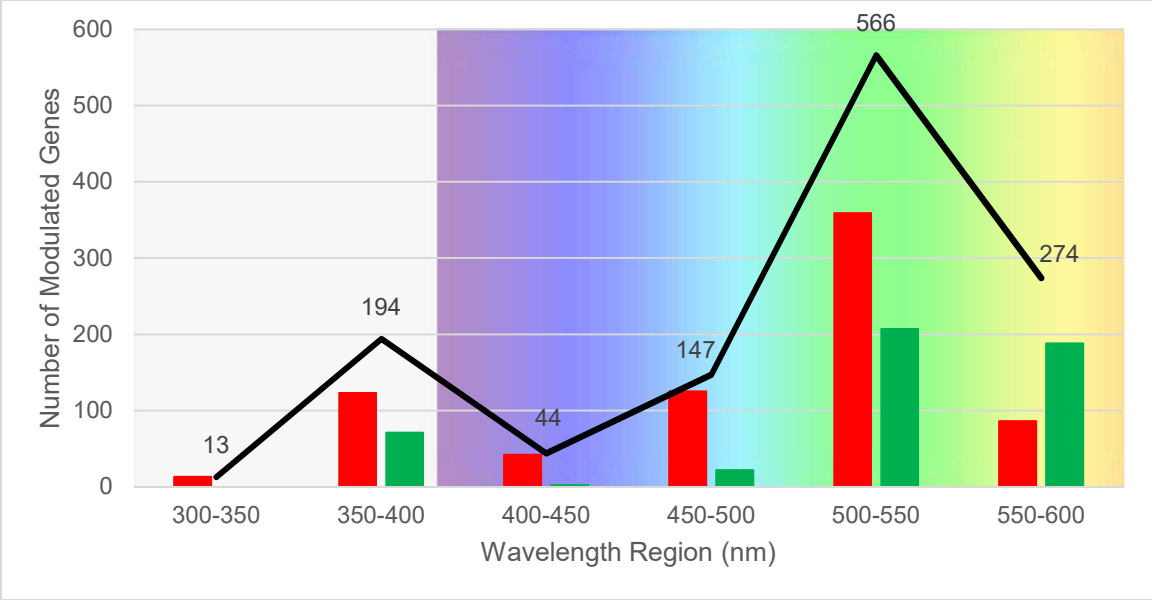

Figure 3-2. Distribution of differential expressed genes in male *X. maculatus* Jp 163 B in response to 50 nm wavebands. Bar and line graphs represent the number of DE genes that were ± 2-fold (*p*-adj ≤ 0.05). The black line represents the total number of DE genes, including up-modulated genes (red bars) and down-modulated genes (green bars). DE genes were determined using RNA-Seq and EdgeR software employed with data from two biological replicates at each waveband. Two waveband regions were observed to exhibit the greatest number of modulated genes (350-400 nm and 500-550 nm) with a decreased number of modulated genes in between (400-500 nm).

Circadian Gene Differential Expression and RNA-Seq Validations

Modulation of light responsive circadian genes have been well documented (Whitmore et al., 2000; Cermakian et al. 2002; Reppert and Weaver, 2002). Differentially expressed circadian genes were identified to determine whether the light dose utilized (10 kJ/m^2) at various waveband regions mimicked what had previously been observed in *Xiphophorus* skin (Walter et al., 2015; Yang et al., 2014). Eight differentially expressed circadian genes were identified that met the statistical cut off (± 2-fold and *p*-adj ≤ 0.05) in at least one

of the six waveband regions: *per1b*, *per2*, *per3*, *arntla* [also called *bmal1*], *clocka*, *bhlhe40*, and *nr1d2b* [also called *Rev-Erb-β*] (Figure 3-3). While *per2*, *arntla*, and *clocka* were consistently up-modulated across all six regions, *per1b*, *per2*, *bhlh240*, and *nr1d2* were down-modulated. Moreover, *per1b*, *per3*, and *nr1d2* become more down-modulated in longer, compared to shorter, wavebands (Figure 3-3). The observed expression patterns of these circadian genes (350-400 nm: *per3*, *arntla*, *bhlhe40*, *clocka*, and *per2*; 500-550: *per3*, *per1*, *bhlhe40, and nr1d2b*) are consistent in magnitude and direction with previous light exposure reports (Yang et al., 2014; Walter et al., 2015).

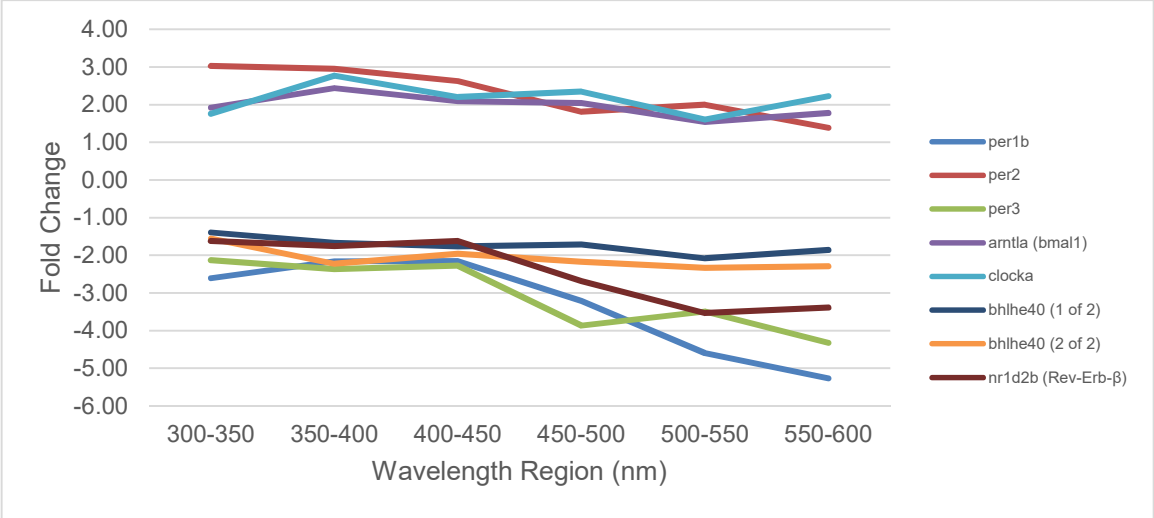

Figure 3-3. Light responsive expression of circadian rhythm genes to various regions of light. Depicted is a line graph representation of circadian rhythm genes with a ± 2-fold (p-adj ≤ 0.05) in at least one wavelength region in adult male *X. maculatus* skin. Fold change was determined by RNA-Seq transcriptome analysis of two biological replicates at each waveband region by comparison of exposed fish to basal expression of control fish. Expression of light responsive genes are consistent with previous reports (Yang et al., 2014; Walter et al., 2015).

To confirm the fold change expression values observed from RNA-Seq, two different and independent experimental technologies were employed, NanoString nCounter and qRT-PCR analyses. The genes tested were DE in at least one of the waveband regions. Five regions were plotted (excluding 400-450 nm) due to the lack of affected gene numbers at the time the NanoString nCounter assay was designed. Among the 7 genes tested by NanoString, 4 genes (*ppp1r27*, *ybx2*, *clocka*, and *per2*) were compared only to the RNA-Seq data (Figure 3-4A-D). The remaining 3 genes (*tgm8*, *dnah7*, and *klhl238b*) were compared using all three technologies: NanoString, RNA-Seq, and qRT-PCR (Figure 3-4E-G). In addition, 2 genes (*atm* and *per1b*) were assessed using RNA-Seq and qRT-PCR (Figure 3-4H-I).

Based on our collective comparison between all three gene expression platforms, the observed changes in expression derived from RNA-Seq were validated. Although the exact fold change values between the three independent experimental platforms were not equal, the trends in gene expression pattern were very similar for each of the 9 genes tested throughout all waveband regions in all platforms (Figure 3-4). Differences in fold change value is likely due to different amounts of samples used during RNA amplification (RNA-Seq: 1 µg; qRT-PCR: 1.5 µg; NanoString: 100 ng) and probe sequences. Thus, both NanoString and qRT-PCR confirmed the expression patterns observed by RNA-Seq at each independent wavelength exposure tested.

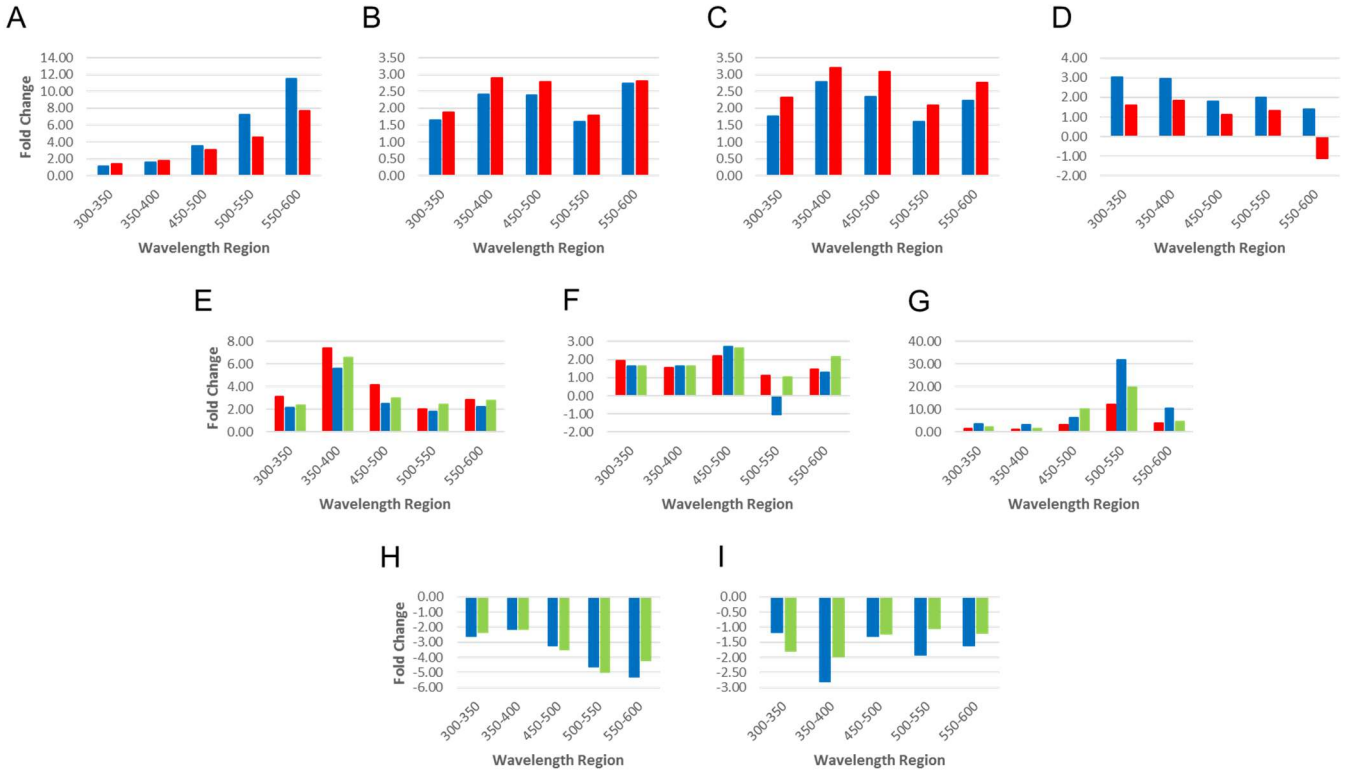

Figure 3-4. Gene expression validations. Validation of RNA-Seq (blue) gene expression by comparison to two other independent technologies, NanoString nCounter assay (red) and qRT-PCR (green). Fold changes were determined represents 2 biological replicates. NanoString samples were normalized to standard NanoString probes and a set of 10 housekeeping genes (Table 2-5). Gene counts were collected for each target gene and compared to basal levels of unexposed fish samples to determine fold change. All qRT-PCR samples were normalized to an 18S rRNA internal standard. mRNA expression of target genes (Table 2-6) was used in a ratio comparison to expression of unexposed fish to determine fold change. qRT-PCR data was tabulated from 2 biological replicates and 3 technical replicates for each sample at each exposure treatment. Y-axis have been adjusted to fit the data of each gene. Gene comparisons of RNA-Seq and NanoString: (A) *ppp1r27*, (B) *ybx2*, (C) *clock*, (D), *per2*. Gene comparisons of RNA-Seq, NanoString, and qRT-PCR: (E) *tgm8*, (F) *dnah7*, (G) *klhl38b*. Gene comparisons of RNA-Seq and qRT-PCR: (H) *atm* and (I) *per1b*. Relative gene modulation trends were observed to be similar across all independent methods.

Shared Genetic Response for 350-400 and 500-550 nm

As shown in Figure 3-2, exposure to different wavelengths of light produced varied genetic responses. To further investigate if each waveband region elicits a similar or unique genetic response, DE genes from each 50 nm waveband region were compared to other wavebands. Adjacent waveband regions shared a larger fraction of DE genes (Figure 3-5A and 3-5B) as one may expect. For example, 137 genes (50% of DE genes in 550-600 nm) were shared between 500-550 and 550-600 nm while only 38 genes (13.9% of DE genes in 550-600 nm) were shared between 450-500 and 550-600 nm (Figure 3-5B).

Examination of the number of shared DE genes between the two most transcriptionally responsive regions (350-400 and 500-550 nm) identified 56 shared DE genes (28.9% of DE genes in 350-400 nm or 9.9% of DE genes in 500-550 nm; Figure 3-5C). Functional analyses of these 56 genes were examined using GeneCards. Five different functional categories were identified: cell signaling (12 genes), circadian rhythm (2 genes), metabolism (8 genes), molecular transport (4 genes), and muscle/cytoskeleton remodeling (10 genes). The other 20 genes appear to be involved in disparate biological functions.

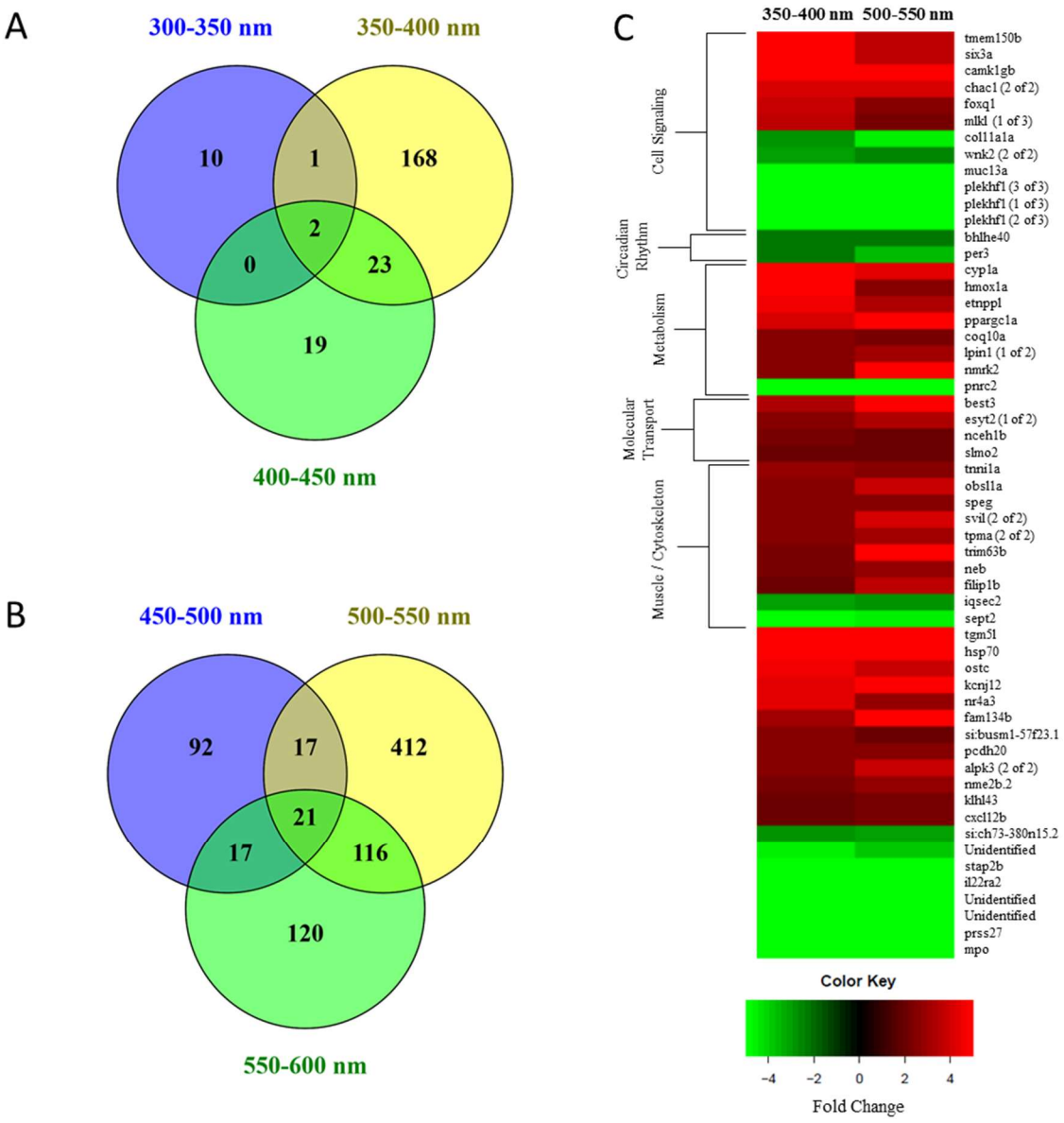

Figure 3-5. Comparison of differentially expressed genes between different wavelength regions from 300-600 nm. Multi-Venn diagram of DE genes between (A) 300-450 and (B) 450-600 nm wavelength regions were generated using Venny 2.1. (C) Heat map representation genes shared and their fold change response for each gene between 350-400 and 500-550 nm (56 genes). Up-modulated genes (red) and down-modulated genes (green) were manually categorized using GeneCards and are bracketed along the heat map: cell signaling (12 genes), circadian rhythm (2 genes), metabolism (8 genes), molecular transport (4 genes), and muscle/cytoskeleton remodeling (10 genes).

Genetic Response in 350-400 and 500-550 nm Regions

Following analysis of shared response between 350-400 and 500-550 nm regions, differentially expressed genes in each region were independently assessed for pathways and functional characterization using Ingenuity IPA and gene ontology, respectively. Pathways (i.e. circadian signaling, eNOS signaling, etc.) include a series of genes and proteins that lead to a particular change in the cell or product. Gene ontology identifies sets of genes that directly or indirectly affect cell function. Examination of both types of analyses provides a greater understanding of how DE genes impact the cell.

Among the 194 DE genes within the 350-400 nm region, human homologs IDs (HUGO ID's) could be assigned to 169 genes (87.1%) and analyzed through the human genome database. Eighty-four genes (49.7%) clustered in 5 canonical pathways and 10 functional categories (Table 3-1 and 3-2). Pathways include circadian rhythm signaling (5 genes, *p*-value = 5.58e-06), calcium signaling (6 genes, *p*-value = 2.86e-03), eNOS signaling (5 genes, *p*-value = 5.31e-03), NRF2-mediated oxidative stress response (5 genes, *p*-value = 1.39e-02), and actin cytoskeleton signaling (5 genes, *p*-value = 2.81e-02) (Table 3-1). In addition to canonical pathways, 10 functional categories were identified representing the majority of the 169 genes (79 genes): regulation of circadian rhythm (6 genes, *p*-value = 4.40e-04), regulation of transport (30 genes, *p*-value = 1.14e-03), tissue development (36 genes, *p*-value = 1.53e-05), epithelium development (24 genes, *p*-value = 1.40e-04), cell proliferation (26 genes, *p*-value = 4.73e-02), fatty acid metabolic process (13 genes, *p*-value = 5.14e-05),

coenzyme biosynthetic process (6 genes, *p*-value = 9.28e-04), muscle tissue development (11 genes, *p*-value = 6.50e-04), response to oxidative stress (15 genes, *p*-value = 3.24e-06), and hydrogen peroxide metabolic process (6 genes, *p*-value = 4.33e-06) (Table 3-2). The remaining 74 genes did not did not readily cluster in GO categories. Additionally, GO categories with similar gene sets and functions, such as *tissue development*, *epithelium development*, and *cell differentiation*, were grouped into broader categories (e.g. cell differentiation). GO terms *fatty acid metabolic process* and *coenzyme biosynthetic process* were grouped with metabolism while GO terms response to *oxidative stress* and *hydrogen peroxide metabolic process* were grouped with stress response.

Table 3-1. Canonical pathways and *p*-values (cutoff p-value ≤ 0.05) of genes clustered at 350-400 nm using Ingenuity IPA. Name of the pathway and the number of DE genes (count) that fall within each pathway are presented: circadian rhythm signaling (5 genes, *p*-value = 5.58e-06), calcium signaling (6 genes, *p*-value = 2.86e-03), eNOS signaling (5 genes, *p*-value = 5.31e-03), NRF2-mediated oxidative stress response (5 genes, *p*-value = 1.39e-02), and actin cytoskeleton signaling (5 genes, *p*-value = 2.81e-02). Z-score was determined by the Ingenuity software to represent the activation or inhibition of the pathway. Z-score of N/A represents the pathway was affected, but not in a particular direction. Gene names and their associated fold change expression are listed. Genes listed may overlap into different pathways due to multiple gene functions.

Canonical Pathway	***p*-value**	**Z-score**	**Count**	**Gene Name**
Circadian Rhythm Signaling	5.58E-06	N/A	5	per3 (-2.37), arntl (2.45), bhlhe40 (-2.22), clock (2.78), per2 (2.95)
Calcium Signaling	2.86E-03	N/A	6	myh14 (2.26), camk1g (5.70), tpm1 (2.49), tnni1 (2.70), itpr1 (2.26), myh7b (2.72)
eNOS Signaling	5.31E-03	-2.00	5	hspa1a/hspa1b (5.98), hspa6 (5.98), itpr1 (2.26), pdgfc (-2.26), atm (-2.80)
NRF2-mediated Oxidative Stress Response	1.39E-02	N/A	5	map2k6 (-3.89), hmox1 (4.97), mgst1 (-2.00), cdc34 (2.01), atm (-2.80)
Actin Cytoskeleton Signaling	2.81E-02	1.00	5	ezr (2.19), myh14 (2.26), myh7b (2.72), pdgfc (-2.26), atm (-2.80)

Table 3-2. GO terms and p-values (cutoff *p*-value ≤ 0.05) of genes clustered at 350-400 nm using Gene Ontology. Among the 194 *Xiphophorus* transcripts ID's, 169 were converted to human homolog ID's. Listed are 79 genes that were clustered into 10 GO clusters: regulation of circadian rhythm (6 genes, *p*-value = 4.40e-04), regulation of transport (30 genes, *p*-value = 1.14e-03), tissue development (36 genes, *p*-value = 1.53e-05), epithelium development (24 genes, *p*-value = 1.40e-04), cell proliferation (26 genes, *p*-value = 4.73e-02), fatty acid metabolic process (13 genes, *p*-value = 5.14e-05), coenzyme biosynthetic process (6 genes, *p*-value = 9.28e-04), muscle tissue development (11 genes, *p*-value = 6.50e-04), response to oxidative stress (15 genes, *p*-value = 3.24e-06), and hydrogen peroxide metabolic process (6 genes, *p*-value = 4.33e-06). GO categories that were similar in gene set and function were grouped into a broader category shown on the left. GO ID for each GO term (GOBPID) and the number of DE genes (count) that fall within each cluster are presented. Gene names and fold change associated with a particular GO term are listed. Up-modulated genes are presented red while down-modulated genes are in green. Genes listed may overlap into different GO categories due to multiple functions.

	GOBPID	*p*-value	Count	Term	Gene Name
Circadian Rhythm	GO:0042752	4.40E-04	6	Regulation of Circadian Rhythm	ppargc1a (4.00), per2 (2.95), clock (2.78), arntl (2.45), per3 (-2.37), bhlhe40 (-2.22)
Transport	GO:0051049	1.14E-03	30	Regulation of Transport	hspa1a (5.98), hmox1 (4.97), nr4a3 (4.30), ppargc1a (4.00), best3 (3.38), atp1b2 (3.16), snca (3.15), per2 (2.95), ca2 (2.85), rab25 (2.82), clock (2.78)ldlrap1 (2.72), arntl (2.45), sgk2 (2.44), rsad2 (2.32), anxa1 (2.29), itpr1 (2.26), chia (2.22), ezr (2.19), clic3 (2.19), rangap1 (2.06), cxcl12 (2.03), homer2 (2.03), ept1 (2.02), kcnd1 (-67.00), map2k6 (-3.89), tmem173 (-2.54), slc17a9 (2.05), wnk2 (-3.03), wnt5a (-2.41)
Cell Proliferation	GO:0009888	1.53E-05	36	Tissue Development	pax6 (15.63), tgm3 (6.43), tgm5 (6.43), six3 (5.86), cyp1a1 (4.98), nr4a3 (4.30), ppargc1a (4.00), foxq1 (3.77), ca2 (2.85), rab25 (2.82), clock (2.78), tnni1 (2.70), obsl1 (2.69), speg (2.68), svil (2.65), tpm1 (2.49), arntl (2.45), scel (2.37), anxa1 (2.29), myh14 (2.26), nme2 (2.21), dsg2 (2.20), dsg4 (2.20), evpl (2.19), ezr (2.19), fmn1 (2.14), tgm1 (2.10), emp1 (2.07), cxcl12 (2.03), nppc (-8.70), hoxc13 (-3.48), col11a1 (-2.92), atm (-2.80), fat4 (-2.68), wnt5a (-2.41), bmpr1b (-2.18)
	GO:0060429	1.40E-04	24	Epithelium Development	pax6 (15.63), tgm3 (6.43), tgm5 (6.43), six3 (5.86), cyp1a1 (4.98), foxq1 (3.77), ca2 (2.85), rab25 (2.82), clock (2.78), arntl (2.45), scel (2.37), anxa1 (2.29), nme2 (2.21), dsg4 (2.20), evpl (2.19), ezr (2.19), fmn1 (2.14), tgm1 (2.10), emp1 (2.07), cxcl12 (2.03), hoxc13 (-3.48), atm (-2.80), fat4 (-2.68), wnt5a (-2.41)

Table 3.2 Continued. GO terms and p-values (cutoff *p*-value ≤ 0.05) of genes clustered at 350-400 nm using Gene Ontology.

	GOBPID	*p*-value	Count	Term	Gene Name
	GO:0008283	4.73E-02	26	Cell Proliferation	pax6 (15.63), six3 (5.86), cyp1a1 (4.98), hmox1 (4.97), nr4a3 (4.30), ppargc1a (4.00), per2 (2.95), rab25 (2.82), capn1 (2.76), speg (2.68), sgk2 (2.44), anxa1 (2.29), nme1 (2.21), nme2 (2.21), styk1 (2.16), emp1 (2.07), srms (2.07), cxcl12 (2.03), nppc (-8.70), wnk2 (-3.03), atm (-2.80), irf1 (-2.78), wnt5a (-2.41), pdgfc (-2.26), bmpr1b (-2.18), ctbp2 (-2.03)
Metabolism	GO:0006631	5.14E-05	13	Fatty Acid Metabolic Process	cyp1a1 (4.98), cyp1a2 (4.98), nr4a3 (4.30), ppargc1a (4.00), snca (3.15), per2 (2.95),elovl7 (2.44), lpin1 (2.51), anxa1 (2.29), elovl1 (2.19), hsd17b12 (2.14), hacl1 (-2.49), faah (-2.41)
	GO:0009108	9.28E-04	6	Coenzyme Biosynthetic Process	snca (3.15), nmrk2 (2.50), elovl7 (2.44), elovl1 (2.19), hsd17b12 (2.14), nadk (2.01)
Muscle / Cytoskeleton Remodeling	GO:0060537	6.50E-04	11	Muscle Tissue Development	ppargc1a (4.00), tnni1 (2.70), obsl1 (2.69), speg (2.68), svil (2.65), tpm1 (2.49), arntl (2.45), myh14 (2.26), dsg2 (2.20), col11a1 (-2.92), wnt5a (-2.41)
Stress Response	GO:0006979	3.24E-06	15	Response to Oxidative Stress	hspa1a (5.98), hspa1b (5.98), hmox1 (4.97), nr4a3 (4.30), ppargc1a (4.00), snca (3.15), ca3 (2.85), tpm1 (2.49), arntl (2.45), sgk2 (2.44), anxa1 (2.29), lpo (-215.89), mpo (-215.89), epx (-215.89), mgst1 (-2.00)
	GO:0042743	4.33E-06	6	Hydrogen Peroxide Metabolic Process	cyp1a1 (4.98), cyp1a2 (4.98), snca (2.44), lpo (-215.89), mpo (-215.89), epx (-215.89)

Similar functionalization of the 566 DE genes observed in the 500-550 nm waveband region allowed 496 genes (87.6%) to be assigned human homolog ID's. Clustering of these genes segregated 251 (50.6%) of these genes into 8 canonical pathways and 9 functional categories (Table 3-3 and 3-4). Pathways include AMPK signaling (15 genes, *p*-value = 1.52e-05), glycolysis I (6 genes, *p*-value = 1.68e-05), aldosterone signaling in epithelial cells (13 genes, *p*-value = 4.32e-05), calcium signaling (14 genes, *p*-value = 6.22e-05), actin cytoskeleton signaling (12 genes, *p*-value = 4.18e-03), eNOS signaling (9 genes, *p*-value = 5.39e-03), ILK signaling (10 genes, *p*-value = 1.03e-02), and circadian rhythm signaling (3 genes, *p*-value = 3.89e-02) (Table 3-3). Moreover, 9 functional categories were identified: cell differentiation (134 genes, *p*-value = 7.67e-05), cell death (69 genes, *p*-value = 8.22e-03), glucose metabolic process (18 genes, *p*-value = 3.32e-05), regulation of fatty acid metabolic process (9 genes, *p*-value = 4.35e-04), oxidation-reduction process (47 genes, *p*-value = 5.67e-04), muscle cell differentiation (35 genes, *p*-value = 3.35e-11), actin cytoskeleton organization (32 genes, *p*-value = 2.43e-05), response to heat (16 genes, *p*-value = 4.74e-06) and response to oxidative stress (21 genes, *p*-value = 9.57e-04) (Table 3-4). The remaining 242 genes did not cluster significantly in a GO category. Categories such as cell death were grouped with cell differentiation. Smaller GO terms *glucose metabolic process* and *regulation of fatty acid metabolic process* were grouped into metabolism. *Muscle cell differentiation* and *actin cytoskeleton organization* were grouped into a broader category muscle/cytoskeleton remodeling. Summary of canonical pathways (Tables 3-1 and 3-3) and GO

clusters (Tables 3-2 and 3-4) at both 350-400 and 500-550 nm regions are presented in Figure 3-6.

Table 3-3. Canonical pathways and *p*-values (cutoff p-value ≤ 0.05) of genes clustered at 500-550 nm using Ingenuity IPA. Name of the pathway and the number of DE genes (count) that fall within each pathway are presented: AMPK signaling (15 genes, *p*-value = 1.52e-05), glycolysis I (6 genes, *p*-value = 1.68e-05), aldosterone signaling in epithelial cells (13 genes, *p*-value = 4.32e-05), calcium signaling (14 genes, *p*-value = 6.22e-05), actin cytoskeleton signaling (12 genes, *p*-value = 4.18e-03), eNOS signaling (9 genes, *p*-value = 5.39e-03), ILK signaling (10 genes, *p*-value = 1.03e-02), and circadian rhythm signaling (3 genes, *p*-value = 3.89e-02). Z-score was determined to represent the activation or inhibition of the pathway. Z-score of N/A represents the pathway was affected, but not in a particular direction. Gene names and their associated fold change expression are listed. Genes listed may overlap into different pathways due to multiple gene functions.

Canonical Pathway	*p*-value	Z-score	Count	Gene Name
AMPK Signaling	1.52E-05	1.27	15	pik3c2b (-2.43), arid1a (-2.26), ckm (2.13), pfkfb1 (3.51), eef2 (2.52), cpt1b (2.40), chrnb1 (3.07), gys2 (5.87), pfkm (2.49), mtor (-2.00), crtc2 (-2.12), fasn (-2.13), prkaa2 (2.01), irs2 (2.88), ppargc1a (5.34)
Glycolysis I	1.68E-05	N/A	6	gpi (2.15), pkm (2.65), pgam2 (2.91), aldoa (2.31), gapdh (2.17), pfkm (2.49)
Aldosterone Signaling in Epithelial Cells	4.32E-05	-1.00	13	hspa8 (2.99), hspa4 (2.38), pik3c2b (-2.43), dnajb4 (2.97), itpr3 (-2.22), hspa1a/hspa1b (15.64), asic1 (5.47), hspb8 (2.99), hspa6 (15.64), hsp90aa1 (2.94), hspb7 (3.52), plch2 (-2.46), dnajb5 (2.67)
Calcium Signaling	6.22E-05	0.00	14	myh6 (2.10), myh13 (4.10), tnnt3 (2.00), itpr3 (-2.22), casq1 (2.38), chrnb1 (3.07), camk1g (5.74), myh7 (3.53), tpm1 (2.99), tnni1 (2.57), tpm2 (2.06), actc1 (3.12), myl3 (2.30), atp2a1 (2.50)
Actin Cytoskeleton Signaling	4.18E-03	1.90	12	pik3c2b (-2.43), myh6 (2.10), flna (-2.31), myh13 (4.10), mylpf (2.27), actn2 (2.50), fgf12 (3.63), myh7 (3.53), actc1 (3.12), ttn (2.48), myl3 (2.30), iqgap3 (-3.43)
eNOS Signaling	5.39E-03	-1.63	9	hspa8 (2.99), hspa4 (2.36), pik3c2b (-2.43), chrnb1 (3.07), itpr3 (-2.22), hspa1a/hspa1b (2.94), hspa6 (15.64), prkaa2 (2.01), hsp90aa1 (2.94)
ILK Signaling	1.03E-02	1.90	10	pik3c2b (-2.43), mtor (-2.00), myh6 (2.10), flna (-2.31), myh13 (4.10), actn2 (2.50), irs2 (2.88), myh7 (3.53), actc1 (3.12), myl3 (2.30)
Circadian Rhythm Signaling	3.89E-02	N/A	3	per3 (-3.49), per1 (-4.60), bhlhe40 (-2.33)

Table 3-4. GO terms and p-values (cutoff *p*-value ≤ 0.05) of genes clustered at 500-550 nm using Gene Ontology. Among the 566 *Xiphophorus* transcripts ID's, 496 were converted to human homolog ID's. Listed are 219 genes that were clustered into 10 GO clusters: cell differentiation (134 genes, *p*-value = 7.67e-05), cell death (69 genes, *p*-value = 8.22e-03), glucose metabolic process (18 genes, *p*-value = 3.32e-05), regulation of fatty acid metabolic process (9 genes, *p*-value = 4.35e-04), oxidation-reduction process (47 genes, *p*-value = 5.67e-04), muscle cell differentiation (35 genes, *p*-value = 3.35e-11), actin cytoskeleton organization (32 genes, *p*-value = 2.43e-05), response to heat (16 genes, *p*-value = 4.74e-06) and response to oxidative stress (21 genes, *p*-value = 9.57e-04). GO categories that were similar in gene set and function were grouped into a broader category shown on the left. GO ID for each GO term (GOBPID) and the number of DE genes (count) that fall within each cluster are presented. Gene names and fold change associated with a particular GO term are listed. Up-modulated genes are presented red while down-modulated genes are in green. Genes listed may overlap into different GO categories due to multiple functions.

Table 3-4. GO terms and p-values (cutoff *p*-value ≤ 0.05) of genes clustered at 500-550 nm using Gene Ontology.

	GOBPID	*p*-value	Count	Term	Gene Name
Cell Proliferation	GO:0030154	7.67E-05	134	Cell Differentiation	helt (27.40), tgm3 (11.01), epb42 (11.01), apoa4 (9.87), etp (9.72), scrt1 (8.90), scrt2 (8.90), prom1 (6.46), fbxo40 (6.39), ppdpf (6.33), lmod2 (5.76), nmrk2 (5.58), ppargc1a (5.34), ankrd1 (5.13), yp1a1 (4.31), chac1 (4.20), crem (4.13), clic5 (4.01, 2.59), nptx1 (4.00), lmod3 (4.00), obsl1 (3.92), coro1c (3.79), myoc (3.66), nebl (3.63), strc (3.63), tcap (3.63), six3 (3.62), nr1d2 (3.53), cyp24a1 (3.44), klhl40 (3.33), dhh (3.19), bcap29 (3.14), lgi1 (3.10), chrnb1 (3.06), myod1 (3.05), wfikkn2 (2.99), hspa8 (2.99), esrrb (2.99), tpm1 (2.99), hsp90aa1 (2.94), usp13 (2.93), nr4a3 (2.92), irs2 (2.88), sept4 (2.83), nme1 (2.77), nme2 (2.77), ddit4 (2.69), fhl1 (2.68), plpp7 (2.67), murc (2.65), foxq1 (2.65), eef2 (2.52), nexn (2.52), speg (2.51), actn2 (2.50), ttn (2.48), obscn (2.45), asb2 (2.42), cxcl12 (2.40), pbld (2.38), casq1 (2.38), wnt2b (2.37), scn1b (2.35), cap2 (2.31), nr4a2 (2.31), klhl41 (2.30), hacd1 (2.26), rps6ka2 (2.24), anpep (2.23), myoz1 (2.23), bin1 (2.22), steap4 (2.17), gadd45g (2.15), actc1 (2.12), myf6 (2.10), myh6 (2.10), chrd (2.10), mlf1 (2.08), gprc5b (2.08), insig1 (2.03), smyd1 (2.02), psme4 (2.02), cacna1s (2.01), esrra (2.00), ccol11a1 (-4.72), celsr2 (-4.07), col27a1 (-4.07), ehf (-3.80), pcsk9 (-3.70), col1a1 (-3.67), rhcg (-3.56), wdr78 (-3.35), kiaa1109 (-3.03), ptprf (-2.44), lama5 (-3.22), plk4 (-3.15), cacna1d (-3.05), tnc (-2.99), wnk1 (-2.94), agrn (-2.90), bag6 (-2.67), slitrk3 (-2.65), znf703 (-2.64), jarid2 (-2.58), col7a1 (-2.57), tnik (-2.55), e2f8 (-2.50), herc1 (-2.47), clasp1 (-2.37), mkl2 (-2.34), flna (-2.31), casz1 (-2.28), lrp6 (-2.27), arid1a (-2.26), ephb4 (-2.24), abca1 (-2.22), bcl9 (-2.22), kdm6a (-2.17), col15a1 (-2.13), fasn (-2.13), gata3 (-2.12), rere (-2.12), mmp15 (-2.11), sfxn1 (-2.08), lamb1 (-2.05), dnm1 (-2.04), ephb3 (-2.04), prrc2c (-2.02), ambra1 (-2.02), col5a2 (-2.01), sipa1l3 (-2.01), mtor (-2.00), col18a1 (-2.00)

Table 3-4 Continued. GO terms and p-values (cutoff *p*-value ≤ 0.05) of genes clustered at 500-550 nm using Gene Ontology.

	GOBPID	*p*-value	Count	Term	Gene Name
Cell Proliferation	GO:0008219	8.22E-03	69	Cell Death	hspa1a (15.64), hspa1b (15.64), fam134b (10.74), hp (10.28), scrt2 (8.90), cideb (6.38), ppargc1a (5.34), ankrd1 (5.13), chac1 (4.20), cd38 (4.16), sbk2 (4.13), nptx1 (4.00), gls2 (3.81), six3 (3.62), dusp22 (3.37), bcap29 (3.14), aimp1 (3.09), nr4a2 (2.92), nr4a3 (2.92), irs2 (2.88), sept4 (2.83), nme1 (2.77), nme2 (2.77), slc25a4 (2.74), ddit4 (2.69), pkm (2.65), hmox1 (2.62), pdk2 (2.59), atp2a1 (2.50), actn2 (2.50), obscn (2.45), cxcl12 (2.40), acer2 (2.35), rps6ka2 (2.24), bin1 (2.22), mlkl (2.21), gapdh (2.17), wisp2 (2.17), gadd45g (2.15), gpi (2.15), ifi27 (2.12), actc1 (3.12), serpinb9 (2.08), pycr1 (2.07), psme4 (2.02), wisp1 (2.02), prkaa2 (2.01), mpo (-52.37), nox1 (-13.29), tax1bp1 (-7.44), bub1 (-4.23), gata3 (-3.72), pcsk9 (-3.70), klf11 (-3.27), hsh2d (-3.24), clspn (-3.12), agrn (-2.90), bag6 (-2.67), magi1 (-2.61), tnik (-2.55), plekhf1 (-2.41), birc6 (-2.37), flna (-2.31), lrp6 (-2.27), cecr2 (-2.22), phip (-2.03), ambra1 (-2.02), col18a1 (-2.02)
Metabolism	GO:0006006	3.32E-05	18	Glucose Metabolic Process	gys2 (5.87), ppargc1a (5.34), crem (4.13), pfkfb1 (3.51), aimp1 (3.09), pygm (2.98), pgam2 (2.91), irs2 (2.88), gpd1 (2.73), pkm (2.65), pdk2 (2.59), pfkm (2.49), aldoa (2.31), gapdh (2.17), gpi (2.14), hk1 (2.02), crtc2 (-2.12), mtor (-2.00)
	GO:0019217	4.35E-04	9	Regulation of Fatty Acid Metabolic Process	apoa4 (9.87), pdk2 (2.59), ppargc1a (5.34), nr4a3 (2.92), irs2 (2.88), insig1 (2.03), prkaa2 (2.01), srebf1 (-2.12), mtor (-2.00)
Oxidation Reduction	GO:0055114	5.67E-04	47	Oxidation-Reduction Process	cyp2w1 (15.11), apoa4 (9.87), gys2 (5.87), ppargc1a (5.34), cyp1a1 (4.31), cyp1a2 (4.31), cyp24a1 (3.44), dhrs3 (3.02), pygm (2.98), abcc8 (2.95), nr4a3 (2.93), pgam2 (2.91), prkaa2 (2.91), irs2 (2.88), dio3 (2.77), slc25a4 (2.74), gpd1 (2.73), pkm (2.65), hmox1 (2.62), me1 (2.55), dhrs7c (2.51), pfkfb1 (3.51), ppp1r3a (2.90), pfkm (2.49), cpt1b (2.40), aldoa (2.31), ldhb (2.24), gmpr (2.23), creg1 (2.21), gapdh (2.17), steap4 (2.17), gpi (2.14), aldh3a1 (2.08), aldh3a2 (2.08), pycr2 (2.07), pycr1 (2.07), hk1 (2.02), lpo (-52.37), mpo (-52.37), epx (-52.37), nox1 (-13.29), cacna1d (-3.05), kdm6a (-2.17), uty (-2.17), itpr3 (-2.22), fasn (-2.13), mtor (-2.00)

Table 3-4 Continued. GO terms and p-values (cutoff *p*-value ≤ 0.05) of genes clustered at 500-550 nm using Gene Ontology.

	GOBPID	*p*-value	Count	Term	Gene Name
Muscle / Cytoskeleton Remodeling	GO:0042692	3.35E-11	35	Muscle Cell Differentiation	fbxo40 (6.39), lmod2 (5.76), nmrk2 (5.58), ankrd1 (5.13), lmod3 (4.00), myf6 (3.95), obsl1 (3.92), tcap (3.63), nebl (3.63), klhl40 (3.63), actc1 (3.12), chrnb1 (3.06), myod1 (3.05), tpm1 (2.99), wfikkn2 (2.99), plpp7 (2.67), nexn (2.52), speg (2.51), actn2 (2.50), ttn (2.48), obscn (2.45), asb2 (2.42), cxcl12 (2.40), casq1 (2.38), klhl41 (2.30), hacd1 (2.26), myoz1 (2.23), bin1 (2.22), myh6 (2.10), smyd1 (2.02), cacna1s (2.01), mkl2 (-2.34), bcl9 (-2.22), arid1a (-2.15), mtor (-2.00)
	GO:0030036	2.43E-05	32	Actin Cytoskeleton Organization	xirp1 (7.91), lmod2 (5.76), ankrd1 (5.13), lmod3 (4.00), obsl1 (3.92), coro1c (3.79), myoc (3.66), nebl (3.63), xirp2 (3.59, 3.15), tpm1 (2.99), tacr1 (2.83), neb (2.74), tcap (3.63), coro6 (2.55), actn2 (2.50), ttn (2.48), obscn (2.45), cxcl12 (2.40), casq1 (2.38), aldoa (2.31), klhl41 (2.30), baiap2l2 (2.27), myoz1 (2.23), actc1 (2.12), myh6 (2.10), iqsec2 (-2.71), tenm1 (-2.58), tnik (-2.55), espn (-5.15), clasp1 (-2.37), flna (-2.31), mtor (-2.00)
Stress Response	GO:0009408	4.74E-06	16	Response to Heat	hspa1a (15.64), hspa1b (15.64), hspa6 (15.64), hspb7 (3.52), hspa8 (2.99), dnajb4 (2.97), hsp90aa1 (2.94), tacr1 (2.83), hmox1 (2.62), cxcl12 (2.40), casq1 (2.38), myh6 (2.10), atr (-2.42), nup205 (-2.34), nup98 (-2.02), mtor (-2.00)
	GO:0006979	9.57E-04	21	Response to Oxidative Stress	hspa1a (15.64), hspa1b (15.64), hp (10.28), apoa4 (9.87), ppargc1a (5.34), cd38 (4.16)chrna4 (3.00), tpm1 (2.99), nr4a3 (2.92), tacr1 (2.83), hmox1 (2.62), pdk2 (2.59), sesn1 (2.57), nr4a2 (2.31), pycr1 (2.07), lpo (-52.37), mpo (-52.37), epx (-52.37), nox1 (-13.29), col1a1 (-3.67), atrn (-2.18),

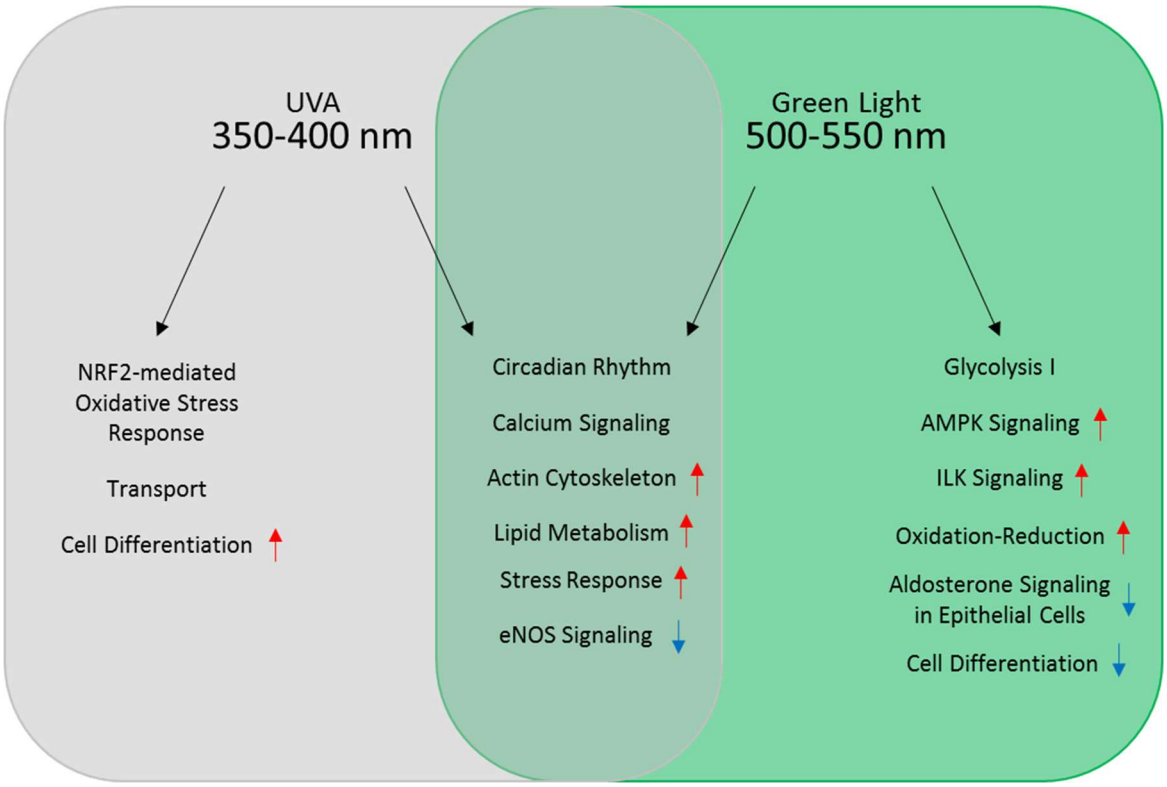

Figure 3-6. Chart summary of canonical pathways identified by Ingenuity IPA and GO categories in male 350-400 and 500-550 nm regions. Pathways and GO terms at the 350-400 nm region is shown on the left (Table 3-1 and 3-2) while those at the 500-550 nm region are shown on the right (Table 3-3 and 3-4). Pathways and GO terms shared between both regions are listed in the center. Up-modulation and down-modulation of clusters are indicated by red and blue arrows, respectively.

To visualize genetic associations, ConsensusPathDB (CPDB) was employed to independently analyze DE genes at both 350-400 nm and 500-550 nm (Figure 3-7 and 3-8, respectively). Human gene ID's previously used for Ingenuity IPA and gene ontology were also inputted into CPDB (350-400 nm: 169 genes; 500-550 nm: 496 genes). The fold change values for each gene displayed within each network are shown as a heat map. Two large DE gene networks appear to be modulated at the 350-400 nm (Figure 3-7) and 500-550 nm (Figure 3-8a) exposures, centered exclusively around *atm* and *atr*, respectively. Both

networks include a circadian rhythm cluster involving known circadian genes (e.g. *bhlhe40*, *per3*, *arntl*, etc.; Hunt and Sassone-Corsi, 2007). Additionally, genes related to cell signaling, muscle/cytoskeletal remodeling, metabolism, and transcription/translation were DE in both transcriptionally active regions (Figure 3-7 and 3-8b) while genes related to cell adhesion/motility were only observed with the 500-550 nm exposure (Figure 3-8b). DE genes related to cellular stress were observed in both 350-400 and 500-550 nm regions. However, each stress related gene cluster contained genes that are expected to have substantially different functions (see below).

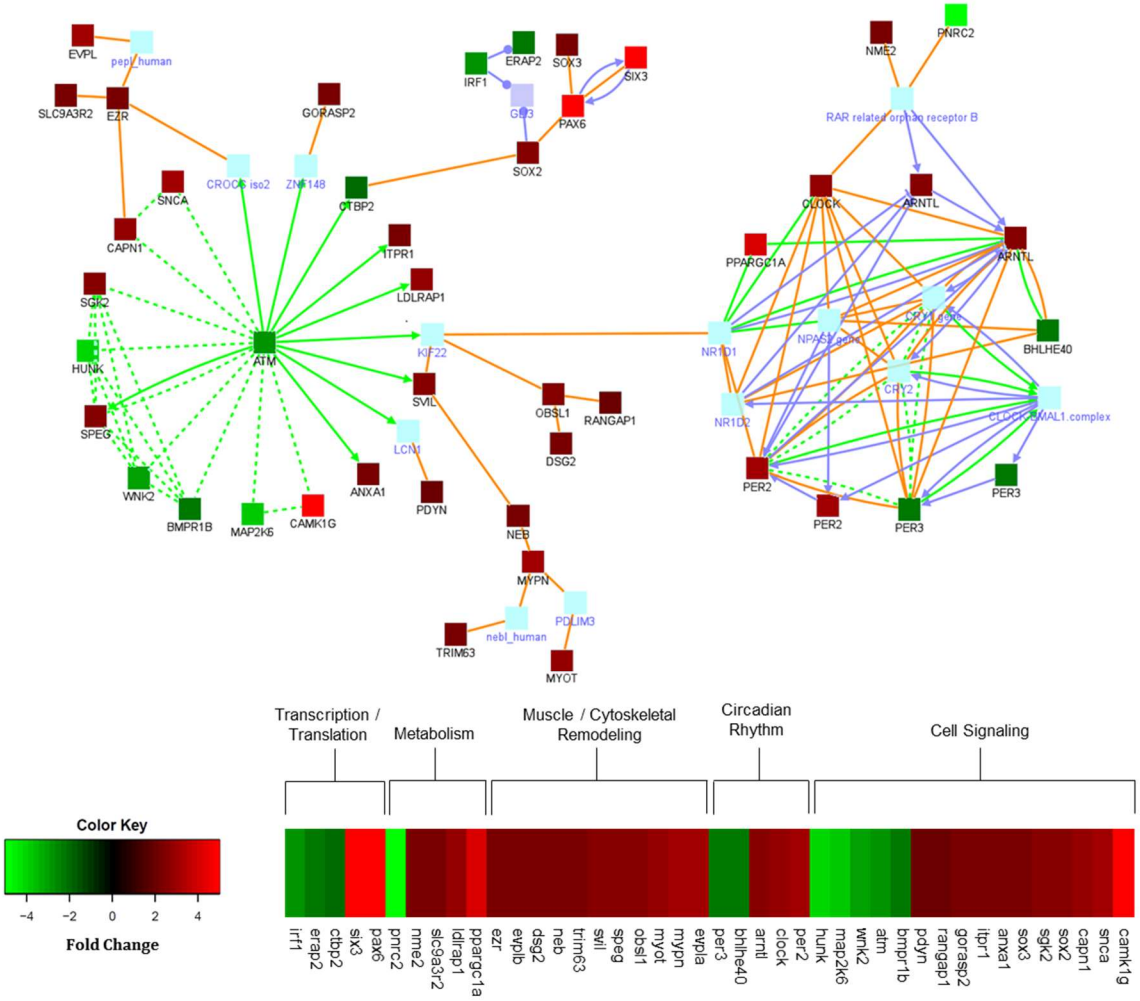

Figure 3-7. Protein and genetic associations of differentially expressed genes (± 2-fold) of male *X. maculatus* skin exposed to 350-400 nm. Network was created through ConsensusPathDB gene analysis software. A total of 169 genes were queried and the following associations were made (42 genes; Z-score = 30): protein (orange), genetic (blue), and biochemical (green) interactions. Dotted lines represent a physical interaction, solid arrows show substrate/product interaction, and solid lines with a circle represent enzyme interaction. Colored boxes indicate fold change scaled to the heat map colors. Boxes in blue and purple represent predicted genes and proteins CPDB used to make associations. Up-modulated (red) and down-modulated (green) genes within the heat map were functionally categorized. Within the 350-400 nm region, genes were clustered into cell signaling (16 genes), circadian rhythm (5 genes), muscle/cytoskeletal (11 genes), metabolism (5 genes), and transcription/translation (5 genes).

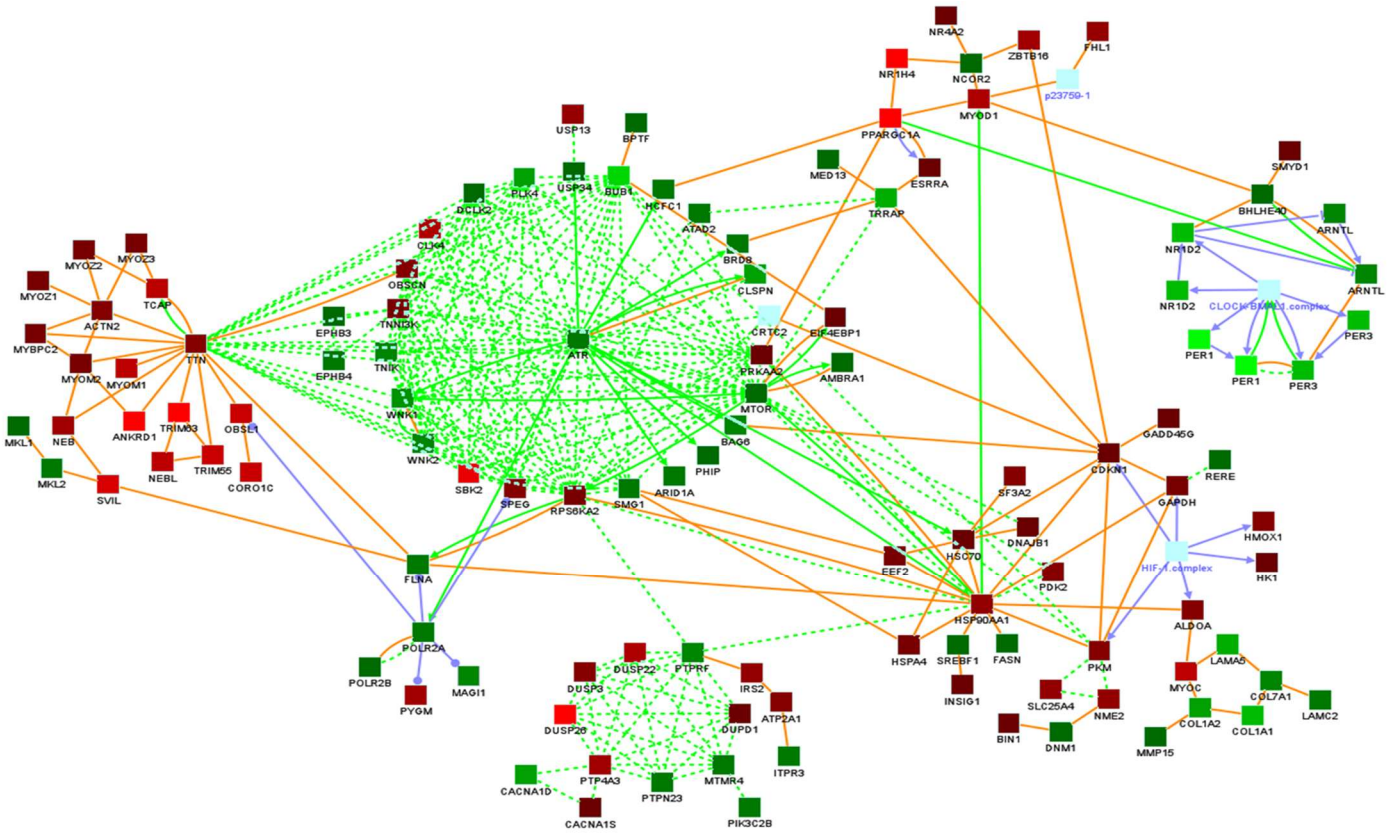

Figure 3-8A. Protein and genetic associations of differentially expressed genes (± 2-fold) of male *X. maculatus* skin exposed to 500-550 nm. Network was created through ConsensusPathDB gene analysis software. A total of 496 genes were queried and the following associations were made (119 genes; Z-score = 30): protein (orange), genetic (blue), and biochemical (green) interactions. Dotted lines represent a physical interaction, solid arrows show substrate/product interaction, and solid lines with a circle represent enzyme interaction. Colored boxes indicate fold change scaled to heat map colors (Figure 3-6b). Boxes in blue and purple represent predicted genes and proteins CPDB used to make associations.

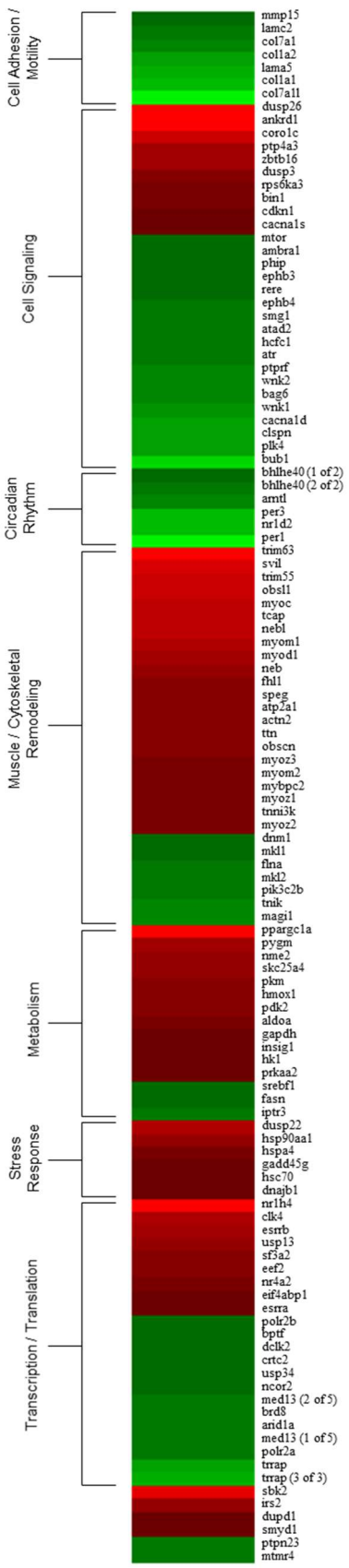

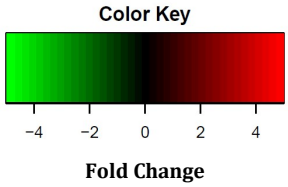

Figure 3-8B Continued. Heat map indicating fold change for the 119 genes observed within the 500-550 nm ConsensusPath network (Figure 3-6a). Up-modulated (red) and down-modulated (green) genes within the heat map were functionally categorized. Within the 500-550 nm region, genes were clustered into cell adhesion/motility (7 genes), cell signaling (28 genes), circadian rhythm (6 genes), muscle/cytoskeletal (29 genes), metabolism (15 genes), stress response (6 genes), and transcription/translation (22 genes). Additionally, 6 genes were uncategorized.

Discussion

DE Gene Induction at 350-400 nm and 500-550 nm Waveband Regions

Light has been documented to play an important role in circadian cycling and other various biological processes (e.g. metabolism, cytoskeletal, and detoxification) in mammalian systems (Albrecht et al., 1997; Akhtar et al., 2002) and, more recently, in fish skin (Walter et al., 2014; Boswell et al., 2015; Walter et al., 2015). However, while these previous reports dealt exclusively with ultraviolet wavelengths or broad-spectrum fluorescent lights, little is known on how specific wavelengths may affect transcriptional responses. As presented in Figure 3-2, the distribution of DE genes across wavelength regions between 300-600 nm is not uniform. In particular, the most robust transcriptional responses cluster around two waveband regions: 350-400 nm (UVA light) and 500-550 nm (green light). Interestingly, fish exposed to 400-450 nm (violet light) and 450-500 nm (blue light) wavelengths exhibited fewer genes modulated. The low genetic response exhibited in the violet-blue region is interesting considering that certain proteins undergo photoactivation via blue light (Mitani et al., 1996), such as photolyase and cryptochrome proteins. As previously discussed, photolyases are activated through the photoreduction of flavin for DNA repair (Li et al., 1991) while cryptochrome family proteins undergo a similar reaction to regulate the circadian cycle (Thompson and Sancar, 2002; Bouly et al., 2007). Considering a number of proteins are blue light responsive, the genetic response observed within these regions were surprising.

Use of all wavelengths by fish skin to regulate homeostasis may not be surprising given our evolution, but such clustering of transcriptional response is novel and unexpected. Since many proteins and cofactors have been documented to be light responsive and absorb violet-blue light, the clustering of transcriptional response outside of the violet-blue region (400 to 500 nm) in skin may suggest intracellular biomolecules and receptors specifically absorb violet-blue wavelengths to provide energy for cellular processes, while transcriptional activators are conscripted to the wavelength regions shown here (350-400 and 500-550 nm) for gene regulation. Although it is unclear what mechanisms and intracellular receptors might absorb specifically in the transcriptional hotspots at 350-400 or 500-550 nm and what mechanism(s) might be involved to produce the observed modulated gene expression, this presents an interesting avenue for future study.

Shared Genetic Response at Both 350-400 nm and 500-550 nm Regions

Ingenuity IPA was employed to identify canonical pathways modulated at both wavelength regions (Figure 3-6). Exposure to both 300-350 and 500-550 nm wavebands affected several common signaling pathways (e.g. calcium, eNOS, and actin cytoskeleton signaling) similarly, but apparently through different gene sets (Table 3-1 and 3-3). In Figure 3-9 the pathway diagrams show DE genes in calcium signaling at both 350-400 and 500-550 nm. Calcium signaling plays key roles in regulation of various biological process (e.g. transcription, cellular proliferation, cell motility, etc.; for review, see Clapham, 2007). However, it has

been reported that accumulation of reactive oxygen species (ROS) serves to enhance calcium signaling causing an influx of calcium and disrupting calcium pump regulators (Graier et al., 1998; Ermak and Davies, 2001). Furthermore, calcium signaling may inhibit nitric oxide production and lead to a suppression of the inflammatory response (Korhonen et al., 2001). This notion is supported by the down-regulation of endothelial nitric oxide synthase (eNOS) signaling observed at both wavelength regions (Figure 3-10).

Additionally, actin cytoskeleton signaling is up-regulated in response to 350-400 and 500-550 nm wavebands (Figure 3-11). This is accompanied by a set of 10 shared genes involved in muscle/cytoskeleton that exhibited an overall up-modulation (8 of 10 genes; Figure 3-5C). Furthermore, GO clustering of genes related to muscle/cytoskeleton remodeling was also observed to be up-modulated at both wavelength regions (350-400 nm: 9 of 11 genes, Table 3-2; 500-550 nm: 40 of 50 genes, Table 3-4). It has been documented that cellular stress and damage, particularly oxidative damage, may induce cytoskeletal remodeling and reorganization of endothelial and skin cells in mammals (Paladini et al., 1996; Houle et al., 2003). Altogether, the changes observed within these signaling pathways indicate the skin is undergoing cellular stress when exposed to either 350-400 nm or 500-550 nm light.

Among the shared genetic response, genes encoding proteins involved in oxidation of lipids were observed modulated in skin following 350-400 and 500-550 nm exposures. Although only 8 genes involved in metabolism were shared between both peak regions (Figure 3-5C), independent functional analyses of

both regions clustered more DE genes into this category (350-400 nm: 13 genes, Table 3-2; 500-550 nm: 9 genes, Table 3-4). An overall up-modulation of lipid metabolism was observed at both waveband regions. While fatty acids and lipids are essential to maintaining various cellular components (e.g. cellular membrane and energy storage; Spector and Yorek, 1985), increased oxidative degradation of fatty acids to free fatty acids is associated with cellular stress by ROS generation (Dias et al., 2013). Oxidation of fatty acids utilizes the electron transfer flavoprotein quinone oxidoreductase (ETF-QOR) in the matrix of the mitochondria within complex I of the electron transfer chain, which can generate ROS (St Pierre et al., 2002). The overall up-modulation of lipid metabolic genes (350-400 nm: 11 of 13 genes, Table 3-2; 500-550 nm: 7 of 9 genes, Table 3-4) suggests the increased lipid metabolism may be contributing to the cellular stress response in fish skin.

Modulation of Cell Cycle Regulators, *atm* and *atr*, at Both 350-400 nm and 500-550 nm Regions

As previously mentioned, circadian rhythm pathway regulates cell cycle control and response to DNA damage (Hunt and Sassone-Corsi, 2007; Sancar et al., 2010). CPDB identified two main nodes (one at each wavelength region) involved in cell signaling, *atm* (at 350-400 nm; Figure 3-7) and *atr* (at 500-550; Figure 3-8a). Both ataxia telangiectasia mutated (ATM) and ataxia telangiectasia and Rad3-related protein (ATR) respond to cellular stress and damage by initiating a cascade of events to either repair damaged DNA or initiate apoptosis

(for reviews, see Tibbetts et al., 1999; Abraham, 2001; Liu et al., 2007; Malewicz and Perlmann, 2014). While an up-regulation of *atm* and *atr* are usually observed to initiate these events, transcriptional activation of *atm* and *atr* may have occurred rapidly after light exposure, followed by down-modulation of the *atm* and *atr* transcription factors during the 6-hour post-exposure period. Future experiments are needed to assess the time course of gene regulation following exposure to specific wavelengths of light.

Examination of the genes around the *atm* and *atr* cluster (Figure 3-7 and Figure 3-8, respectively) confirm the results observed in the Ingenuity IPA analyses. Genes clustered around *atm* at the 350-400 nm region exhibited an overall up-modulation (11 of 16 genes) while genes around *atr* at the 500-550 nm region showed more down-modulation (18 of 28 genes). The cellular stress response observed at both peak wavelength regions suggest 350-400 nm and 500-550 nm light may be inducing cellular damage. However, cell proliferation appears to be occurring after exposure to 350-400 nm light while it is suppressed in 500-550 nm light.

Genetic Response after Exposure to 350-400 nm Light

Gene ontology analyses revealed differentially expressed genes were associated with circadian rhythm, transport, cell differentiation, metabolism, muscle/cytoskeleton remodeling, and stress response at the 350-400 nm region (Table 3-2). While genes related to transport represent a large number of DE genes (30 genes), this broad GO term encompass a wide array of overlapping

cellular function. Thus, for the purpose of discussion, we focus on the other major GO clusters and canonical pathways.

Besides the shared pathways previously discussed (e.g. calcium, eNOS, and actin cytoskeleton signaling), one other pathway was identified in Ingenuity IPA at the 350-400 nm region (Figure 3-6). Five genes (*map2k6*, *hmox1*, *mgst1*, *cdc34*, and *atm*; Table 3-1) were clustered into the NRF2-mediated oxidative stress response pathway. NRF2 is an antioxidant transcriptional protein that regulates the gene expression of detoxification enzymes and antioxidant stress proteins (Ishii et al., 2000; Nguyen et al., 2009). Furthermore, genes related to stress were differentially expressed according to gene ontology (Table 3-2). In particular, GO identified 2 smaller clusters, response to oxidative stress (15 genes) and hydrogen peroxide metabolic process (6 genes). The up-modulation of these clusters (13 of 17 genes) suggests cells may be reacting to oxidative stress following exposure to 350-400 nm UVA light. The canonical pathways and GO categories presented that are affected by exposure to 350-400 nm light are indicative of a cellular stress response. Despite the stress, cells may be undergoing following exposure to 350-400 nm light, our data does not suggest apoptotic or suppression of cellular progression. In fact, genes related to tissue development, epithelium development, and cell proliferation were identified in the 350-400 nm region. Among the 169 genes assigned with human homolog ID's, 47 genes were found to encode proteins involved in cell differentiation (*six3*, *cyp1a1*, *rab25*, *wnt5a*, *atm*, *col11a1*, *pdgfc*, *nr4a3*, *tpm1*, *scel*, *anxa1*, etc.; Table 3-2). Most (36 of 47) of the genes within this cluster were up-modulated,

suggesting promotion of cell proliferation. Our results are consistent with previous reports that have shown non-lethal UVA exposure can promote cellular survival (He et al., 2008). Thus, the dose of UVA used here for fish skin exposures (10 kJ/m^2) may be enough to elicit a stress response, but not enough to induce apoptosis.

It is well known that exposure to UVA (defined as 320-400 nm; Maverakis et al., 2010) produces ROS upon absorption by intracellular photosensitizers (Kielbassa et al., 1997; Wood et al., 2006). The increase in ROS generation and oxidative stress in the cell can induce DNA damage, leading to apoptosis (Simon et al., 2000; Lesser et al., 2001; Apel and Hirt, 2004). Therefore, stress induced by UVA exposure in production of ROS may explain the uptick in expression of genes associated with cellular reorganization. However, from the pattern of DE genes affected, we speculate that the dose used in the 350-400 nm exposure is not adequate to induce apoptosis.

Genetic Response after Exposure to 500-550 nm Light

Different canonical pathways are observed at 500-550 nm (e.g. ILK signaling, AMPK signaling, aldosterone signaling, etc.; Table 3-3) compared to the 300-350 waveband exposure. Integrin-linked kinase (ILK) signaling was observed up-modulated according to Ingenuity IPA (Table 3-3). Overexpression of ILK has been shown to induce actin cytoskeletal rearrangement in chicken embryo fibroblast cells (Qian et al., 2005). As previously discussed, reorganization of the cytoskeleton can be associated with cellular stress and

damage. This notion is supported by an overall up-modulation of cytoskeletal genes clustered in the CPDB network (22 of 29 genes; Figure 3-8). Coupled with the up-modulated actin cytoskeleton signaling pathway (Figure 3-11) and the overlap of genes involved in both pathways, this suggests 500-550 nm light induces ILK signaling within the skin to remodel the actin cytoskeleton in response to cellular stress.

One of the other pathways up-modulated by 500-550 nm light involves AMPK signaling (Table 3-3). Adenosine monophosphate-activated protein kinase (AMPK) signaling is slightly up-regulated following exposure to 500-550 nm light. The AMPK protein complex regulates metabolic processes and cellular proliferation in adaptation to stress (Bungard et al., 2010) and has been shown able to induce cell cycle arrest through interactions with p53 and glucose depletion (Jones et al., 2005). This is also observed in our data set by the up-modulation of glucose metabolic process cluster (*gpi*, *pkm*, *pgam2*, *aldoa*, *gapdh*, and *pfkm*; Table 3-4). Carbohydrate metabolism plays a critical role in resistance to oxidative stress by providing cellular energy to maintain active defense (Thorpe et al., 2004). The increase in glucose metabolism may be the result of AMPK signaling in response to cellular stress and the beginning of cell cycle arrest.

Additionally, after 500-550 nm exposure, a down-regulation of the aldosterone signaling in epithelial cells (13 genes) is observed (Table 3-3). Aldosterone stimulates fibroblast proliferation through the activation of cellular growth cascades, such as MAPK1/2 (Stockand and Meszaros, 2002). The down-

regulation of the aldosterone signaling suggests a suppression of cell proliferation. Among the 13 genes within this cluster, 9 heat shock stress related genes are up-modulated (*hspa8*, *hspa4*, *dnajb4*, *hspa1a/hspa1b*, *hspb8*, *hspa6*, *hsp90aa1*, *hspb7*, and *dnajb5*). Furthermore, these genes were also identified by GO in 2 other clusters; response to heat (16 genes) and response to oxidative stress (21 genes), exhibiting an up-regulation in both (12 of 16 genes and 16 of 21 genes, respectively) (Table 3-4). This set of genes supports the contention that 500-550 nm light initiates a cell based stress response in *Xiphophorus* skin (Santoro, 2000).

Aside from the various pathways modulated by 500-550 nm wavebands, gene ontology identified several other clusters that support our speculations (e.g. oxidation-reduction process and cell death). Forty-nine genes associated with oxidation-reduction (redox) processes were observed modulated following exposure to 500-550 nm light (Table 3-4). This process involves the transfer of electrons and is vital to various biological processes, such as cell growth signaling and metabolism (Moldovan and Moldovan, 2004). However, these reactions can lead to the formation of ROS as a byproduct (Kohen and Nyska, 2002; Spitz et al., 2004). We observed an overall up-modulation of genes associated with redox process (37 of 47 genes). Examination of these genes reveal many within the cluster are involved with lipid (*apoa4*, *nr4a3*, *prkaa2*, *abcc8*, *me1*, *fasn*, *cyp2w1*, *cyp1a1*, *cyp1a2*, and *cpt1b*) and glucose metabolism (*gys2*, *pygm*, *pgam2*, *gpd*, *pkm*, *pfkfb1*, *pfkm*, aldoa, *gapdh*, *gpi*, *hk1*, *ppp1r3a*,

and *ldhb*) that suggest genes within this cluster is contributing to the cellular stress response observed at the 500-550 nm region.

In addition to the implication of cellular stress at 500-550 nm region, 2 large clusters of DE genes involved in cell differentiation (134 genes) and cell death (69 genes) were identified (Table 3-4). Although there was not an apparent down-modulation of the cell differentiation cluster (50 of 134 genes down-modulated), many of the genes found within this cluster were also found within the muscle/cytoskeleton clusters (33 up-modulated genes). Since we observe an active actin cytoskeleton remodeling, the overlapping up-modulated cell differentiation genes could be due to the reorganization of the cytoskeleton. Furthermore, we observe an up-modulation of genes related to cell death (47 of 69 genes). Thus, stress induced by 500-550 nm exposure may be suppressing cell proliferation in the *Xiphophorus* skin, in contrast to 350-400 nm exposure where we found up-regulated DE genes involved with promotion of cell proliferation.

Conclusions

Collectively, these data show fish skin exposed to 350-400 and 500-550 nm exhibited the highest transcriptional response among 50 nm waveband exposures between 300 to 600 nm. Within these two peak regions, skin cells may be undergoing light induced cellular stress that has similarities and differences between these two wavebands. Exposure to both wavebands showed various metabolic signaling cascades affected (e.g. calcium signaling,

eNOS signaling, AMPK signaling, and glycolysis). The genetic effects induced by either wavelength region suggest a cell based stress response that includes cytoskeletal remodeling and lipid oxidation. Our observation that cellular proliferation appears to be unaffected following 350-400 nm exposure is consistent with previous reports (He et al., 2008). However, exposure to 500-550 nm caused the suppression of many genes associated with cell proliferation. A recent report involving differential gene expression in *Xiphophorus* skin exposed to “cool white” fluorescent lights showed a robust suppression of mitotic progression (Walter et al., 2015). The cellular stress response observed within the 500-550 nm region may contribute to the cell cycle suppression induced by fluorescent lights. Nonetheless, exposure to fluorescent light encompasses more than one waveband region. Based on the results presented herein, cell cycle genes modulated by fluorescent light are likely due to high radiance of longer wavelengths emitted by fluorescent lights (500 nm and above; Figure 1-5). Further experimentation would be needed to confirm this speculation and to assess the effects of fluorescent light wavelengths above 600 nm.

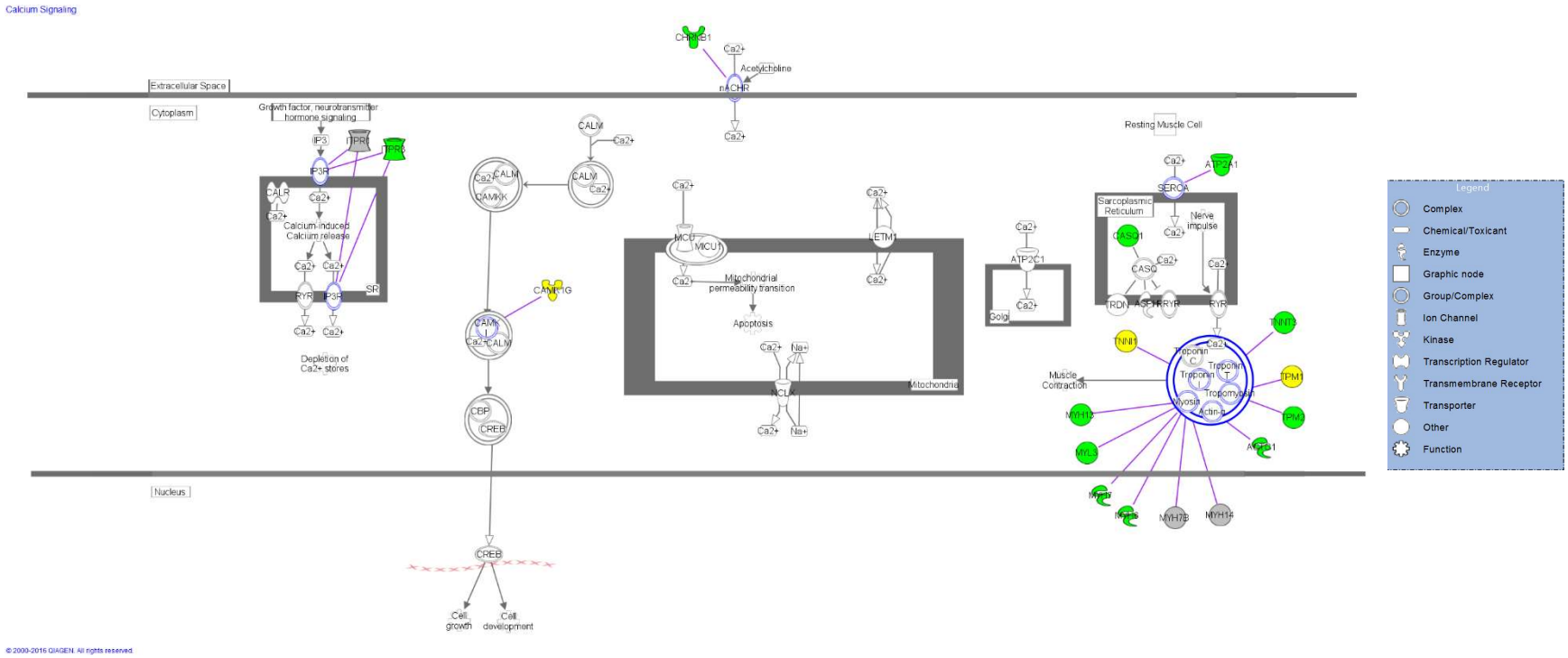

Figure 3-9. Representation of the calcium signaling pathway generated by Ingenuity IPA. Pathway contains genes that were DE following exposure to 350-400 nm (grey) or 500-550 nm (green) wavelengths. Genes DE in both data sets are colored yellow. Blue outlined symbols represent complexes that were affected and the genes affecting the complex are connected by purple lines. Displayed on the right is a legend for the various symbols. Solid lines symbolize direct interactions and dashed lines symbolize indirect interactions. Solid arrows represent activation/causation while white arrows represent translocation. Lines with perpendicular end represent inhibition.

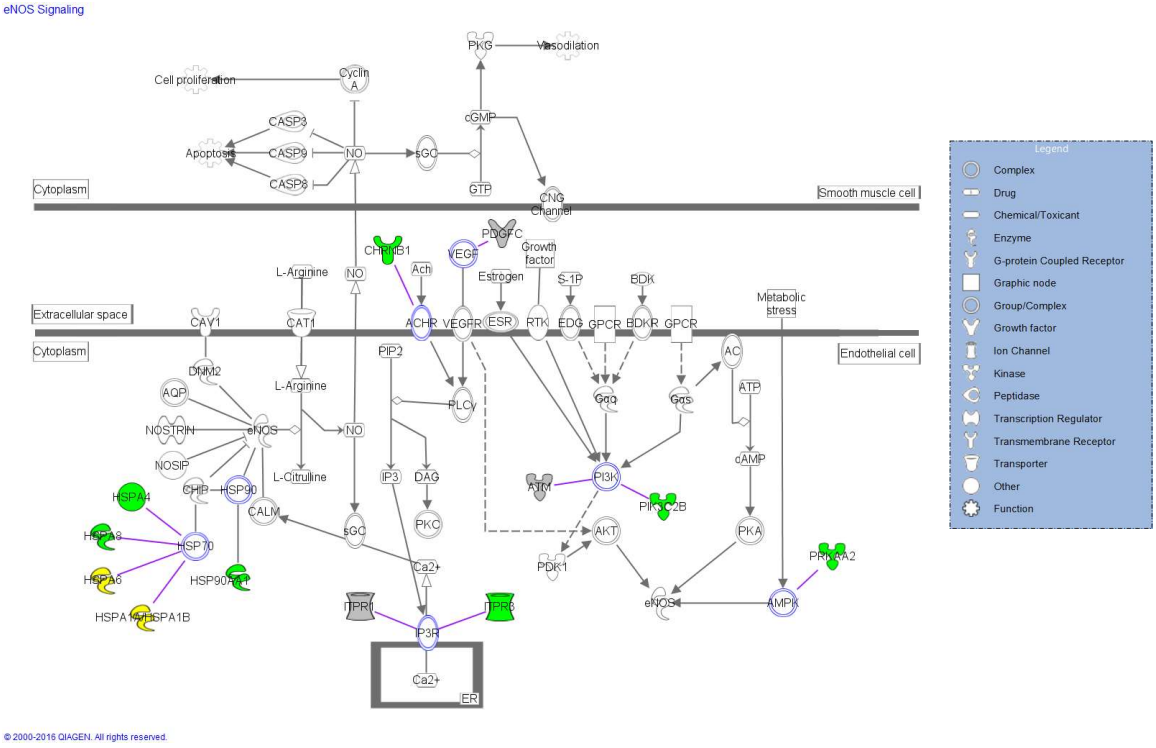

Figure 3-10. Representation of the eNOS signaling pathway generated by Ingenuity IPA. Pathway contains genes that were DE following exposure to 350-400 nm (grey) or 500-550 nm (green) wavelengths. Genes DE in both data sets are colored yellow. Blue outlined symbols represent complexes that were affected and the genes affecting the complex are connected by purple lines. Displayed on the right is a legend for the various symbols. Solid lines symbolize direct interactions and dashed lines symbolize indirect interactions. Solid arrows represent activation/causation while white arrows represent translocation. Lines with perpendicular end represent inhibition and lines with diamonds signify enzyme catalysis.

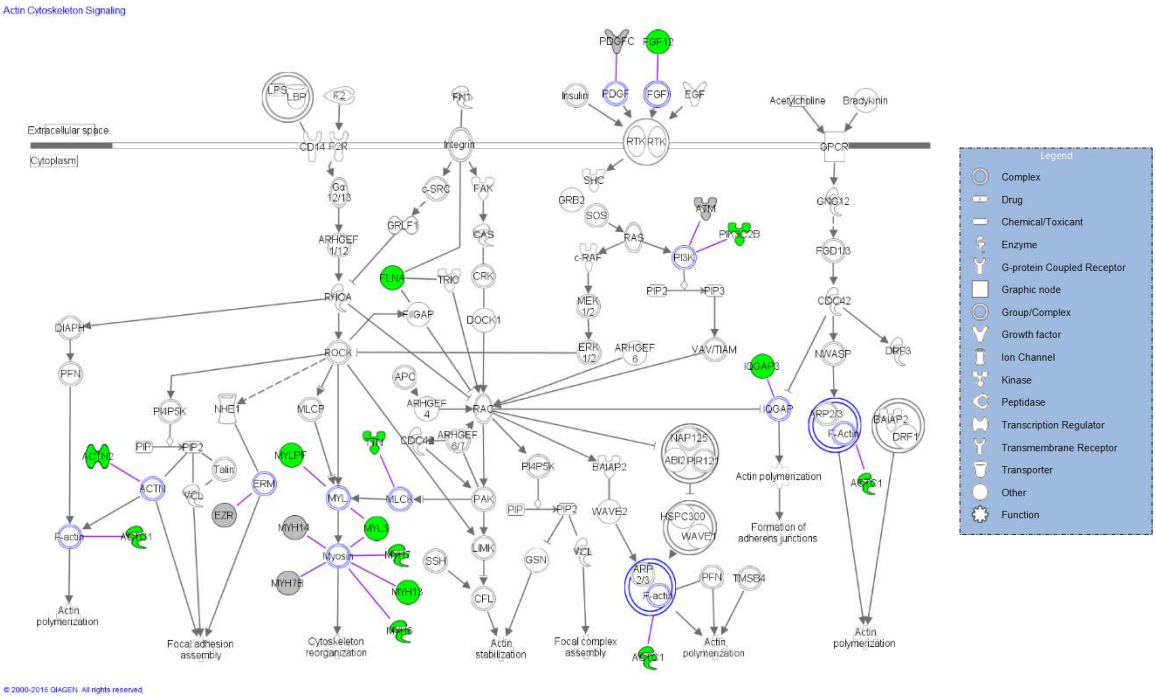

Figure 3-11. Representation of the actin cytoskeleton signaling pathway generated by Ingenuity IPA. Pathway contains genes that were DE following exposure to 350-400 nm (grey) or 500-550 nm (green) wavelengths. Blue outlined symbols represent complexes that were affected and the genes affecting the complex are connected by purple lines. Displayed on the right is a legend for the various symbols. Solid lines symbolize direct interactions and dashed lines symbolize indirect interactions. Solid arrows represent activation/causation while white arrows represent translocation. Lines with perpendicular end represent inhibition and lines with diamonds signify enzyme catalysis. Lines containing both a perpendicular line and arrow head represents inhibition and act on.

IV. GENETIC RESPONSE OF FEMALE *XIPHOPHORUS* SKIN TO VARYING WAVELENGTHS OF LIGHT

Introduction

As stated previously, the incidence of human melanoma has increased over the last 40 years and shows a higher frequency in males than females (Reed et al., 2012). This trend is also present in the *Xiphophorus* interspecies hybrids, particularly in the F_1 hybrids of the Gordon-Kosswig cross (*X. maculatus* Jp 163 A × *X. hellerii*). Siciliano et al. (1971) observed a significant difference in the percentage of males and females with melanoma, 85.2% versus 53.2%, respectively. With the recent advancement of genomic sequencing and bioinformatics, the difference between male and females became apparent at a molecular genetic level. Over 2,250 genes are differentially expressed between male and female *Xiphophorus maculatus* Jp 163 A at basal expression (Zhang et al., 2011). Furthermore, a sex specific response to UVB (311 nm) light has been documented and each sex showed induction of different pathways, such as *ucp3* and AMPK signaling in males but not females (Boswell et al., 2015). Thus, it is of interest to determine how the genetic response of females exposed to specific wavebands of light for comparison with that of similarly exposed males.

To determine the global genetic effect of females in response to varying wavebands of light, female *X. maculatus* Jp 163 B were exposed to the same six 50 nm waveband regions previously conducted in male *Xiphophorus* (Chapter 3). RNA-Seq and bioinformatic tools were employed to analyze the transcriptional

response following exposures. Overall, we observed a greater transcriptional response in longer wavelengths compared shorter wavelengths (within the ultraviolet region). Female fish skin exhibited two different genetic responses between the UV and visible light region. Exposure to either wavelength region elicited an upregulated response in genes associated with cellular stress and corresponding suppression of inflammatory response genes. However, the downstream effects of stress upon exposure to each waveband region differed in its effects on the cell proliferation and cell signaling pathways.

Results

Distribution of Differentially Expressed Genes in Females to Varying Wavebands

To determine the number of differentially expressed genes, two replicate biological samples from each waveband exposed fish skin were compared to 8 control fish that were not exposed to light. DE genes were identified across the same six 50 nm wavebands as were utilized in the male analyses (Chapter 3). The distribution of DE genes across the 300-600 nm region showed higher numbers of DE genes in wavebands above 400 nm compared to shorter wavelengths (300-400 nm) (Figure 4-1). Differential transcriptional response in the visible light region appeared to peak at 400-450 nm. Female skin exposed to 400-450 nm light showed 343 DE genes, of which 34% (117 genes) were up-modulated and 66% (226 genes) were down-modulated while fish skin exposed to UV wavebands (i.e. 300-350 and 350-400 nm) exhibited substantially lower numbers of DE genes (151 and 113 genes, respectively). We found 48.3% (73

genes) of the DE genes in the 300-350 nm region were up-modulated and 51.7% (78 genes) were down-modulated. Overall, more genes were observed down-modulated than up-modulated, across all six 50 nm regions (Figure 4-1).

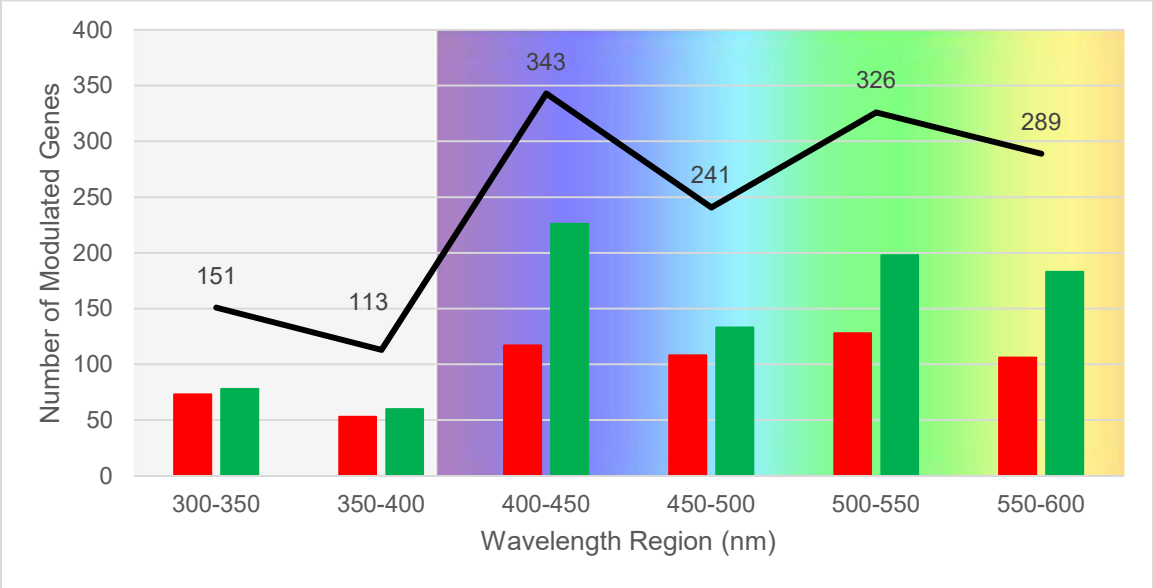

Figure 4-1. Distribution of DE genes in female *X. maculatus* Jp 163 B in response to 50 nm wavebands. Bar and line graphs represent the number of DE genes that were ± 2-fold (*p*-adj ≤ 0.05). The black line represents the total number of DE genes, including u*p*-modulated genes (red bars) and down-modulated genes (green bars).

Circadian Gene Expression in Females Over Six Waveband Regions

Examination of genes known to be involved with circadian cycling validate that female fish skin responds to light similarly to what has been established in the literature. Four light responsive circadian genes were identified to be differentially modulated in at least one of the six waveband regions (*cry1ab*, *nr1d2a* [also termed *rev-erb-β1*], *per1b*, and *per3*) (Figure 4-2). All 4 genes exhibited a down-modulation. While *cry1ab* was consistently 2-fold down-

modulated, the expression trend of both period genes (*per1b* and *per3*) was similar (Figure 4-2). The observed expression patterns of these circadian genes were consistent in magnitude and direction with previous light reports (Yang et al., 2014; Walter et al., 2015).

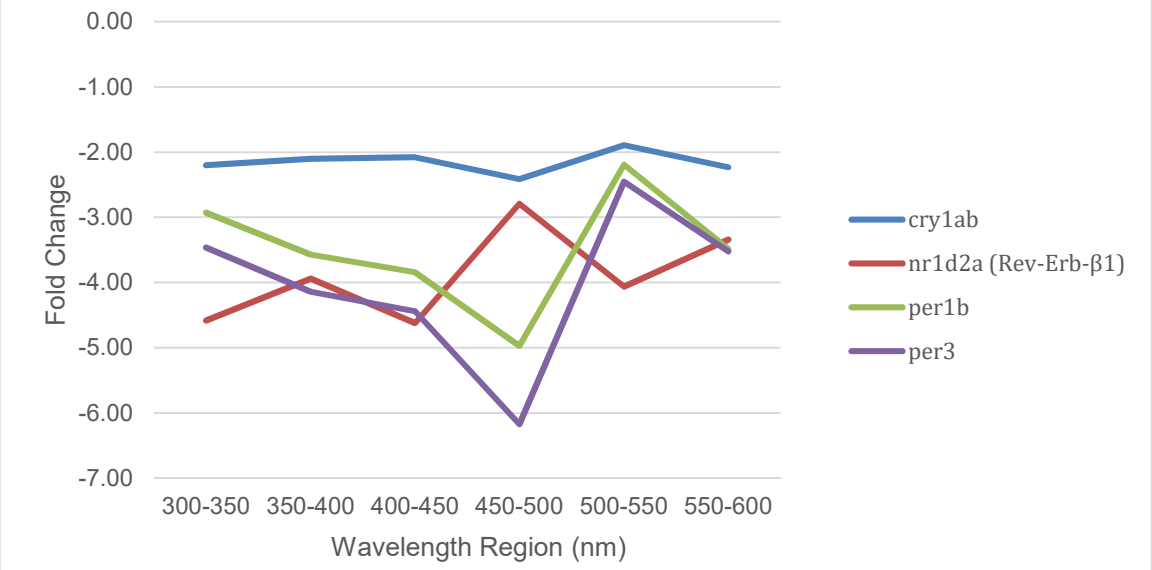

Figure 4-2. Light responsive circadian rhythm gene expressions when exposed to various waveband regions of light. Depicted is a line graph representation of circadian rhythm genes with a ± 2-fold (*p*-adj ≤ 0.05) in at least one wavelength region in adult female *X. maculatus* skin.

Shared Response between 300-350 and 400-450 nm Waveband Regions

Figure 4-1 shows exposure of female fish skin to different wavebands of light induces varied genetic responses, particularly between the UV region and the visible region. To further determine the differences and similarities between the waveband regions, DE genes from each 50 nm waveband region were compared to all other wavebands (Figure 4-3). Larger fractions of genes were shared between wavebands in the same wavelength regions (i.e. UV region or

visible region) than between different regions. For example, 41.1% of the DE genes found in the 300-350 nm region (62 genes) were shared with the 350-400 nm region while only 22.7% of the DE genes in the 400-450 nm region (78 genes) were shared with the 350-400 nm region (Figure 4-3A). Comparison of the waveband regions (e.g. 450-500 and 550-600 nm) adjacent to 500-550 nm region exhibited a similar fraction of shared DE genes. For example, 58.5% of the DE genes in the 450-500 nm region (141 genes) were shared with the 500-550 nm region and 56.1% of the DE genes in the 550-600 nm region (162 genes) were shared with the 500-550 nm region (Figure 4-3B). Comparison of DE genes from the visible light regions (400-450 nm, 450-500 nm, 500-550 nm, and 550-550 nm) is shown in Figure 4-3C.

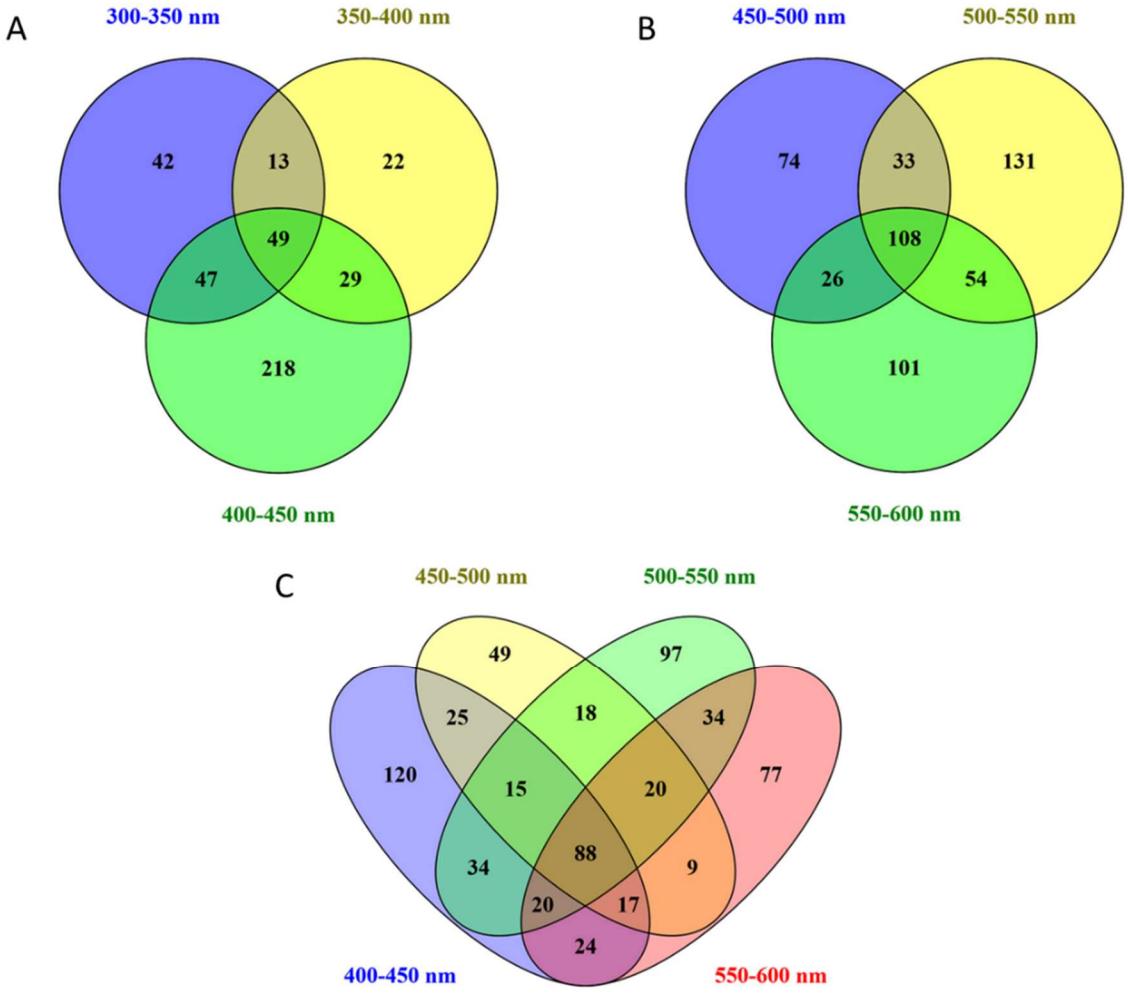

Figure 4-3. Comparison of differentially expressed genes between different wavelength regions from 300-600 nm based on RNA-Seq analysis. Multi-Venn diagram of DE genes between (A) 300-450 nm, (B) 450-600 nm, and (C) 400-600 nm wavelength regions were generated using Venny 2.1. Figure 4-3C represents comparison of the 4 most transcriptionally active 50 nm regions observed in the female exposures.

To include a representation of both UV and visible light region, as presented in the male exposure analyses, we selected the most transcriptionally active wavebands from each region, 300-350 nm (UVB) and 400-450 nm (blue light). Differentially expressed genes from these 2 regions were compared for shared and unique responses. A total of 96 genes were found shared between both wavelength regions with 40 genes up-modulated (41.7%) and 56 genes down-modulated (58.3%). Each shared gene exhibited similar gene up- or down-modulation between the 300-350 and 400-450 nm wavelength regions (Figure 4-4). Among the 96 genes, 71 genes were able to be assigned human homolog gene ID's. GO analyses of the shared genes clustered 43 of these 71 unique genes into 8 GO categories: circadian rhythm (7 genes, *p*-value = 1.05e-05), cell differentiation (21 genes, *p*-value = 2.42e-02), regulation of homeostatic process (5 genes, *p*-value = 1.22e-02), lipid metabolic process (9 genes, *p*-value = 4.91e-02), inflammatory response (7 genes, *p*-value = 8.02e-03), regulation of signaling (18 genes, *p*-value = 1.51e-02), response to hypoxia (5 genes, *p*-value = 3.44e-03), regulation of response to stress (12 genes, *p*-value = 5.13e-03), and response to external stimulus (18 genes, *p*-value = 3.96e-03) (Table 4-1). The remaining 28 genes did not readily cluster by GO term.

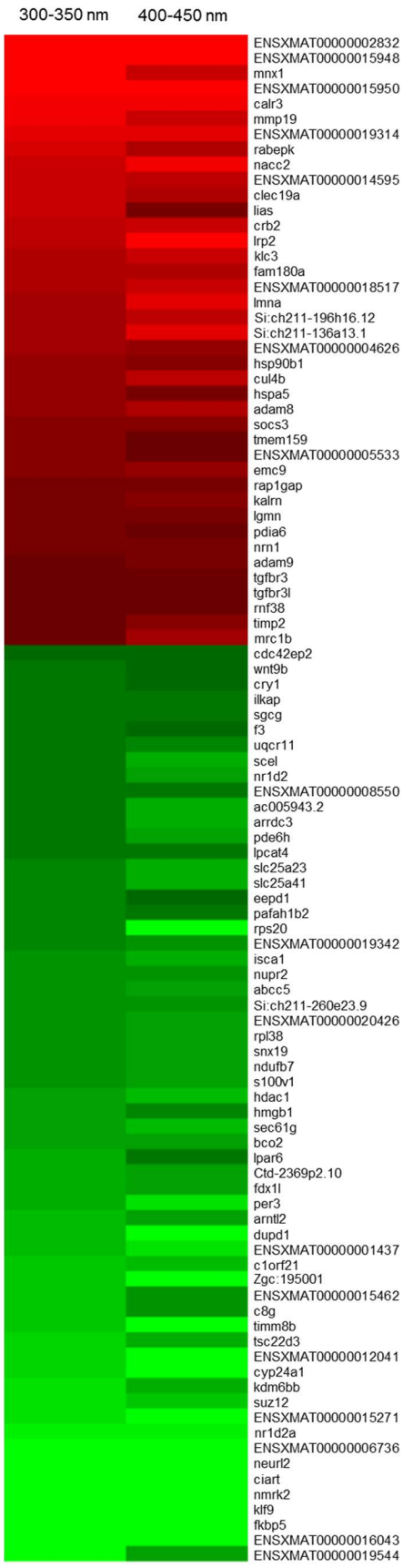

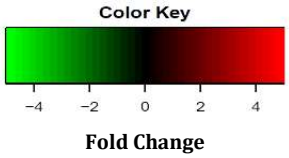

Figure 4-4. Shared DE genes between 300-350 and 400-450 nm light. Heat map indicating fold change for the 96 genes shared. U*p*-modulated (red) and down-modulated (green) genes within the heat map were sorted based on fold change expression in the 300-350 nm region. GO characterization of shared genes can be found in Table 4-1.

Table 4-1. GO terms and *p*-values (cutoff *p*-value ≤ 0.05) of genes shared between 300-350 and 400-450 nm wavelength regions using Ingenuity IPA. Among the 96 *Xiphophorus* transcript ID's, 71 were converted to human homolog ID's. Listed are 43 genes clustered into 9 GO categories: circadian rhythm (7 gene, *p*-value = 1.05e-05), cell differentiation (21 genes, *p*-value = 2.42e-02), regulation of homeostatic process (5 genes, *p*-value = 1.22e-02), lipid metabolic process (9 genes, *p*-value = 4.91e-02), inflammatory response (7 genes, *p*-value = 8.02e-03), regulation of signaling (18 genes, *p*-value = 1.51e-02), response to hypoxia (5 genes, *p*-value = 3.44e-03), regulation of response to stress (12 genes, *p*-value = 5.13e-03), and response to external stimulus (18 genes, *p*-value = 3.96e-03). GO ID for each GO term (GOBPID) and the number of DE genes (count) that fall within each cluster are presented. Up-modulated genes are presented red while down-modulated genes are in green. Genes of similar functions were grouped as shown on the right. Genes listed may overlap into different pathways due to multiple gene functions.

	GOBPID	*p*-value	Count	Term	Gene Name
Circadian Rhythm	GO:0007623	1.05E-05	7	Circadian Rhythm	cry1, ciart, hdac1, arntl2, klf9, per3, nr1d2
Cell Differentiation	GO:0030154	2.42E-02	21	Cell Differentiation	adam8, crb2, mnx1, lmna, mmp19, tgfbr3, timp2, adam9, kalrn, socs3, neurl2, cyp24a1, suz12, nmrk2, hdac1, hmgb1, snx19, sgcg, wnt9b, scel, nr1d2
Metabolism	GO:0032844	1.22E-02	5	Regulation of Homeostatic Process	adam8, tsc22d3, arrdc3, slc25a23, nr1d2
	GO:0006629	4.91E-02	9	Lipid Metabolic Process	lias, lgmn, fdx1l, cyp24a1, lpcat4, lrp2, pafah1b2, bco2, nr1d2
Immune Response	GO:0006954	8.02E-03	7	Inflammatory Response	adam8, lias, socs3, f3, hmgb1, c8g, nr1d2
Signaling	GO:0023051	1.51E-02	18	Regulation of Signaling	adam8, nacc2, crb2, hspa5, lmna, lgmn, rap1gap, tgfbr3, timp2, adam9, kalrn, socs3, cry1, f3, hdac1, hmgb1, pde6h, arrdc3
Stress	GO:0001666	3.44E-03	5	Response to Hypoxia	adam8, lmna, tgfbr3, hsp90b1, socs3
	GO:0080134	5.13E-03	12	Regulation of Response to Stress	adam8, nacc2, hspa5, lgmn, hsp90b1, socs3, cry1, f3, hmgb1, pafah1b2, c8g, nr1d2
	GO:0009605	3.96E-03	18	Response to External Stimulus	adam8, lias, mnx1, hspa5, lrp2, adam9, kalrn, socs3, cry1, cyp24a1, f3, hmgb1, pafah1b2, arntl2, c8g, wnt9b, bco2, nr1d2

Genetic Response in the 300-350 and 400-450 nm Waveband Regions

While the shared genetic response between the 300-350 and 400-450 nm regions revealed several functional gene ontology (GO) categories (e.g. circadian rhythm, cell differentiation, metabolism, etc.), we investigated whether exposure to specific wavebands elicited unique responses. Differentially expressed genes from both wavelength regions (300-350 nm and 400-450 nm) were independently assessed for pathway and functional characterization using Ingenuity IPA and gene ontology as previously described (Chapters 2 and 3).

Female fish exposed to 300-350 nm wavebands modulated 151 genes (Figure 4-1). Among the 151 *Xiphophorus* transcripts, 115 HUGO ID's were able to be assigned (76.2%). Ingenuity IPA and gene ontology (GO) clustered 64 genes (55.7%) into 4 canonical pathways and 9 GO categories (Table 4-2 and 4-3). Pathway clusters include circadian rhythm signaling (2 genes, *p*-value = 1.22e-02), endoplasmic reticulum stress response (3 genes, *p*-value = 1.59e-04), glucocorticoid receptor response (7 genes, *p*-value = 5.19e-04), and acute phase response (4 genes, *p*-value = 1.10e-02) (Table 4-2). GO identified 9 categories: circadian rhythm (7 genes, *p*-value = 2.04e-04), tissue development (25 genes, *p*-value = 2.39e-05), cell differentiation (35 genes, *p*-value = 1.65e-03), regulation of apoptotic process (15 genes, *p*-value = 1.65e-02), inflammatory response (11 genes, *p*-value = 1.04e-03), muscle structure development (12 genes, *p*-value = 1.32e-04), actin cytoskeleton organization (7 genes, *p*-value = 3.96e-02), response to stress (36 genes, *p*-value = 2.70e-03), and regulation of external stimulus (33 genes, *p*-value = 2.94e-03) (Table 4-3). The remaining 51 genes did

not readily cluster in a pathway or category. Small gene clusters with similar functions were grouped into broader categories, for example, *tissue development* and *cell differentiation* were grouped into cell proliferation. Also, GO clusters *muscle structure development* and *actin cytoskeleton organization* were grouped into muscle/cytoskeleton remodeling.

Table 4-2. Canonical pathways and *p*-values (cutoff *p*-value ≤ 0.05) of genes clustered at 300-350 nm using Ingenuity IPA. Name of the pathway and the number of DE genes (count) that fall within each pathway are presented: circadian rhythm signaling (2 genes, *p*-value = 1.22e-02), endoplasmic reticulum stress response (3 genes, *p*-value = 1.59e-04), glucocorticoid receptor response (7 genes, *p*-value = 5.19e-04), and acute phase response (4 genes, *p*-value = 1.10e-02). Z-score was determined by the Ingenuity software to represent the activation or inhibition of the pathway. Z-score of N/A represents the pathway was affected, but not in a particular direction. Gene names and their associated fold change expression are listed. Genes listed may overlap into different pathways due to multiple gene functions.

Canonical Pathway	***p*-value**	**Z-score**	**Count**	**Gene Name**
Circadian Rhythm Signaling	1.22E-02	N/A	2	cry1 (-2.20), per3 (-3.46)
Endoplasmic Reticulum Stress Response	1.59E-04	N/A	3	calr (2.02), hsp90b1 (2.94), hspa5 (2.85)
Glucocorticoid Receptor Response	5.19E-04	N/A	7	fkbp5 (-10.51), grb2 (2.11), hmgb1 (-2.98), hsp90aa1 (2.49), hsp90b1 (2.94), hspa5 (2.85), tsc22d3 (-4.01)
Acute Phase Response	1.10E-02	-1.00	4	apcs (-3.13), crp (-3.13), grb2 (2.11), socs3 (2.61)

Table 4-3. GO terms and *p*-values (cutoff *p*-value ≤ 0.05) of genes clustered at 300-350 nm using Gene Ontology. Among the 151 *Xiphophorus* transcripts ID's, 115 were converted to human homolog ID's. Listed are 63 genes that were clustered into 9 GO clusters: circadian rhythm (7 genes, *p*-value = 2.04e-04), tissue development (25 genes, *p*-value = 2.39e-05), cell differentiation (35 genes, *p*-value = 1.65e-03), regulation of apoptotic process (15 genes, *p*-value = 1.65e-02), inflammatory response (11 genes, *p*-value = 1.04e-03), muscle structure development (12 genes, *p*-value = 1.32e-04), actin cytoskeleton organization (7 genes, *p*-value = 3.96e-02), response to stress (36 genes, *p*-value = 2.70e-03), and regulation of external stimulus (33 genes, *p*-value = 2.94e-03). GO categories that were similar in gene set and function were grouped into a broader category shown on the left. GO ID for each GO term (GOBPID) and the number of DE genes (count) that fall within each cluster are presented. Gene names and fold change associated with a particular GO term are listed. Up-modulated genes are presented red while down-modulated genes are in green. Genes listed may overlap into different GO categories due to multiple functions.

	GOBPID	*p*-value	Count	Term	Gene Name
Circadian Rhythm	GO:0007623	2.04E-04	7	Circadian Rhythm	klf9 (-8.10), ciart (-6.34), arntl2 (-3.47), per3 (-3.46), hdac1 (-2.96), nr1d2 (-2.34), cry1 (-2.20)
Cell Proliferation	GO:0009888	2.39E-05	25	Tissue Development	stc1 (304.69), mnx1 (5.74), lias (3.78), crb2 (3.66), lmna (3.14), rpl24 (2.82), socs3 (2.61), adam9 (2.14), tgfbr3 (2.13), grb2 (2.11), ctsv (2.08), calr (2.02), klf5 (-17.04), tsc22d3 (-4.01), s100a4 (-3.82), csf1r (-3.13), adm (-3.04), hdac1 (-2.96), snx19 (-2.85), rpl38 (-2.85), arrdc3 (-2.36), nr1d2 (-2.34), scel (-2.31), sgcg (-2.22), wnt9b (-2.20)
	GO:0030154	1.65E-03	35	Cell Differentiation	stc1 (304.69), apoe (33.82), mnx1 (5.74), mmp19 (4.49), crb2 (3.66), lmna (3.14), rpl24 (2.82), adam8 (2.80), socs3 (2.61), hsp90aa1 (2.49), kalrn (2.38), adam9 (2.14), tgfbr3 (2.13), grb2 (2.11), ctsv (2.08), timp2 (2.08), calr (2.02), klf5 (-17.04), nmrk2 (-6.93), neurl2 (-6.12), suz12 (-4.32), cyp24a1 (-4.20), s100a4 (-3.82), s100a6 (-3.82), csf1r (-3.13), crp (-3.13), apcs (-3.13), adm (-3.04), hdac1 (-2.96), hmgb1 (-2.98), snx19 (-2.85), nr1d2 (-2.34), scel (-2.31), sgcg (-2.22), wnt9b (-2.20)
Apoptosis	GO:0042981	1.65E-02	15	Regulation of Apoptotic Process	apoe (33.82), nacc2 (3.92), lmna (3.14), hsp90b1 (2.94), hspa5 (2.85), adam8 (2.80), socs3 (2.61), lgmn (2.38), kalrn (2.38), calr (2.02), tsc22d3 (-4.01), adm (-3.04), hmgb1 (-2.98), hdac1 (-2.96), f3 (-2.27)
Immune Response	GO:0006954	1.04E-03	11	Inflammatory Response	apoe (33.82), lias (3.78), adam8 (2.80), socs3 (2.61), c8g (-3.94), crp (-3.13), csf1r (-3.13), apcs (-3.13), hmgb1 (-2.98), nr1d2 (-2.34), f3 (-2.27)

Table 4-3 Continued. GO terms and *p*-values (cutoff *p*-value ≤ 0.05) of genes clustered at 300-350 nm using Gene Ontology.

	GOBPID	*p*-value	Count	Term	Gene Name
Muscle / Cytoskeleton Remodeling	GO:0061061	1.32E-04	12	Muscle Structure Development	mnx1 (5.74), lmna (3.14), tgfbr3 (2.13), calr (2.02), klf5 (-17.04), nmrk2 (-6.93), neurl2 (-6.12), tsc22d3 (-4.01), csf1r (-3.13), adm (-3.04), nr1d2 (-2.34), sgcg (-2.22)
	GO:0030036	3.96E-02	7	Actin Cytoskeleton Organization	hsp90b1 (2.94), grb2 (2.11), ctsv (2.08), calr (2.02), neurl2 (-6.12), csf1r (-3.13), cdc42ep3 (-2.17)
Stress Response	GO:0006950	2.70E-03	36	Response to Stress	stc1 (304.69), apoe (33.82), nacc2 (3.92), lias (3.78), lmna (3.14), hsp90b1 (2.94), hspa5 (2.85), adam8 (2.80), socs3 (2.61), hsp90aa1 (2.49), lgmn (2.38), pdia5 (2.36), pdia6 (2.34), pdia4 (2.20), adam9 (2.14), tgfbr3 (2.13), grb2 (2.11), ctsl (2.08), ctsv (2.08), calr (2.02), tsc22d3 (-4.01), c8g (-3.94), crp (-3.13), csf1r (-3.13), apcs (-3.13), sec61g (-3.06), adm (-3.04), hmgb1 (-2.98), hdac1 (-2.96), pafah1b2 (-2.48), eepd1 (-2.46), nr1d2 (-2.34), f3 (-2.27), cry1 (-2.20), wnt9b (-2.20), c2orf40 (-2.18)
	GO:0048583	2.94E-03	33	Regulation of External Stimulus	apoe (33.82), nacc2 (3.92), crb2 (3.66), lmna (3.14), hsp90b1 (2.94), hspa5 (2.85), adam8 (2.80), socs3 (2.61), hsp90aa1 (2.49), rap1gap (2.42), lgmn (2.38), kalrn (2.38), adam9 (2.14), grb2 (2.11), ctsl (2.08), calr (2.02), guca1c (-11.31), c8g (-3.94), s100a4 (-3.82), csf1r (-3.13), apcs (-3.13), adm (-3.04), hmgb1 (-2.98), hdac1 (-2.96), pafah1b2 (-2.48), per3 (-3.46), pde6h (-2.38), arrdc3 (-2.36), nr1d2 (-2.34), f3 (-2.27), cry1 (-2.20), tgfbr3 (2.13), timp2 (2.08)

Female fishes exposed to 400-450 nm wavebands modulated 343 genes (Figure 4-1). Among the 343 DE genes, HUGO ID's were assigned to 301 genes (87.8%) and analyzed through the human genome database, resulting in clustering of 163 genes (54.2%) into 6 canonical pathways and 14 GO clusters (Table 4-4 and 4-5). Pathways include circadian rhythm (3 genes, *p*-value = 1.06e-02), calcium signaling (18 genes, *p*-value = 5.94e-11), eNOS signaling (5 genes, *p*-value = 4.80e-02), oxidative phosphorylation (11 genes, *p*-value = 3.46e-07), ILK signaling (9 genes, *p*-value = 1.15e-03), and acute phase response signaling (6 genes, *p*-value = 3.07e-02) (Table 4-4). Functional GO identified 14 categories: circadian rhythm (11 genes, *p*-value = 6.06e-04), epidermis development (20 genes, *p*-value = 2.22e-07), epithelial cell differentiation (18 genes, *p*-value = 9.23e-03), respiratory electron transport chain (10 genes, *p*-value = 3.69e-05), oxidation-reduction process (31 genes, *p*-value = 1.59e-03), nucleotide metabolic process (25 genes, *p*-value = 9.20e-05), regulation of defense response (22 genes, *p*-value = 8.52e-03), inflammatory response (17 genes, *p*-value = 2.89e-02), muscle cell differentiation (15 genes, *p*-value = 8.72e-04), cytoskeleton organization (26 genes, *p*-value = 2.64e-02), regulation of cell migration (16 genes, *p*-value = 3.98e-02), collagen metabolic process (9 genes, *p*-value = 1.57e-04), regulation of stress response (33 genes, *p*-value = 2.53e-02), and cellular response to external stimulus (16 genes, *p*-value = 1.14e-02) (Table 4-5). The remaining 138 genes did not readily cluster in a GO category. Additionally, GO categories with similar functions were grouped into a broader category. For example, *epidermis development* and epi*thelial cell*

differentiation were grouped into cell differentiation. GO categories *respiratory electron transport chain* and *oxidation-reduction process* were grouped into oxidation-reduction. *Regulation of defense response* and *inflammatory response* were grouped as immune response while *muscle cell differentiation* and *cytoskeleton organization* were grouped into muscle/cytoskeleton remodeling. Lastly, *regulation of cell migration* and *collagen metabolic process* were grouped into cell adhesion. Summary of canonical pathways (Tables 4-2 and 4-4) and GO clusters (Tables 4-3 and 4-5) at both 300-350 and 400-450 nm regions are presented in Figure 4-5.

Table 4-4. Canonical pathways and *p*-values (cutoff *p*-value ≤ 0.05) of genes clustered at 400-450 nm using Ingenuity IPA. Name of the pathway and the number of DE genes (count) that fall within each pathway are presented: circadian rhythm (3 genes, *p*-value = 1.06e-02), calcium signaling (18 genes, *p*-value = 5.94e-11), eNOS signaling (5 genes, *p*-value = 4.80e-02), oxidative phosphorylation (11 genes, *p*-value = 3.46e-07), ILK signaling (9 genes, *p*-value = 1.15e-03), and acute phase response signaling (6 genes, *p*-value = 3.07e-02). Z-score was determined by the Ingenuity software to represent the activation or inhibition of the pathway. Z-score of N/A represents the pathway was affected, but not in a particular direction. Gene names and their associated fold change expression are listed. Genes listed may overlap into different pathways due to multiple gene functions.

Canonical Pathway	***p*-value**	**Z-score**	**Count**	**Gene Name**
Circadian Rhythm	1.06E-02	N/A	3	cry1 (-2.08), per1 (-3.84), per3 (-4.44)
Calcium Signaling	5.94E-11	-1.63	18	atp2a1 (-6.30), casq2 (-3.54), chrna1 (-8.83), chrne (-4.53), hdac1 (-3.61), myh7 (-4.88), myh13 (-6.90), myl2 (-8.78), myl3 (-5.41), myl4 (-5.45), tnnc1 (-6.23), tnnc2 (-4.66), tnni2 (-4.71), tnnt1 (-3.80), tnnt3 (-3.72), tpm2 (-4.89), tpm3 (-6.90), trdn (-3.63)
eNOS Signaling	4.80E-02	-2.00	5	chrne (-4.53), hsp90b1 (2.51), hspa5 (2.34), lpar6 (-2.29), prkg1 (-6.71)
Oxidative Phosphorylation	3.46E-07	N/A	11	cox5b (-5.95), cox6a2 (-9.81), cox7a1 (-5.79), ndufa3 (-3.65), ndufa7 (-2.21), ndufb1 (-3.79), ndufb2 (-2.84), ndufb7 (-3.18), ndufv3 (-3.38), sdhb (-5.28), uqcr11 (-2.58)
ILK Signaling	1.15E-03	-1.00	9	fn1 (2.28), ilkap (-2.35), map2k4 (-2.07), myh7 (-4.88), myh13 (-6.90), myl2 (-8.78), myl3 (-5.41), myl4 (-5.45), ppp1r14b (2.04)
Acute Phase Response Signaling	3.07E-02	-1.34	6	apcs (-3.03), crabp2 (-2.21), crp (-3.03), fn1 (2.28), map2k4 (-2.07), socs3 (2.45)

Table 4-5. GO terms and *p*-values (cutoff *p*-value ≤ 0.05) of genes clustered at 400-450 nm using Gene Ontology. Among the 343 *Xiphophorus* transcripts ID's, 301 were converted to human homolog ID's. Listed are 146 genes that were clustered into 14 GO clusters: circadian rhythm (11 genes, *p*-value = 6.06e-04), epidermis development (20 genes, *p*-value = 2.22e-07), epithelial cell differentiation (18 genes, *p*-value = 9.23e-03), respiratory electron transport chain (10 genes, *p*-value = 3.69e-05), oxidation-reduction process (31 genes, *p*-value = 1.59e-03), nucleotide metabolic process (25 genes, *p*-value = 9.20e-05), regulation of defense response (22 genes, *p*-value = 8.52e-03), inflammatory response (17 genes, *p*-value = 2.89e-02), muscle cell differentiation (15 genes, *p*-value = 8.72e-04), cytoskeleton organization (26 genes, *p*-value = 2.64e-02), regulation of cell migration (16 genes, *p*-value = 3.98e-02), collagen metabolic process (9 genes, *p*-value = 1.57e-04), regulation of stress response (33 genes, *p*-value = 2.53e-02), and cellular response to external stimulus (16 genes, *p*-value = 1.14e-02). GO categories that were similar in gene set and function were grouped into a broader category shown on the left. GO ID for each GO term (GOBPID) and the number of DE genes (count) that fall within each cluster are presented. Gene names and fold change associated with a particular GO term are listed. Up-modulated genes are presented red while down-modulated genes are in green. Genes listed may overlap into different GO categories due to multiple functions.

	GOBPID	*p*-value	Count	Term	Gene Name
Circadian Rhythm	GO:0007623	6.06E-04	11	Circadian Rhythm	nlgn1 (2.95), six3 (-24.65), klf9 (-10.71), ciart (-8.60), nr1d2 (-4.62, -2.97), per3 (-4.44), per1 (-3.84), dbp (-3.72), hdac1 (-3.61), arntl2 (-3.02), cry1 (-2.08)
Cell Proliferation	GO:0008544	2.22E-07	9	Epidermis Development	adam9 (2.36), slc4a7 (-5.75), clic5 (-5.61), krt16 (-5.57), hdac1 (-3.61), tgm3 (-3.56), scel (-3.29), aldh3a2 (-3.02), crabp2 (-2.21)
	GO:0030855	9.23E-03	14	Epithelial Cell Differentiation	c1galt1 (5.26), fat4 (3.17), adam9 (2.36), col18a1 (2.10), eng (2.10), six3 (-24.65), slc4a7 (-5.75), clic5 (-5.61), hdac1 krt16 (-5.57), (-3.61), tgm3 (-3.56), scel (-3.29), gpat4 (-2.36), wnt9b (-2.12)
Oxidation-Reduction	GO:0022904	3.69E-05	10	Respiratory Electron Transport Chain	cox5b (-5.95), sdhb (-5.28), sco2 (-4.70), ndufb1 (-3.79), ndufa3 (-3.65), ndufv3 (-3.38), ndufb7 (-3.18), ndufb2 (-2.84), uqcr11 (-2.58), ndufa7 (-2.21)
	GO:0055114	1.59E-03	31	Oxidation-Reduction Process	nos1 (16.95), vat1 (2.10), abcc4 (-7.90), cyp24a1 (-7.50), cox5b (-5.95), gapdh (-5.76), gmpr (-5.31), sdhb (-5.28), pgam2 (-5.25), ldhb (-4.90), dhrs7c (-4.30), ppp1r3a (-4.71), sco2 (-4.70), ndufb2 (-2.84), ndufb1 (-3.79), ndufa3 (-3.65), tecr (-3.53), ndufv3 (-3.38), ugp2 (-3.35), slc25a23 (-3.28), cpt1b (-3.19), ndufb7 (-3.18), hsd11b2 (-3.11), aldh3a1 (-3.02), aldh3a2 (-3.02), bco2 (-2.97), fdx1l (-2.96), uqcr11 (-2.58), prodh (-2.29), ndufa7 (-2.21), mgst3 (-2.14)

Table 4-5 Continued. GO terms and *p*-values (cutoff *p*-value ≤ 0.05) of genes clustered at 400-450 nm using Gene Ontology.

	GOBPID	*p*-value	Count	Term	Gene Name
Metabolism	GO:0009117	9.20E-05	25	Nucleotide Metabolic Process	nos1 (16.95), entpd5 (3.50), oxer1 (3.28), slc25a23 (3.28), timp2 (2.58), htr4 (-13.17), nmrk2 (-6.14), gapdh (-5.76), gmpr (-5.31), pgam2 (-5.25), ldhb (-4.90), myh7 (-4.88), adssl1 (-4.76), dnm1l (-3.98), ndufb1 (-3.79), atpif1 (-3.76), ndufa3 (-3.65), ndufv3 (-3.38), ugp2 (-3.35), ndufb7 (-3.18), ndufb2 (-2.84), ak1 (-2.25), ndufa7 (-2.21), nt5c (-2.01), nt5m (-2.01)
Immune Response	GO:0031347	8.52E-03	22	Regulation of Defense Response	tlr5 (8.15), adam8 (3.46), polr3g (3.07), hsp90b1 (2.51), socs3 (2.45), lgmn (2.31), tnfaip6 (2.30), dhx58 (2.22), sbno2 (2.13), clec4e (2.02), clec4d (2.02), clec4a (2.02), clec4c (2.02), clec6a (2.02), cd209 (2.02), nr1d2 (-4.62, -2.97), per1 (-3.84), apcs (-3.03), c8g (-2.75), hmgb1 (-2.61), xiap (-2.12), map2k4 (-2.07)
	GO:0006954	2.89E-02	17	Inflammatory Response	tlr5 (8.15), adam8 (3.46), socs3 (2.45), lias (2.37), tnfaip6 (2.30), fn1 (2.28, 2.07), sbno2 (2.13), krt16 (-5.57), nr1d2 (-4.62, -2.97), per1 (-3.84), crp (-3.03), apcs (-3.03), aimp1 (-3.02), c8g (-2.75), hmgb1 (-2.61), xiap (-2.12), f3 (-2.00)
Muscle / Cytoskeleton Remodeling	GO:0042692	8.72E-04	15	Muscle Cell Differentiation	nos1 (16.95), lmna (4.33), myl2 (-8.78), rbm24 (-7.36), nmrk2 (-6.14), neurl2 (-5.80), krt16 (-5.57), klhl41 (-4.41), bin1 (-4.30), smyd1 (-4.02), lmod3 (-3.90), casq2 (-3.54), cxcl12 (-2.42), sgcg (-2.35), speg (-2.27)
	GO:0007010	2.64E-02	20	Cytoskeleton Organization	lmna (4.33), nlgn1 (2.95), hsp90b1 (2.51), fat1 (2.29), lrp1 (2.15), ccdc88a (2.05), trpv4 (2.04), myl2 (-8.78), prkg1 (-6.71), neurl2 (-5.80), gapdh (-5.76), krt16 (-5.57), klhl41 (-4.41), coro6 (-4.23), lmod3 (-3.90), trdn (-3.63), casq2 (-3.54), myoc (-2.57), cxcl12 (-2.42), cdc42ep3 (-2.04)
Cell Adhesion	GO:0030334	3.98E-02	16	Regulation of Cell Migration	lmna (4.33), has1 (4.01), adam8 (3.46), olfm1 (2.56), hspa5 (2.36), adam9 (2.36), fn1 (2.28, 2.07), ret (2.27), lrp1 (2.15), eng (2.10), col18a1 (2.10), krt16 (-5.57), hmgb1 (-2.61), myoc (-2.57), cxcl12 (-2.42), f3 (-2.00)
	GO:0032963	1.57E-04	9	Collagen Metabolic Process	mmp19 (3.80), col11a2 (3.19), mmp11 (3.06), col10a1 (2.79), adam9 (2.36), col4a5 (2.31), serpinh1 (2.23), col18a1 (2.10), col13a1 (-37.57)

Table 4-5 Continued. GO terms and *p*-values (cutoff *p*-value ≤ 0.05) of genes clustered at 400-450 nm using Gene Ontology.

	GOBPID	*p*-value	Count	Term	Gene Name
Stress Response	GO:0080134	2.53E-02	33	Regulation of Stress Response	tlr5 (8.15), nacc2 (4.50), adam8 (3.46), polr3g (3.07), hsp90b1 (2.51), socs3 (2.45), hspa5 (2.36), lgmn (2.31), tnfaip6 (2.30), dhx58 (2.22), wdfy3 (2.16), sbno2 (2.13), trpv4 (2.04), clec4m (2.02), clec4c (2.02), clec4e (2.02), clec4d (2.02), clec4a (2.02), clec6a (2.02), cd209 (2.02), f3 (2.02), prkg1 (-6.71), nr1d2 (-4.62, -2.97), dnm1l (-3.98), per1 (-3.84), apcs (-3.03), c8g (-2.75), hmgb1 (-2.61), cxcl12 (-2.42), pafah1b2 (-2.26), xiap (-2.12), cry1 (-2.08), map2k4 (-2.07)
	GO:0071496	1.14E-02	16	Cellular Response to External Stimulus	nos1 (16.95), tlr5 (8.15), atf3 (3.38), hspa5 (2.36), wdfy3 (2.16), cyp24a1 (-7.50), myh13 (-6.90), prkg1 (-6.71), kcnj2 (-5.62), krt15 (-5.57), dnm1l (-3.98), atpif1 (-3.76), pdk2 (-2.70), pafah1b2 (-2.26), wnt9b (-2.12), map2k4 (-2.07)

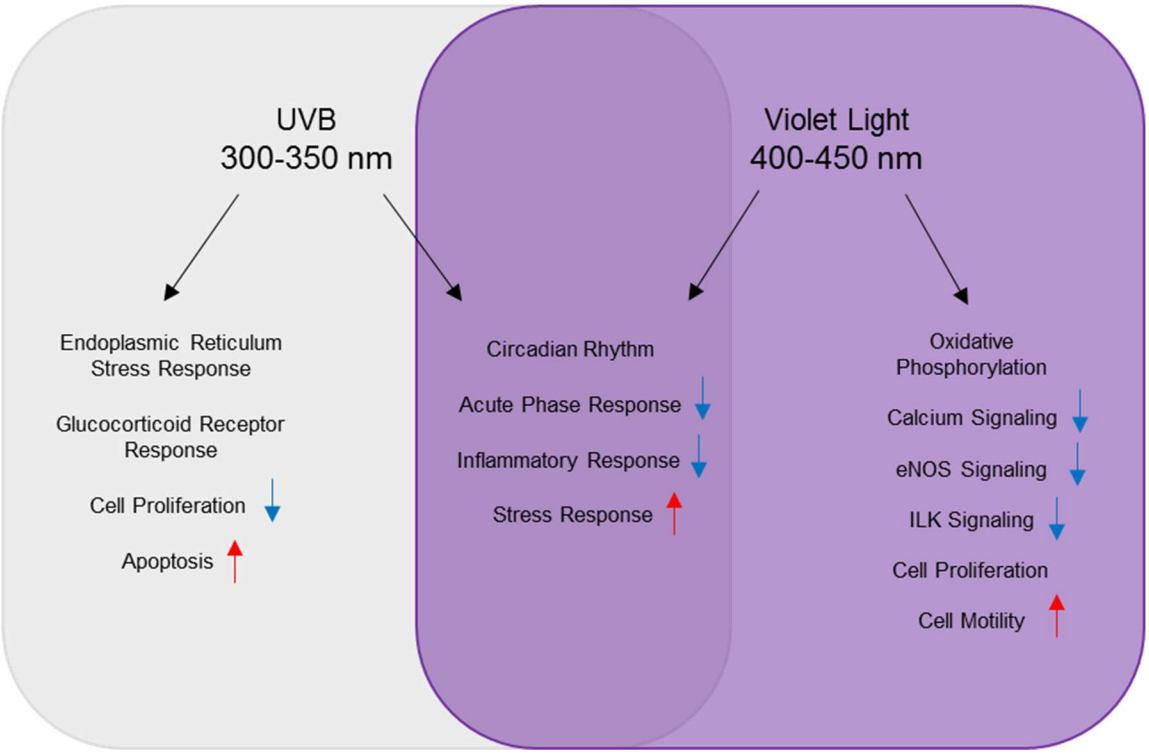

Figure 4-5. Chart summary of canonical pathways identified by Ingenuity IPA and GO categories in female 300-350 and 400-450 nm regions. Pathways and GO terms at the 300-350 nm region is shown on the left (Table 4-2 and 4-3) while those at the 400-450 nm region are shown on the right (Table 4-4 and 4-5). Pathways and GO terms shared between both regions are listed in the center. Up-modulation and down-modulation of clusters are indicated by red and blue arrows, respectively.

Visualization of the genetic associations within the 300-350 and 400-450 nm waveband regions were assessed using ConsensusPath Database (CPDB). HUGO ID's previously generated for Ingenuity IPA and gene ontology were uploaded into CPDB (300-350 nm: 115 genes; 400-450 nm: 301 genes, respectively). The fold change values for each gene displayed within the networks are shown as a heat map (Figure 4-6 and 4-7). Large gene clusters were identified within each network. Networks in the 300-350 nm region showed genes clustered around the heat shock proteins (e.g. *hsp90b1*, *hspa5*, and *hsp90aa1*) (Figure 4-6). Additionally, a small cluster of genes was found surrounding *tg* (thyroglobulin). Functional characterization of the genes displayed on the network (29 genes) revealed 10 categories: circadian rhythm (4 genes), chromatin organization (3 genes), cell proliferation (3 genes), immune response (7 genes), metabolism (4 genes), apoptosis (3 genes), stress (3 genes), transcription (2 genes), translation (2 genes) and transport (5 genes) (Figure 4-6).

CPDB was used to identify genetic associations for the 400-450 nm region. A large cluster of genes centered on *hnf4a* (Figure 4-7). Moreover, a subset of genes related to circadian rhythm was also displayed. A total of 9 categories was identified: circadian rhythm (6 genes), cell differentiation (4 genes), muscle/cytoskeleton remodeling (18 genes), cell motility (16 genes), metabolism (8 genes), oxidation-reduction (15 genes), transcription (7 genes), transport (3 genes), and immune response (4 genes) (Figure 4-7).

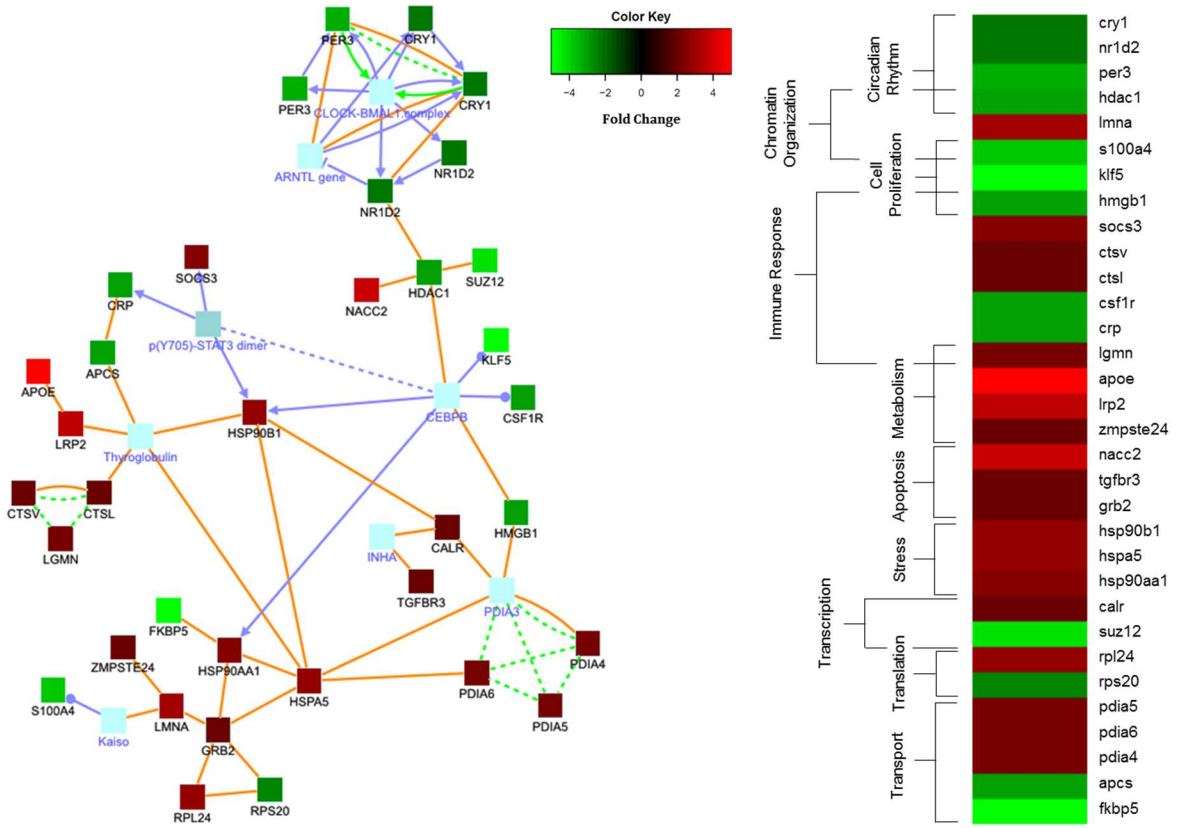

Figure 4-6. Protein and genetic associations of differentially expressed genes (± 2-fold) of female *X. maculatus* skin exposed to 300-350 nm. Network was created through CPDB gene analysis software. A total of 115 genes were queried and the following associations were made (32 genes; Z-score = 30): protein (orange), genetic (blue), and biochemical (green) interactions. Dotted lines represent a physical interaction, solid arrows show substrate/product interaction, and solid lines with a circle represent enzyme interaction. Colored boxes indicate fold change scaled to the heat map colors. Boxes in blue and purple represent predicted genes and proteins CPDB used to make associations. Up-modulated (red) and down-modulated (green) genes within the heat map were functionally categorized. Functional characterization was performed using gene ontology. Genes not clustered by GO were manually grouped through literature. Within the 300-350 nm region, genes were clustered into circadian rhythm (4 genes), chromatin organization (3 genes), cell proliferation (3 genes), immune response (7 genes), metabolism (4 genes), apoptosis (3 genes), stress (3 genes), transcription (2 genes), translation (2 genes) and transport (5 genes).

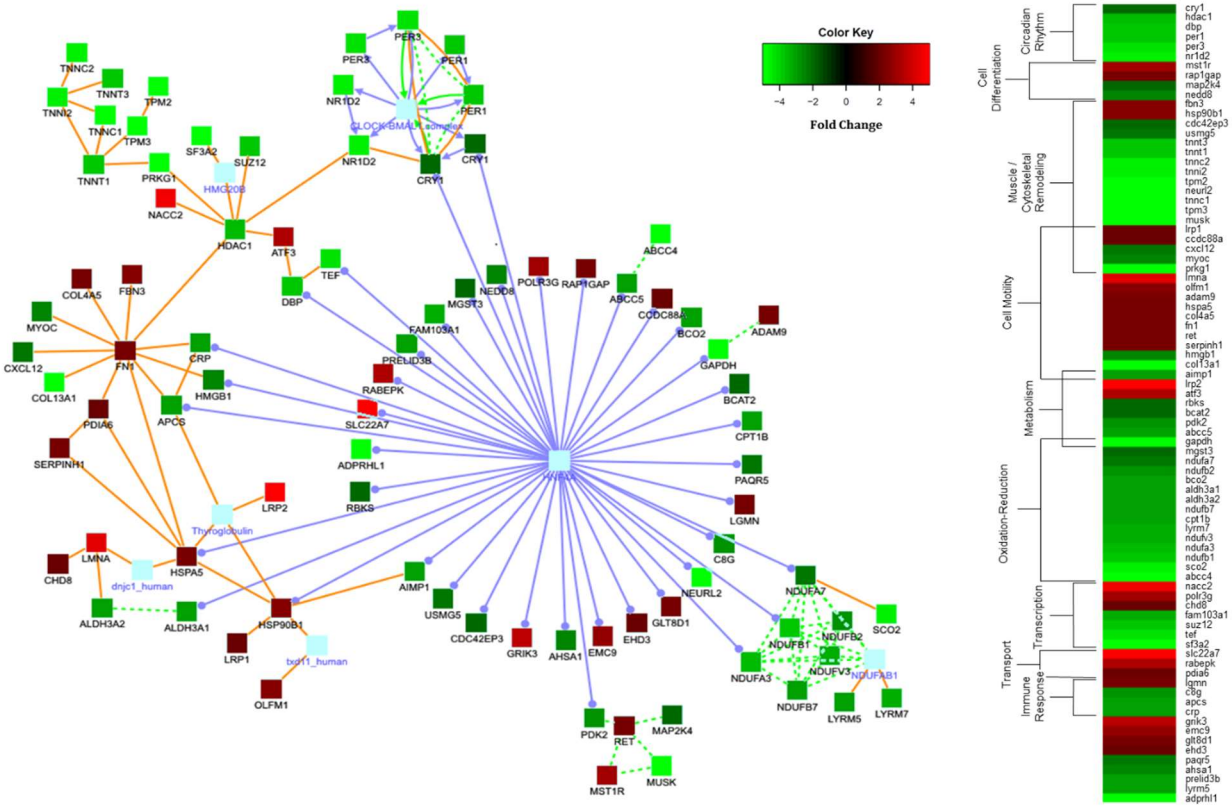

Figure 4-7. Protein and genetic associations of differentially expressed genes (± 2-fold) of female *X. maculatus* skin exposed to 400-450 nm. Network was created through ConsensusPathDB gene analysis software. A total of 301 genes were queried and the following associations were made (83 genes; Z-score = 30): protein (orange), genetic (blue), and biochemical (green) interactions. Dotted lines represent a physical interaction, solid arrows show substrate/product interaction, and solid lines with a circle represent enzyme interaction. Colored boxes indicate fold change scaled to the heat map colors. Boxes in blue and purple represent predicted genes and proteins CPDB used to make associations. Up-modulated (red) and down-modulated (green) genes within the heat map were functionally categorized. Functional characterization was performed using gene ontology. Genes not clustered by GO were manually grouped through literature. Within the 400-450 nm region, genes were clustered into circadian rhythm (6 genes), cell differentiation (4 genes), muscle / cytoskeleton remodeling (18 genes), cell motility (16 genes), metabolism (8 genes), oxidation-reduction (15 genes), transcription (7 genes), transport (3 genes), and immune response (4 genes).

Discussion

DE Gene Distribution across 300-600 nm Waveband Regions

Gender-specific bias in melanoma induction has been observed in both human and *Xiphophorus* backcross hybrids (Siciliano et al., 1971; Fernandez, 2010; Reed et al., 2013). These differences are in part due to hormonal influence on gene expression (Klein, 2000; Rinn and Snyder, 2005). Moreover, reports on sex specific genetic responses following exposure to UVB (311 nm) show females exhibit differential modulation in *ucp3* and AMPK pathways (Boswell et al., 2015). As discussed in Chapter 3, different wavelengths of light elicit unique genetic responses in male *Xiphophorus*. Here we present results from genetic examination of specific wavelengths of light on female skin.

Following exposure to varying 50 nm wavebands DE genes in females exhibited a robust response following exposure to wavebands in the visible light region (e.g. 400-600 nm). Conversely, fish exposed to 300-350 nm (UVB light) and 350-400 nm (UVA light) wavebands exhibited fewer genes modulated (Figure 4-1). The production of reactive oxygen species by exposure to ultraviolet light has been well documented (Kielbassa et al., 1997; Wood et al., 2006). Accumulation of ROS have also been shown to increase the expression of several transcription factors, such as Erk-1/2, MAPK and NFκB (Gupta et al., 1999). The lower transcriptional response observed in female skin after UV exposure may be due to the higher basal concentrations of antioxidants in the skin (Thomas-Ahner et al., 2007) that serve to reduce levels of ROS produced by

UV exposure. This may explain the fewer differentially expressed genes at both the 300-350 nm and 350-400 nm wavelength exposures.

Alternatively, female fish skin exposed to visible light appears to differentially modulate expression of substantially more genes than does UV exposure. While the exact intracellular receptors or biomolecules that absorb visible light and regulate transcription are unknown, it is likely that genes regulated by estrogen and estradiol in female fish are affected by these unknown light absorbing intermediates. It has been well documented that estrogen and progesterone are involved in activation of many transcription factors like GAL4 and TAF, such as androgen through androgen receptors (Webster et al., 1988; Gronemeyer, 1991; Shang et al., 2000). Recent reports suggest visible light is able to degrade estradiol, the primary estrogen hormone, through photodegradation and this is accelerated in water and by ROS (Díaz et al., 2009; Leech et al., 2009). This may explain the greater number of down-modulated genes across each of the visible light wavebands (Figure 4-1). It is unknown whether visible light is able to directly target estrogen in the skin. Experiments measuring estrogen levels in the skin upon exposure to visible light would be an interesting avenue for future study.

Shared Response between 300-350 and 400-450 nm Waveband Regions

Among the canonical pathways identified by Ingenuity IPA at the 300-350 nm and 400-450 nm wavelength region, several pathways and GO categories were shared (acute phase response signaling, immune response, and stress

response) (Figure 4-5). Additionally, a major pathway shared at both 400-450 nm and 500-550 nm region involves the acute phase response signaling (Figure 4-8). Both regions are predicted to suppress the acute phase signaling pathway (Table 4-2 and 4-4; Figure 4-8). The acute phase response is an innate immunity response that becomes activated in the presence of infection or tissue damage (for review, see Gabay and Kushner, 1999; Suffredini et al., 1999). Moreover, genes related to inflammation are observed slightly down-modulated (300-350 nm: 7 of 11 genes, Table 4-3; 400-450 nm: 11 of 17 genes, Table 4-5). Suffredini et al. (1999) report the inflammatory response may be affected by modifying agents such as stress hormones, epinephrine and cortisol. Induced stress is shown to decrease acute phase response proteins and inflammation (Bierman et al., 1952; Barber et al., 1993). Additionally, DE genes related to stress response are identified in the 300-350 nm and 400-450 nm exposure regions (36 genes and 33 genes, respectively) (Table 4-3 and 4-5). Our observations support our previous speculation that female fish exposed to both UVB and blue light may be undergoing a cellular stress response. To confirm this, future experiments measuring stress hormone levels released in the water would be needed.

Modulation of Regulators Affected at 300-350 and 400-450 nm Regions

Analysis of the 300-350 nm region using ConsensusPath DB (CPDB) identified a cluster of genes that were primarily centered on heat shock proteins (*hsp90b1*, *hspa5*, and *hsp90aa1*) (Figure 4-6). Heat shock proteins are documented to be up-regulated in response to cellular stress (Santoro, 2000).

The identification of these particular nodes suggest modulations of pathways in response to cellular stress. Moreover, a small cluster of genes was identified surrounding thyroglobulin (*tg*). TG proteins are primarily produced in the thyroid gland to regulate cellular growth and hormonal levels (Luo et al., 2014). TG has also been implicated to play a role in the immune response (Vladutiu and Rose, 1975; Ploth et al., 1978) and is shown within our network to associate with immune response genes (e.g. *cstl* and *crp*) (Figure 4-6). While the role of TG in light exposure is unknown, estrogen has been shown to play a role in TG up-regulation (Santin and Furlanetto, 2011). Perhaps light is affecting estrogen and estrogen receptors, leading to a downstream effect in TG and TG regulated genes.

CPDB identified several clusters of DE genes at each waveband exposure. In particular, the largest cluster of genes involved *hnf4a* (Figure 4-7). Although, *hnf4a* is not DE in our data, the number of DE genes surrounding it suggests *hnf4a* is an upstream regulator. Hepatocyte nuclear factor 4 (*hnf4a*) is generally localized in the liver. However, *hnf4a* expression can be found in other organs such as skin (Taraviras et al., 1994). More importantly, *hnf4a* is a transcriptional regulator in PXR-mediated expression of *cyp3a4*, a cytochrome P450 enzyme that participates in xenobiotic metabolism and cholesterol homeostasis (Tirona et al., 2003; Bodin et al., 2002). Genes shown to be directly associated with *hnf4a* were down-modulated (30 of 42 genes; Figure 4-7), suggesting *hnf4a* is suppressed following exposure to visible light. Expression of *hnf4a* may have occurred prior to the 6 hr post-exposure isolation and thus

expression would have returned to basal levels. The changes we observed in metabolism and oxidation-reduction process may be due to the suppression of the *hnf4a* transcription factor.

Genetic Response after Exposure to 300-350 nm Light

Following examination of the shared responses between waveband exposures, we investigated the unique responses to identify pathways and functions that may be affected by only a specific waveband of light. While the GO term *response to external stimulus* represents a large number of genes (33 genes, Table 4-3; 16 genes, Table 4-5), these genes are mostly involved in a wide array of functions.

Among the different pathways modulated by exposure to UVB light (300-350 nm), two pathways were identified to be unique to this waveband region, endoplasmic reticulum stress response (3 genes, *p*-value = 1.59e-04) and glucocorticoid receptor response (7 genes, *p*-value = 5.19e-04) (Table 4-2). The endoplasmic reticulum (ER) is a vital organelle responsible for the assembly and transport of proteins within the cell. Abnormal changes in the cell can lead to the production and accumulation of misfolded proteins, creating stress in the system (Shröder and Kaufman, 2005). UVB light has been documented to produce oxidative stress (Wang and Kochevar, 2005; Ali et al., 2011). It is likely that exposure to UVB light in female skin may be causing proteins to misfold and in this manner produce stress in the ER, with a subsequent stress response.

Additionally, the glucocorticoid receptor response was affected by UVB exposure. Glucocorticoid receptors participate in various cellular functions regulating metabolism, immune responses, and transcription by binding to glucocorticoid ligands (Lu et al., 2006). Among the different types of glucocorticoids, cortisol is a common ligand that binds to these receptors (Buckingham, 2006). As previously mentioned, cortisol is expressed when an organism is under stress. The predicted modulation of both the ER stress and glucocorticoid response pathways further supports the idea that female fish exposed to 300-350 nm light undergo cellular stress.

Genes related to cell proliferation and apoptosis were identified in the 300-350 nm region. The GO categories grouped in cell proliferation do not exhibit suppression of cell proliferation (about 50% of the genes are up-modulated), and apoptotic processes are suggested to be up-modulated (10 of 15 genes) (Table 4-3). The exposure of UVB light has been shown to induce DNA damage that can lead to apoptosis. While the genes related to cell proliferation are not completely suppressed, the dose of exposure used (10 kJ/m^2) may suggest skin cells initiated an apoptotic response.

Boswell et al. (2015) have documented the female response to UVB (311 nm), particularly in the female immune response and fatty acid biosynthesis pathways. They speculated that decrease in inflammatory response and increase in fatty acid biosynthesis produce cell stress, and this may lead to apoptosis (Boswell et al., 2015). Our data support their speculation of skin cell apoptosis. While their study focused on exposure to a specific wavelength UVB (311 nm),

the apoptotic response may be triggered by other UVB wavelengths as well. It would be informative to expose female fish to narrower wavebands (10 nm regions) to determine the precise wavelengths in the UVB region that elicit different genetic responses.

Genetic Response after Exposure to 400-450 nm Light

Different pathways and GO clusters were identified as responsive to 400-450 nm exposure. Ingenuity IPA identified a set of genes involved in oxidative phosphorylation (11 genes) (Table 4-4). Oxidative phosphorylation is a metabolic pathway that generates ATP to provide energy for the cell. This is accomplished by the transfer of electrons through the electron transport chain (ETC) in the mitochondria in eukaryotes. (For review, see Boyer et al., 1977; Balaban, 1990). While Ingenuity IPA did not predict an activated or suppressed oxidative phosphorylation state, genes involved in the pathway are all observed to be down-modulated (Table 4-4). Gene ontology (GO) also identified a cluster of genes related to oxidation-reduction at the 400-450 nm exposure that were down-modulated (Table 4-5). The modulations in these sets of genes represent a downward shift in the cellular energy homeostasis.

As discussed in Chapter 3, calcium signaling plays a pivotal role in multiple cellular processes, such as calcium homeostasis, cell survival, immune response, etc. (Clapham, 2007). Exposure of 400-450 nm light by female fish skin shows a suppression of calcium signaling gene transcription (Table 4-4). Estrogen has been implicated to play a role in regulating calcium homeostasis

and signaling by up-regulating calcium signaling genes (e.g. calpactin and calmodulin), which become active when bound to intracellular calcium (Das et al., 2000). Besides regulating calcium homeostasis, estrogen has been documented to increase endothelial nitric oxide (eNOS) signaling (Chen et al., 1998; Chambliss and Shaul, 2002). Ingenuity IPA predictes the eNOS signaling pathway (5 genes, *p*-value = 4.80e-02) in the skin are down-modulated following exposure to 400-450 nm light. The down-modulation observed in calcium signaling and eNOS signaling may be the downstream effect of decreased estrogen levels induced by photodegradation (see above).

Additionally, ILK signaling was observed down-modulated following exposure to 400-450 nm light (Table 4-4). Integrin-like kinase (ILK) signaling plays a role in cell migration and actin rearrangement (Qian et al., 2005). Five genes that were identified within this pathway are myosin related genes that plays a direct role in cell motility (*myh7*, *myh13*, *myl2*, *myl3*, and *myl4*) However, our data also indicates an up-modulation of genes related to cell migration and collagen catabolism (11 of 16 genes and 8 of 9 genes, respectively) (Table 4-5). Nho et al., (2005) reports that ILK signaling decreases during collagen matrix contraction, a phenomenon that involves the cell migration and matrix organization (Grinnell and Petroll, 2010). Furthermore, a slight down-modulation of genes related to cell proliferation (11 of 16 genes) and actin cytoskeleton organization (16 of 26 genes) suggest suppression of cell proliferation (Table 4-5). However, we did not observe genes related to p53 induction or apoptosis within the 400-450 nm exposure. Thus, we speculate the exposure to blue light

may be slowing down cell proliferation, but maintaining cell viability.

Conclusions

Overall, female *X. maculatus* Jp 163 B fish skin exposed to varying 50 nm wavebands of light from 300 to 600 nm exhibited distinct transcriptional differences between the UV and visible light regions. Examination of the wavebands producing the highest numbers of modulated transcripts (300-350 nm and 400-450 nm) suggests skin cells were induced to initiate cellular stress pathways. Moreover, the innate immune response is suppressed after exposure to either of these wavebands as shown by the down-modulation of the acute phase response signaling pathway identified by Ingenuity IPA and of the immune response GO cluster. While the cellular stress response is observed at both regions, the downstream effects were different. Fish skin exposed to 300-350 nm (UVB) light induced stress in the endoplasmic reticulum and glucocorticoid receptors and initiated an apoptotic response. However, exposure to 400-450 nm (blue) light exhibited downward shifts of cellular energy homeostasis, perhaps to maintain cell viability. The differences observed at both wavebands suggest cellular stress may be induced through different mechanisms such as direct DNA damage from UVB at short wavebands and ROS generation in longer wavebands (Kielbassa et al., 1997; Tzung and Rünger, 1998; You et al., 2001; Wood et al., 2006; Swalwell et al., 2012). Although it has been shown that estrogen provides antioxidant effects to combat oxidative stress (Strehlow et al.,

2003), it is unclear what specific wavebands of light may affect transcripts that ultimately may modulate estrogen and estrogen receptors *in vivo*.

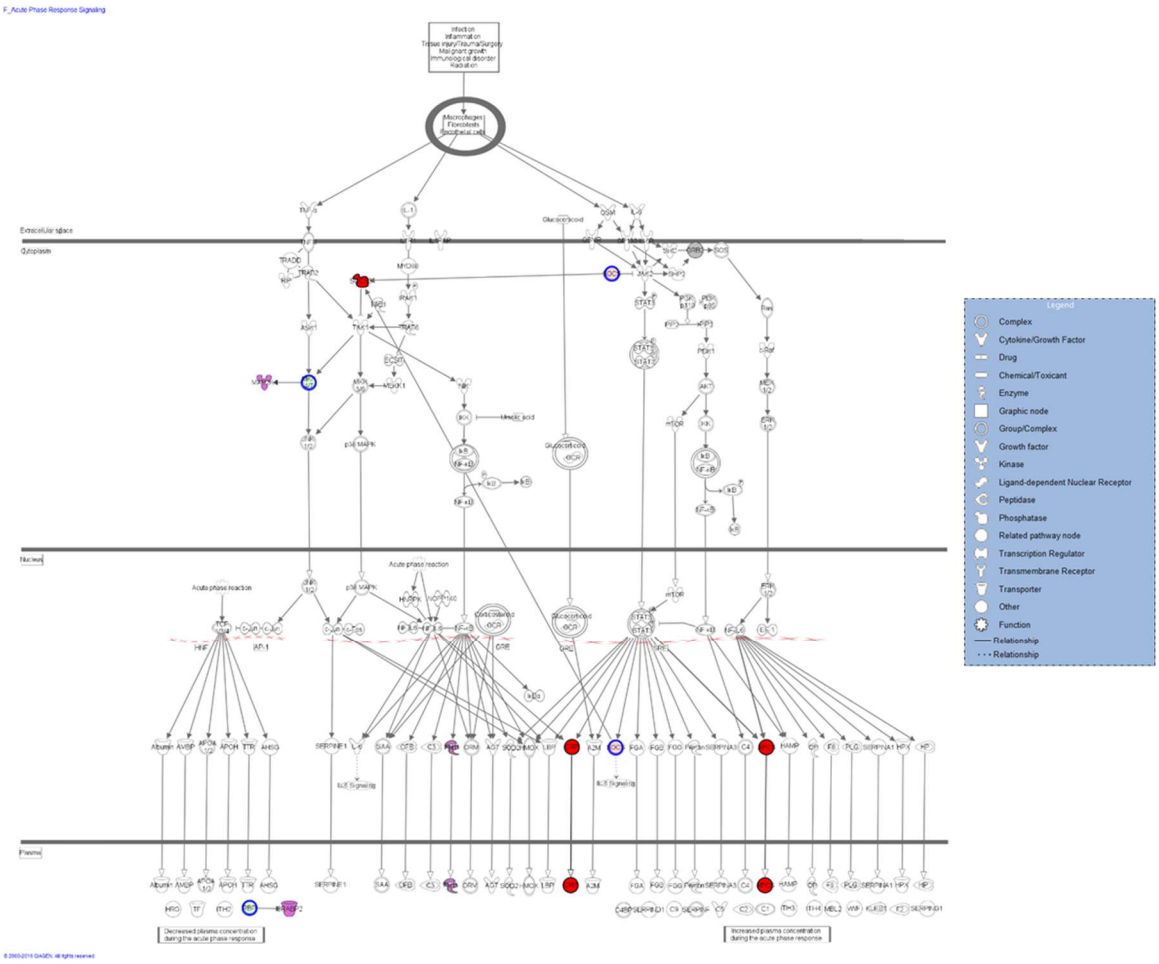

Figure 4-8. Representation of the acute phase response signaling pathway generated by Ingenuity IPA. Pathway contains genes that were DE following exposure to 300-350 nm (grey) or 400-450 nm (purple) wavelengths. Genes DE in both data sets are colored red. Blue outlined symbols represent complexes that were affected and the genes affecting the complex are connected by purple lines. Displayed on the right is a legend for the various symbols. Solid lines symbolize direct interactions and dashed lines symbolize indirect interactions. Solid arrows represent activation/causation while white arrows represent translocation. Lines with perpendicular end represent inhibition and lines with diamonds signify enzyme catalysis.

V. COMPARISON OF SEX SPECIFIC GENETIC RESPONSES OF *XIPHOPHORUS* SKIN TO VARYING WAVELENGTHS OF LIGHT

Introduction

Sex specific responses to various external stimuli and toxins have been previously documented in fish. For example, male Goodeid fish (*Girardinichthys viviparous*) accumulate higher levels of oxidative stress compared to females when exposed to PCBs (Vega-López et al., 2007). Zebrafish (*Brachydanio rerio*) exposed to 4-nitrophenol exhibit differences in hepatocyte morphology and metabolism between male and female liver samples (Braunbeck et al., 1989). More recently, male and female *Xiphophorus* fish exposed to UVB light were shown to modulate different genes associated with metabolic function and inflammation (Boswell et al., 2015). These examples show male and female fish may respond differently to environmental stimuli at the transcriptional level.

In the previous chapters, we independently characterized the genetic response in skin of male and female *Xiphophorus* to varying wavebands of light. To better understand the differences in sex specific genetic responses, here we compare the differentially expressed genes from both data sets to identify sex specific responses within the 50 nm wavebands from 300 to 600 nm.

Results

Differential Modulation of Genes between Male and Female *Xiphophorus*

Differentially expressed (DE) genes generated by EdgeR from both male and female exposures to each 50 nm waveband region were compared between both sexes (Figure 5-1). The trend in the numbers of DE genes exhibited at each region between males and females differed. While males exhibited higher transcriptional responses in the 350-400 nm and 500-550 nm region, females exhibited a much higher response in the visible light region, compared to the UV region. Furthermore, exposure to 300-350 nm, 400-450 nm, and 500-550 nm wavebands produced the greatest difference in the number of DE genes (300-350 nm: 138 genes; 400-450 nm: 299 genes; 500-550 nm: 240) (Figure 5-1). Less than 100 gene differences were observed in the other regions (350-400 nm: 81 genes; 450-500: 94 genes; 15 genes). Additionally, males up-modulate more genes in all 50 nm wavebands, with the exception of 550-600 nm, while females exhibited a more down-modulated genetic response in every waveband region (Figure 5-1).

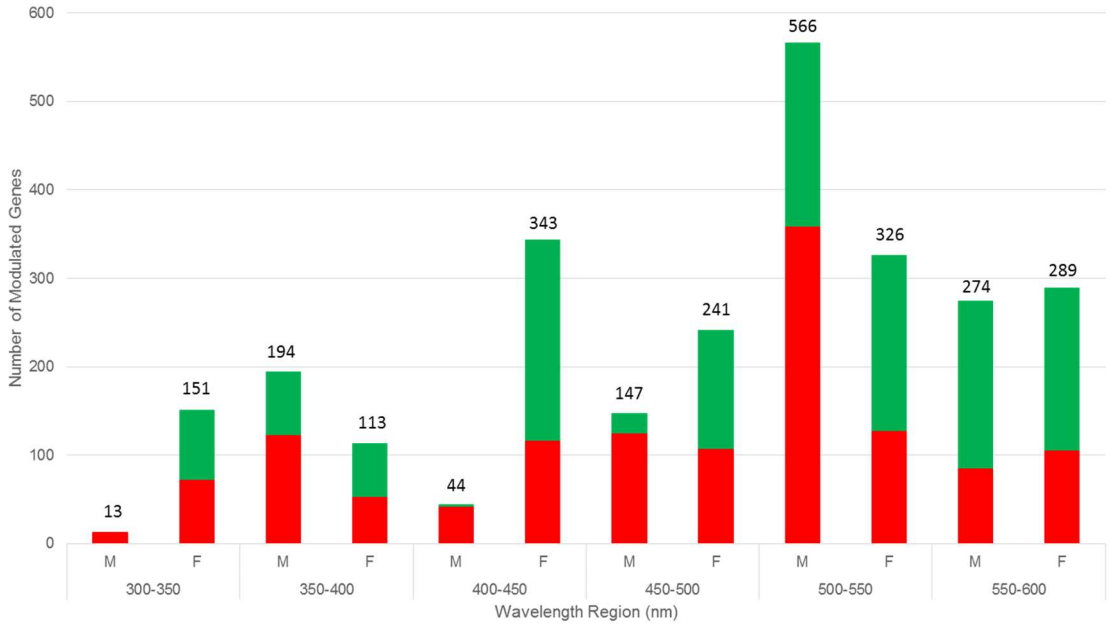

Figure 5-1. Distribution of DE genes between male (M) and female (F) *X. maculatus* Jp 163 B in response to 50 nm waveband exposures. Stacked bar graphs represent the number of DE genes that were ± 2-fold (*p*-adj ≤ 0.05). Up-modulated genes (red bars) and down-modulated genes (green bars) are displayed along with the total number of DE genes above each bar.

Comparison of DE Genes between Each 50 nm Region from Male and Female Exposures

We compared male and female gene lists at each 50 nm waveband to determine which wavelength-dependent genetic responses were similar. Comparison of the DE genes showed few genes (< 5%) were shared in the lower waveband regions (300-350 nm: 0 genes; 350-400 nm: 3 genes; 400-450 nm: 2 genes), while exposure to higher wavebands showed more DE genes (> 5%) were shared (450-500 nm: 20 genes; 500-550 nm: 30 genes; 550-600 nm: 22 genes) (Table 5-1).

Table 5-1. Comparison of the number of DE genes modulated at each 50 nm waveband region in male and female *Xiphophorus* skin. Displayed are the total number of DE genes and shared genes at each waveband region. Percentage of genes shared respective to total genes of each sex are given. While only a small number of genes were shared in lower waveband exposures (300-450; < 5%), more DE genes were shared in the higher waveband exposures (450-600; > 5%).

	Males			Females	
	Total Genes	% Genes Shared	Genes Shared	% Genes Shared	Total Genes
300-350 nm	13	0%	0	0%	151
350-400 nm	194	1.5%	3	2.7%	113
400-450 nm	44	4.5%	2	0.6%	343
450-500 nm	147	13.6%	20	8.3%	241
500-550 nm	566	5.3%	30	9.2%	326
550-600 nm	274	8.0%	22	7.6%	289

Shared DE Genes between Male and Female *Xiphophorus* at 450-500 nm

Since very few genes were shared between 50 nm wavebands in the 300-450 nm regions, we focused on comparisons in the higher wavebands (i.e. 450-500, 500-550, and 550-600 nm). Among the 20 DE genes shared within the 450-500 nm region, all shared genes showed modulations in the same direction (Figure 5-2). Furthermore, genes were segregated into 5 groups by GeneCards: circadian rhythm (3 genes), apoptosis (4 genes), chromatin organization (1 gene), metabolism (4 genes) and stress response (3 genes). The remaining 5 genes were uncharacterized (Figure 5-2).

Ingenuity IPA was employed to determine whether genes could be traced to an upstream transcriptional regulator. Thirteen genes (65.0%) were able to be

assigned human homolog gene ID's (HUGO ID's). Ingenuity IPA identified two upstream regulators, TNF and ERK1/2. Both are predicted to be up-regulated in male and female exposures based on the expression of 7 genes (*dennd4a*, *angpt2*, *timp2*, *hspa5*, *fosl1*, *atf3*, and *hmox1*) (Figure 5-3).

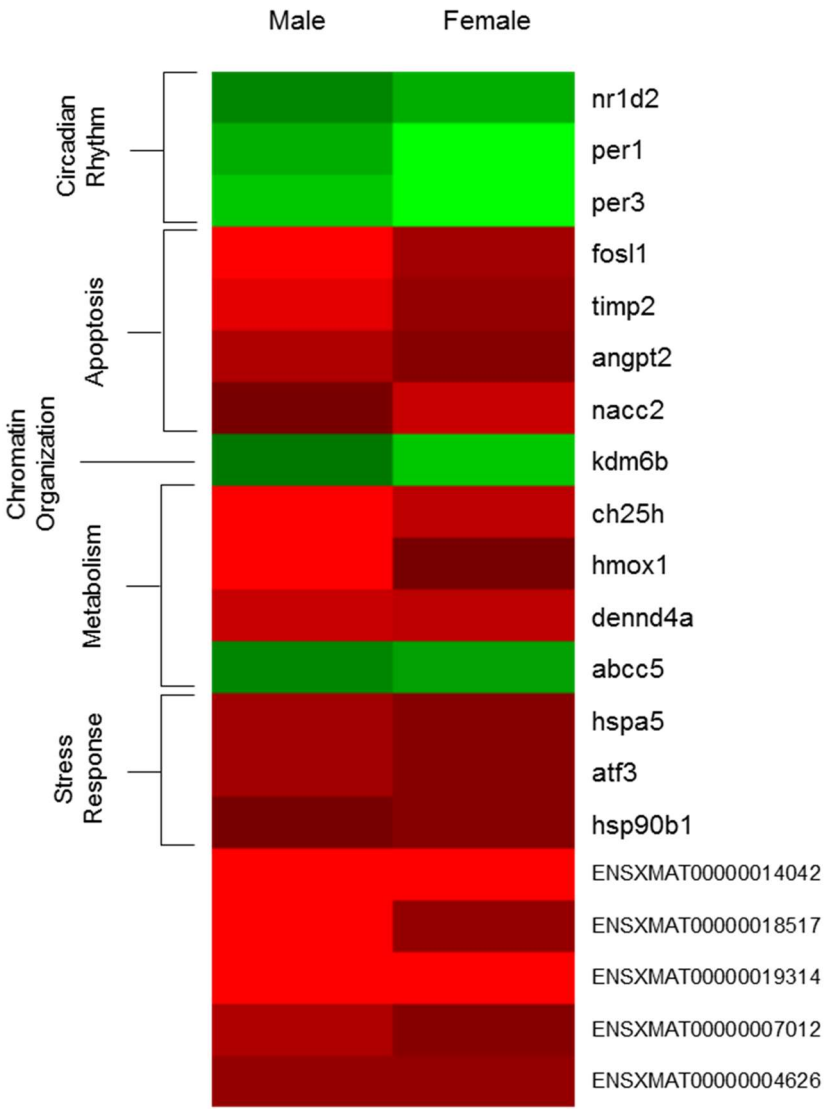

Figure 5-2. Heat map representation of genes shared between male and female exposure to 450-500 nm light (20 genes). Up-modulated genes (red) and down-modulated genes (green) were manually categorized using GeneCards and are bracketed along the heat map. Genes were clustered into 5 categories: circadian rhythm (3 genes), apoptosis (4 genes), chromatin organization (1 gene), metabolism (4 genes) and stress response (3 genes).

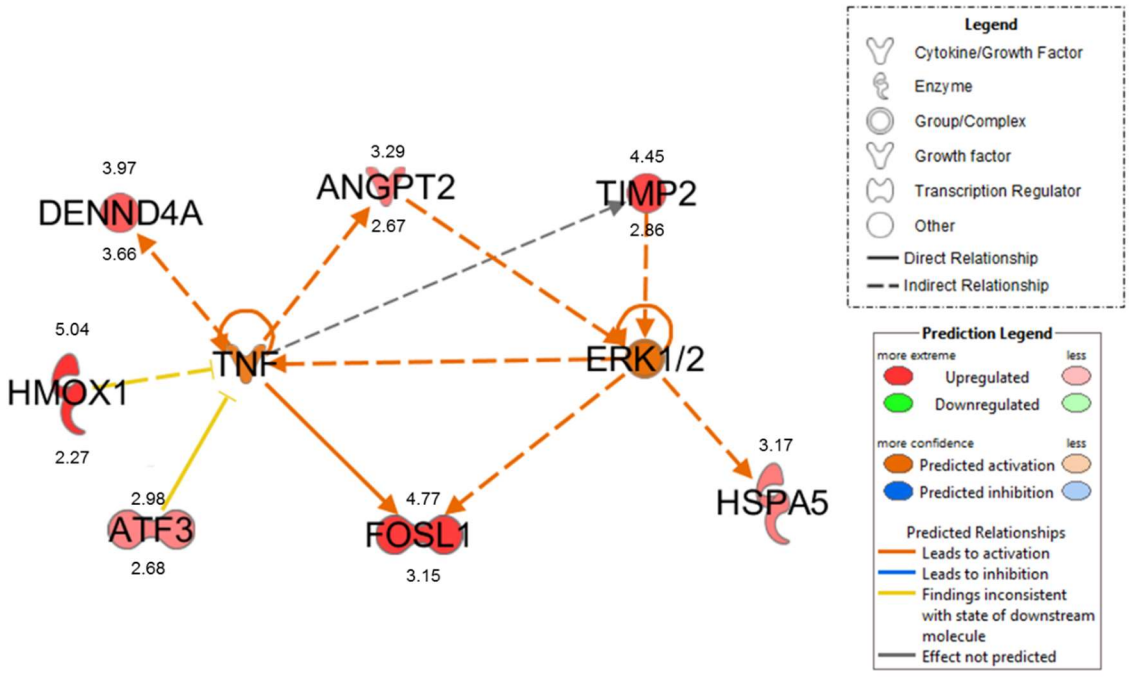

Figure 5-3. Network generated by Ingenuity IPA of upstream transcriptional regulators of males and females 450-500 nm exposures. Genes in red were observed within our data set. Genes in orange are regulators that are predicted to be modulated. Values above each gene represents male fold change while values below represent female fold change. Legend for symbols and colors are displayed on the right.

Shared DE Genes between Male and Female *Xiphophorus* at 500-550 nm

Comparison of DE genes in male and female fish at 550-550 nm identified 30 genes, of which 5 exhibited similar modulation and 25 exhibited opposing modulation (Figure 5-4). Genes were segregated into 7 groups: circadian rhythm (2 genes), chromatin organization (2 genes), metabolism (10 genes), apoptosis (2 genes), cell proliferation (2 genes), cytoskeleton remodeling (3 genes), immune response (1 gene) and transport (3 genes). The remaining 5 genes were functionally uncharacterized (Figure 5-4).

Among the 30 shared DE genes, 26 genes (86.7%) were able to be assigned HUGO ID's. Three transcriptional regulators were predicted to be modulated: PPARGC1A, TP53, and BRCA1. Male exposure to 500-550 nm up-regulated PPARGC1A and TP53, while females are predicted to down-regulate these two regulators. However, down-modulation of BRCA1 was not predictied. Modulation based on 10 genes are presented in a heat map (*myh6*, *myh7*, *lpin1*, *hmox1*, *col18a1*, *ddit4*, *e2f8*, *cyp35a1*, *sesn1*, and *pdk2*) (Figure 5-5).

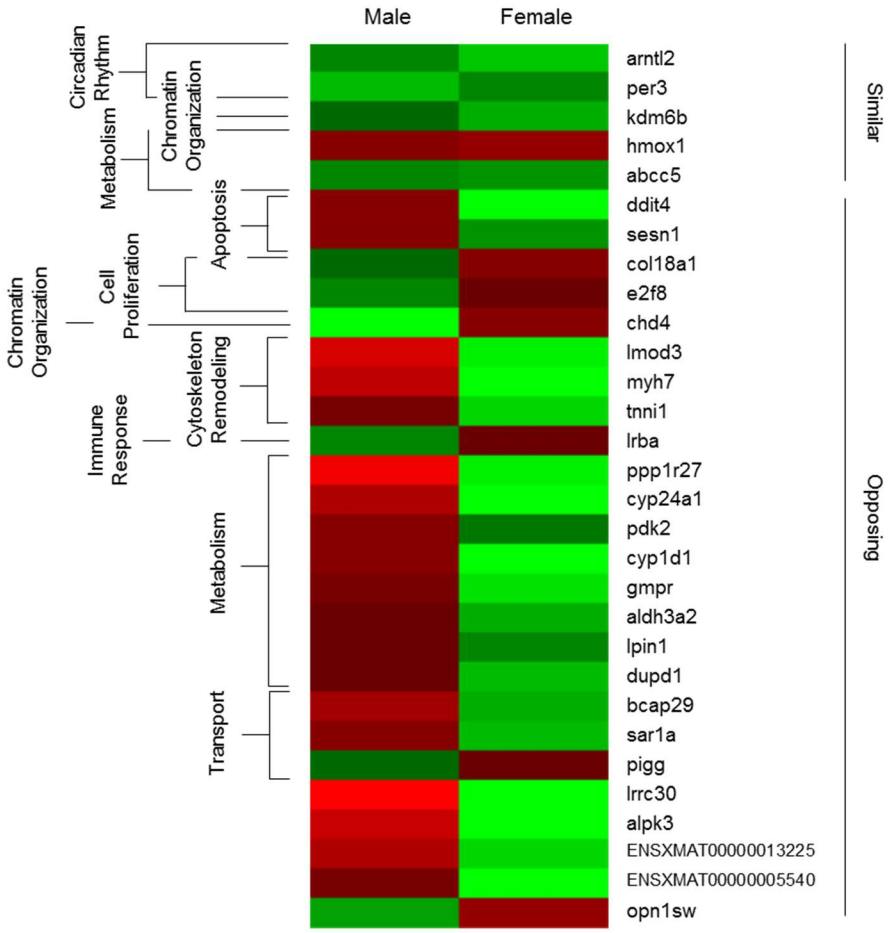

Figure 5-4. Heat map representation of genes shared between male and female exposure to 500-550 nm light (30 genes). Up-modulated genes (red) and down-modulated genes (green) were manually categorized using GeneCards and are bracketed along the heat map. Genes were clustered into 7 categories: circadian rhythm (2 genes), chromatin organization (2 genes), metabolism (10 genes), apoptosis (2 genes), cell proliferation (2 genes), cytoskeleton remodeling (3 genes), immune response (1 gene) and transport (3 genes).

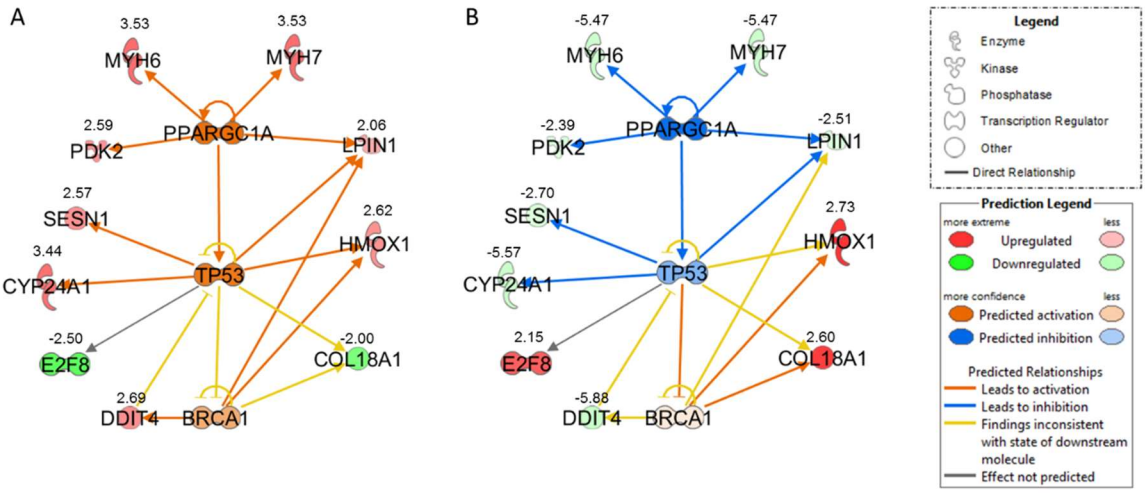

Figure 5-5. Networks generated by Ingenuity IPA of upstream transcriptional regulators in (A) males and (B) females following exposure 500-550 nm light. Genes in red and or green were observed within our data set. Genes in orange or blue are regulators that are predicted to have been modulated. Values displayed represent fold change. Legend for symbols and colors are displayed on the right. (A) Males are predicted to up-regulate PPARGC1A, TP53, and BRCA1 while (B) females down-regulate PPARGC1A and TP53.

Shared DE Genes between Male and Female *Xiphophorus* at 550-600 nm

The sets of modulated genes in male and female fish exposed to 550-600 nm shared 22 genes. Twelve genes displayed similar modulation while 10 genes displayed opposite modulation (Figure 5-6). Genes were segregated into 7 groups: circadian rhythm (5 genes), cell proliferation (6 genes), chromatin organization (2 genes), metabolism (2 genes), stress response (1 gene), apoptosis (1 gene), and cytoskeleton remodeling (1 gene). The remaining 2 genes were functionally uncharacterized (Figure 5-6).

Among the 22 shared DE genes, 16 genes (72.7%) were able to be assigned HUGO ID's. Only one transcriptional regulator was predicted to be modulated, TGFβ1. Males down-regulated TGFβ1 after exposure to 550-600 nm

light, while females up-regulate TGFβ1. Predicted modulations were based on 5 genes (*hspa5, col7a1, col5a1, krt81, and wdfy3*) (Figure 5-7).

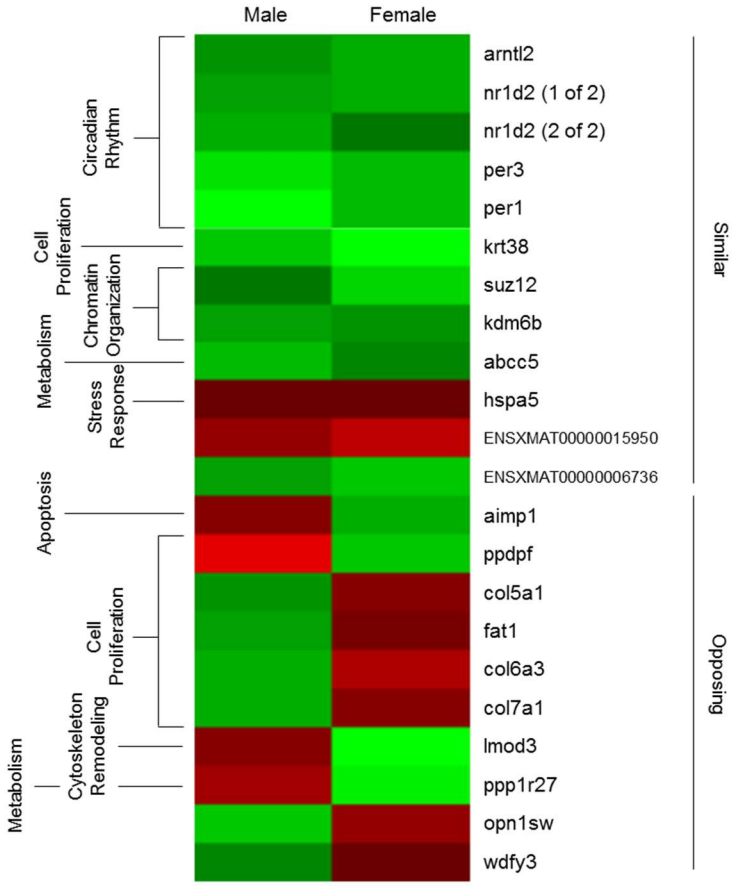

Figure 5-6. Heat map representation of genes shared between male and female exposure to 550-600 nm light (22 genes). Up-modulated genes (red) and down-modulated genes (green) were manually categorized using GeneCards and are bracketed along the heat map. Genes were clustered into 7 categories: circadian rhythm (5 genes), cell proliferation (6 genes), chromatin organization (2 genes), metabolism (2 genes), stress response (1 gene), apoptosis (1 gene), and cytoskeleton remodeling (1 gene).

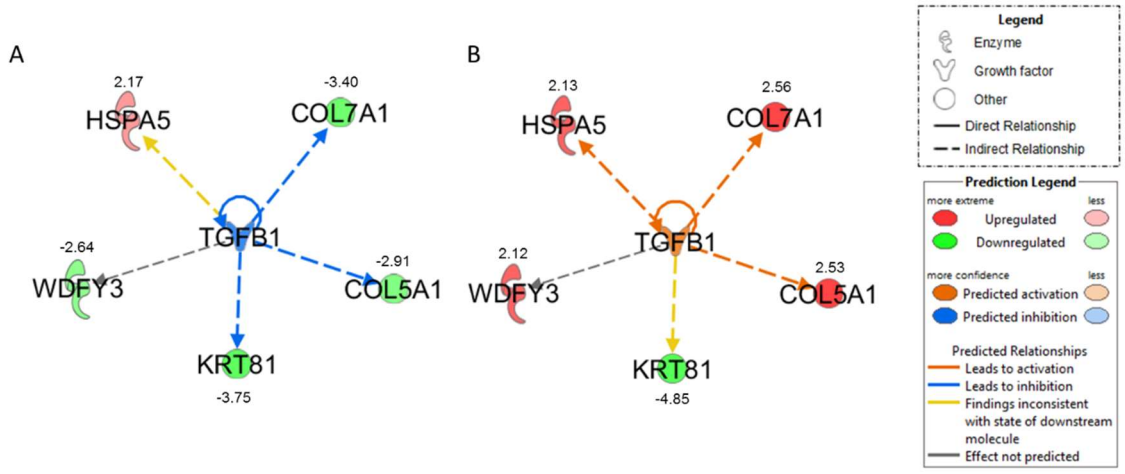

Figure 5-7. Networks generated by Ingenuity IPA of upstream transcriptional regulators in (A) males and (B) females following exposure 550-600 nm light. Genes in red and or green were observed within our data set. Genes in orange or blue are regulators that are predicted to be modulated. Values displayed represent fold change. Legend for symbols and colors are displayed on the right. (A) Males are predicted to up-regulate TGFβ1 while (B) females down-regulate TGFβ1.

Discussion

Comparison of DE Genes between Male and Female Light Exposures

Xiphophorus studies of the genetic effects of light on gene expression, particularly in the UV and visible light regions, has been previously performed. (Yang et al, 2014; Walter et al., 2015). Furthermore, sex specific responses upon exposure to UVB light have been highlighted (Boswell et al., 2015). This study aims to not only define the role specific wavebands have on gene expression, but also characterize sex specific responses to these wavelengths. As previously detailed (Chapters 3 and 4), there are distinctions between male and female transcriptional responses when exposed to varying 50 nm wavebands of light.

Comparison of the number of DE genes modulated at each waveband region in male and female *Xiphophorus* reveal transcriptional response in the sexes is not uniform. In males, only two waveband regions, 350-400 nm (UVA) and 500-550 nm (green light), showed robust transcriptional activity compared to any other regions. However, female transcriptional response to differing wavebands of light appear to segregate into two broader clusters, the UV and visible light regions. Moreover, the waveband region that exhibited the lowest response in males (blue light) is the region that shows the greatest response in females.

There have been many studies showing the effects of sex steroids (i.e. androgens and estrogens) in various biological processes, such as inflammatory response, skeletal development, and dopamine metabolism (Schuurs and Verheul, 1990; Beyer et al., 1991; Spelsberg et al., 1999).
For example, females have increased innate immune response due to the presence of estradiol receptors found on immune cells (Shuurs and Verheul, 1990). Sex steroid receptors for both estrogen and androgen have been found located on osteoblast and osteoclasts, allowing differential bone development and metabolism (Spelsberg et al., 1999). Additionally, the sex difference in dopamine metabolism in the brain contribute to neuronal migration and cell death (Beyer et al., 1991). These examples clearly show sex steroids are multi-functional and regulates many different processes. However, the role of androgens and estrogens on light responsive transcriptional regulation,

particularly in the skin, has not been reported. It is thus of interest to document the sex-specific responses shown herein.

Response of Shared Genes in Male and Female *Xiphophorus* at 450-500 nm

Since male and female *Xiphophorus* were exposed to the same 50 nm waveband, the same intracellular receptors and/or genetic regulators should be activated. Analyses of the shared genes between males and females will provide insight on how sex influences the downstream transcriptional effects. Comparison of the shared genes between males and females exposed to 450-500 nm light indicate cellular stress by up-modulation of *hspa5*, *atf3*, and *hsp90b1* (Figure 5-2). Also, heat shock proteins (i.e. hspa5 and hsp90b1) are up-regulated in response to cellular stress (Santoro, 2000). Activating transcription factor 2 (ATF2) has been reported to increase mRNA expression in the presence of oxidative stress via the JNK and p38 pathways (Liu et al., 2013). Although exposure to blue light has not been shown to generate oxidative stress in the skin, Lockwood et al. (2004) showed blue light was able to generate ROS in normal and oral tumor epithelial cells. Furthermore, up-modulation of apoptotic genes (*fosl1*, *timp2*, *angpt2*, and *nacc2*) (Figure 5-2) may indicate induced cell apoptosis.

Additionally, Ingenuity IPA predicted up-regulation of transcriptional regulators, TNF and ERK1/2 (Figure 5-3). Tumor necrosis factor (TNF) is a cytokine that is involved in regulating cell growth, apoptosis, and inflammation by activation of NF-κB and c-jun (for review, see Gaur and Aggarwal, 2003).

Moreover, activation of ERK1/2 kinases promotes cell proliferation through the suppression of p38 signaling (Lee et al., 2002), but, in the presence of DNA damaging stimuli, activation of ERK promotes apoptosis (Tang et al., 2002). It has been demonstrated that estrogen promotes TNF expression (Chao et al., 1995; Verthelyi and Klinman, 2000) and androgens regulate ERK (Pergola et al., 2008). However, the up-regulation of both TNF and ERK1/2 suggest skin exposed to 450-500 nm light generate and oxidative stress response that may induce apoptosis in both male and female *Xiphophorus* despite the hormonal bias.

Response of Shared Genes in Male and Female *Xiphophorus* at 500-550 nm

Differential expression of shared genes in the 500-550 nm waveband region showed different genetic responses between males and females. Although a small number of genes displayed similar modulations (5 genes; Figure 5-4), two genes (*arntl2* and *per3*) appears to be involved in circadian rhythm. Examination of shared DE genes with opposing modulation in the sexes showed major differences in apoptosis, metabolism, cell proliferation, and cytoskeleton remodeling. Males exposed to 500-550 nm light exhibited an up-modulation of apoptosis, cytoskeleton remodeling, metabolism, and suppression of cell proliferation (Chapter 3). Females, however, displayed opposite effects, suppression of apoptosis, cytoskeleton remodeling, and metabolism while maintain cell proliferation. The effects observed in females were similar to what we previously observed in the 400-450 nm exposures (Chapter 4).

Activation of PPARGC1A (also called PGC1), TP53, and BRCA1 was observed only in males (Figure 5-5A) and these three key cell regulators appear to have been suppressed in females (Figure 5-5B). PGC1 has been shown to directly interact with TP53, activating pro-apoptoic and metabolic genes (Sen et al., 2011). Although we observe an up-modulation of metabolic genes, it is unclear whether this is the result of PGC1-TP53 activation or a metabolic response to initiate the PGC1-TP53 interaction. It is likely that overall suppression of metabolism observed in females induces a starvation response to promote cell survival (Sen et al., 2011). Furthermore, activation of BRCA1 tumor suppressor initiates cell apoptosis in response to cellular stress (Thangaraju et al., 2000). Altogether, the cellular stress induced by 500-550 nm light led to cellular apoptosis in males while females suppressed metabolism to maintain cell viability.

Response of Shared Genes in Male and Female *Xiphophorus* at 550-600 nm

Comparison of the DE genes shared at the 550-600 nm region identified 22 genes, of which, about half exhibited similar modulations (Figure 5-6). Among the similarly DE genes, a cluster of circadian rhythm genes (5 genes) was identified as before. However, unlike the 500-550 nm previously discussed, male and female fish do not exhibit a strong suppression or promotion of cell proliferation. Within the cell proliferation cluster, a small subset of genes related to collagen (*col5a1*, *col6a3*, and *col7a1)* were down-modulated in males and up-modulated in females. The up-modulation of several collagen type genes in

females suggest a progression of cell migration (Grinnell and Petroll, 2010). This effect was previously noted when female *Xiphophorus* was exposed to 400-450 nm light.

Examination of possible upstream transcriptional regulators showed differential regulation of TGFß1. Transforming growth factor beta 1 (TGFß1) primary role is regulating cellular growth, primarily in the extracellular matrix, through cell migration and wound healing (Torsney et al., 2002). Expression of TGFß1 inhibits cellular growth in normal epithelial cells (Lyons and Moses 1990). The predicted down-regulation of TGFß1 in males suggest exposure to 550-600 nm light allows cell division to be maintained. Conversely, females appear to be inhibiting cell growth and initiating a possible wound healing response.

Conclusions

This study aimed to characterize genes that may be differently modulated by specific 50 nm wavebands of light and to identify sex-specific responses to these wavebands. Artificial light, such as fluorescent light, exhibits peaks and valleys within the spectrum that do not mirror our evolutionarily history under the sun (Figure 1-5). Given the widespread use of artificial lighting, it is important to determine which specific wavebands may more likely to alter genetic transcriptional patterns. Exposure to 350-400 and 500-550 nm light in males and 300-350 and 400-450 nm light in females displayed higher transcriptional responses, including the cellular stress response and altered energy homeostasis (Chapter 3 and 4).

Here, we present results from a direct comparison of male and female *Xiphophorus* gene expression in response to the same 50 nm wavebands. Exposure to 450-500 nm (blue light) appears to modulate a subset of genes similarly for both sexes (Figure 5-2). However, exposure to 500-550 and 550-600 nm light produced differential expression of the same genes (Figure 5-4 and 5-6), suggesting a possible role of sex steroids in gene regulation. Sex steroids, such as estrogen and androgen, are known to influence gene regulation but differences in gene expression in response to light has not been reported. Thus, the identification of upstream transcriptional regulators (e.g. PPARGC1A, TGFβ1, etc.; Figure 5-5, and 5-7) that are oppositely regulated is therefore novel and pertinent for further research studies. It would be interesting to determine whether combinatorial exposure of distant waveband regions would produce similar or different results. Further experimentation would be needed to confirm these speculations.

REFERENCES

Abraham, R.T. Cell Cycle Checkpoint Signaling Through the ATM and ATR Kinases. *Genes & Development* **2001**, *15*, 2177–2196.

Akhtar, R.A., Reddy, A.B., Maywood, E.S., Clayton, J.D., King, V.M., Smith, A.G., Gant, T.W., Hastings, M.H., Kyriacou, C.P. Circadian cycling of the mouse liver transcriptome, as revealed by cDNA microarray, is driven by the suprachiasmatic nucleus. *Current Biology* **2002**,*12*, 540–550.

Albrecht, U., Sun, Z.S., Eichele, G., Lee, C.C. A Differential Reponse of Two Putative Mammalian Circadian Regulators, mper1 and mper2, to Light. *Cell* **1997**, *91*, 1055-1064.

Ali, D. , Verma, A., Mujtaba, F., Dwivedi, A., Hans, RK., Ray, R.S. UVB-induced apoptosis and DNA damaging of potential of chrysene via reactive oxygen species in human keratinocytes. *Toxicology Letters* **2011**, *204*, 199-207.

American Cancer Society. What are the key statistics about melanoma skin cancer?. http://www.cancer.org/cancer/skincancer-melanoma/detailedguide/melanoma-skin-cancer-key-statistics (accessed February 01, 2016).

Apel, K., Hirt, H. Reactive oxygen species: metabolism, oxidative stress, and signal transduction. *Annual Review of Plant Biology* **2004**, *55*, 373–399.

Armstrong, B.K., Kricker, A. The epidemiology of UV induced skin cancer. *Journal of Photochemistry and Photobiology B: Biology* **2001**, *63*, 8-18.

Balaban, R.S. Regulation of oxidative phosphorylation in the mammalian cell. *American Journal of Physiology – Cell Physiology* **1990**, *258*, C377-389.

Bandarchi, B., Ma, L., Navab, R., Seth, A., & Rasty, G. From Melanocyte to Malignant Metastatic Melanoma. *Dermatology Research and Practice* **2010***,* 1-8.

Barber, A.E., Coyle, S.M., Marano, M.A., Fischer, E., Calvano, S.E., Fong, Y., Moldawer, L.L., Lowry, S.F. Gluococorticoid therapy alters hormonal and cytokine responses to endotoxin in man. *Journal of Immunology* **1993**, *150*, 1999-2006.

Berneburg, M., Plettenberg, H., Krutmann, J. Photoaging of human skin. *Photodermatology, Photoimmunology & Photomedicine* **2000**, *16*, 239–244.

Beyer, C., Pilgrim, C., Reisert, I. Dopamine content and metabolism in mesencephalic and diencephalic cell cultures: sex differences and effects of sex steroids. *The Journal of Neuroscience,* **1991***, 11*, 1325-1333.

Bierman, H.R., Kelly, K.H., Cordes, F.L., Byron, R.L., Polhemus,J.A., Rappoport, S. The release of leukocytes and platelets from the pulmonary circulation by epinephrine. *Blood* **1952**, *7*, 683-692.

Bodin, K., Andersson, U., Rysted, E., Ellis, E., Norlin, M., Pikuleval, I., Eggertsen, G., Bjorkhem, I., Diczfalusy, U. Metabolism of 4β-hydroxycholesterol in humans. *The Journal of Biological Chemistry* **2002**, *277*, 31534-31540.

Boswell, W., Boswell, M., Titus, J., Savage, M., Lu, Y., Shen, J., Walter, R.B. Sex Specific Molecular Genetic Response to UVB Exposure in *Xiphophorus maculatus* skin. *Comparative Biochemistry and Physiology Part - C: Toxicology and Pharmacology* **2015**, *178*, 76-85.

Bouly, J.P., Schleicher, E., Dionisio-Sese, M., Vandenbussche, F., Van Der Straeten, D., Bakrim, N., Meier, S/. Batschauer, A., Galland, P., Bittl, R., Ahmad, M. Cryptochrome blue light photoreceptors are activated through interconversion of flavin redox states. *Journal of Biological Chemistry* **2007**, *282*, 9383–9391.

Boyer, P.D., Chance, B., Ernster, L., Mitchell, P., Racker, E., Slater, E.C. Oxidative phosphorylation and photophosphorylation. *Annual Review in Biochemistry* **1977**, *46*, 955-1026.

Braunbeck, T., Storch,V., Nagel, R. Sex-specific reaction of liver ultrastructure in zebra fish (*Brachydanio rerio*) after prolonged sublethal exposure to 4-nitrophenol. *Aquatic Toxicology* **1989**, *14*,185-202.

Breider, H. Uber Melanosarkome, Melaninbildung and homologe Zellmechanismen. *Strahlentherapie* **1952**, *88*, 619–639.

Brüning, A., Hölker, F., Franke, S., Preuer, T., & Kloas, W. Spotlight on fish: Light pollution affects circadian rhythms of European perch but does not cause stress. *Science of The Total Environment* **2015***,* 516-522.

Buckingham, J.C., Glucocorticoids: exemplars of multi-tasking. *British Journal of Pharmacology* **2006**, *147*, S258-S268.

Bungard, D., Fuerth, B.J., Zeng, P.Y., Faubert, B., Maas, N.L., Viollet, B., Carling, D., Thompson, C.B., Jones, R.G., Berger, S.L. Signaling kinase AMPK activates stress-promoted transcription via histone H2B phosphorylation. *Science* **2010**, *329*, 1201-1205.

Cermakian, N., Pando, M.P., Thompson, C.L., Pinchak, A.B., Selby, C.P., Gutierrez, L., Wells, D.E., Cahill, G.M., Sancar, A., Sassone-Corsi, P. Light induction of a vertebrate clock gene involves signaling through blue-light receptors and MAP kinases. *Current Biology* **2002**, *12*, 844–848.

Chambliss, K.L., Shaul. P.W. Estrogen modulation of endothelial nitric oxide synthase. *Endocrine Reviews* **2002**, *23*, 665-686.

Chao, T.C., Alten, P.J., Greager, J.A., Walters, R.J. Steroid Sex Hormones Regulate the Release of Tumor Necrosis Factor by Macrophages. *Cellular Immunology* **1995**, *160*, 43-49.

Chen, Z., Yuhanna, I.S., Galcheva-Gargova, Z., Karas, R.H., Mendelsohn, M.E., Shaul, P.W. Estrogen receptor α mediates the nongenomic activation of endothelial nitric oxide synthase by estrogen. *The Journal of Clinical Investigation* **1999***, 103*, 401-406.

Chin, L. 1999. Modeling malignant melanoma in mice: Pathogenesis and maintenance. *Oncogene* **1999***, 18*, 5304-5310.

Clapham, D.E. Calcium Signaling. *Cell* **2007**, *131*: 1047-1058.

Condit, H., & Grum, F. Spectral Energy Distribution of Daylight. *Journal of the Optical Society of America* **1964***, 54*, 937-937.

Das, S.J., Tan, J., Raja, S., Halder, J., Paria, B.C., Dey, S.K., Estrogen targets genes involved in tprotein processing, calcium homeostasis, and wnt signaling in the mouse uterus independent of estrogen receptor-α and –β. *The Journal of Biological Chemistry* **2000**, *275*, 28834-28842.

Dias, V., Junn, E., Mouradian, M. M. The role of oxidative stress in Parkinson's disease. *Journal of Parkinson's Disease* **2013**, 3, 461-491.

Díaz, M., Luiz, M., Alegretti, P., Furlong, J., Amat-Guerri, F., Massad, W., Criado, S., García, N.A. Visible-light-mediated photodegradation of 17β-estradiol: kinetics, mechanism and photoproducts. *Journal of Photochemistry and Photobiology A* **2009**, *202*, 221-227.

Diepgen, T.L., Mahler, V. The Epidemiology of Skin Cancer. British *Journal of Dermatology* **2002**, *146*, 1–6.

Diffey, B. Sources and measurement of ultraviolet radiation. *Methods* **2002***, 28*, 4-13.

Ermak, G., Davies, K.J.A. Calcium and oxidative stress: from cell signaling to cell death. *Molecular Immunology* **2001**, *38*, 713-721.

Fernandez, A.A. A cancer-causing gene is positively correlated with male aggression in *Xiphophorus cortezi. Journal of Evolutionary Biology* **2010**, *23*, 286-296.

Foder, L., Elman, M., & Ullmann, Y. Light Tissue Interactions. *Aesthetic Applications of Intense Pulsed Light* **2011**, 11-20.

Gabay, C., Kushner, I. Actue-phase proteins and other systemic responses to inflammation. *The New England Journal of Medicine* **1999**, *340*, 448-454.

Garcia, T.I., Shen, Y., Crawford, D., Oleksiak, M.F., Whitehead, A., Walter, R.B. RNA-Seq reveals complex genetic response to deepwater horizon oil release in Fundulus grandis. *BMC Genomics* **2012**, *13*, 474.

Garland, C.F., Garland, F.C., Gorham, E.D. Rising trends in melanoma: an hypothesis concerning sunscreen effectiveness. *Annals of Epidemiology* **1993**, *3*, 103-110.

Geiss, G.K., Bumgarner, R.E., Birditt, B., Dahl, T., Dowidar, N., Dunaway, D.L., Fell, H.P., Ferree, S., George, R.D., Grogan, T., James, J.J., Maysuria, M., Mitton, J.D., Oliveri, P., Osborn, J.L., Peng, T., Ratcliffe, A.L., Webster, P.J., Davidson, E.H., Hood, L., Dimitrov, K. Direct multiplexed measurement of gene expression with color-coded probe pairs. *Nature Biotechnology* **2008**, *26,* 317–325.

Gekakis, N., Staknis, D., Nguyen, H.B., Davis, F.C., Wilsbacher, L.D., King, D.P., Takahashi, J.S., Weitz, C.J. Role of the CLOCK protein in the mammalian circadian mechanism. *Science (New York, N.Y.)* **1998**, *280*, 1564–1569.

Gery, S., Komatsu, N., Baldjyan, L., Yu, A., Koo, D., Koeffler, H.P. The Circadian Gene Per1 Plays an Important Role in Cell Growth and DNA Damage Control in Human Cancer Cells. *Molecular Cell* **2006**, *22,* 375–382.

Gimenez-Conti, I., Woodhead, A.D., Harshbarger, J.C., Kazianis, S., Setlow, R.B., Nairn, R.S., Walter, R.B. A proposed classification scheme for *Xiphophorus* melanoma based on histopathologic analyses. *Marine Biotechnology* **2001***, 3,* S100-106.

Gordon M. The genetics of a viviparous top-minnow *Platypoecilus*: The inheritance of two kinds of melanophores. *Genetics* **1927** ,*12*, 253–283.

Gordon, M. The Reappearance of Ancestral Micromelanophores in Offspring of Parents Lacking These Cells. In *Genetics of Melanomas in Fishes*: New York, New York, **1941**; p 656-659.

Graier, W.F., Hoebel, B.G., Paltauf-Doburzynska, J., Kostner, G.M. Effects of superoxide anions on endothelial Ca^{2+} signaling pathways. *Arteriosclerosis, Thrombosis, and Vascular Biology* **1998**, *18*: 1470-1479.

Granda, T.G., Liu, X., Smaaland, R., Cermakian, N., Filipski, E., Sassone-corsi, P., Le, F. Circadian regulation of cell cycle and apoptosis proteins in mouse bone marrow and tumor. *The FASEB Journal* **2005**, *19*, 304–306.

Griffin, E.A., Staknis, D., Weitz, C.J. Light-independent role of CRY1 and CRY2 in the mammalian circadian clock. *Science (New York, N.Y.)* **1999**, 286, 768–771.

Grinnell, F., Petroll, W.M. Cell motility and mechanics in three-dimensional collagen matrices. *Annual Review of Cell and Developmental Biology* **2010**, *26*, 335-361.

Gronemeyer, H. Transcription activation by estrogen and progesterone receptors. *Annual Review Genetics* **1991**, *25*, 89-123.

Gaur, U., Aggarwal, B.B. Regulation of proliferation, survival and apoptosis by members of the TNF superfamily. *Biochemical Pharmacology* **2003**, *66*, 1403-1408.

Gupta, A., Rosenberger, S.F., Bowden, G.T. Increased ROS levels contribute to elevated transcription factor and MAP kinase activities in malignantly progressed mouse keratinocyte cell lines. *Carcinogenesis* **1999**, *20*, 2063-2073.

Ha, L., Noonan, F., Fabo, E., & Merlino, G. Animal Models of Melanoma. *Journal of Investigative Dermatology Symposium Proceedings* **2005***,* 86-88.

Hastings, M., O'Neill, J.S., Maywood, E.S. Circadian clocks: Regulators of endocrine and metabolic rhythms. *Journal of Endocrinology* **2007**, *195,* 187–198.

He, Y.Y., Council, S.E., Feng, L., Chignell, C.F. UVA-Induced Cell Cycle Progression is Mediated by a Disintegrin and Metalloprotease/Epidermal Growth Factor Receptor/AKT/Cyclin D1 Pathways in Keratinocytes. *Cancer Res.* **2008**, *68,* 3752-3758.

Herlyn, M., & Fukunaga-Kalabis, M. What Is a Good Model for Melanoma? *Journal of Investigative Dermatology* **2010***, 130*, 911-912.

Houle, F., Rousseau, S., Morrice, N., Luc, M., Mongrain, S., Turner, C.E., Tanaka, S., Moreau, P., Huot, J. Extracellular Signal-regulated Kinase Mediates Phosphorylation of Tropomyosin-1 to Promote Cytoskeleton Remodeling in Response to Oxidative Stress: Impact on Membrane Blebbing. *Molecular Biology of the Cell* **2003**, *14*,1418–1432.

Hunt, T., Sassone-Corsi, P. Riding tandem: circadian clocks and the cell cycle. *Cell* **2007**, *129*, 461-464.

Ishii, T., Itoh, K., Takahashi, S., Sato, H., Yanagawa, T., Katoh, Y., Bannai, S., Yamamoto. M. Transcription factor Nrf2 coordinately regulates a group of oxidative stress-inducible genes in Macrophages. *The Journal of Biological Chemistry* **2000**, *275*, 16023-16029.

Jaywardana, K., Schramm, S.J., Haydu, L., Thompson J.F., Scolyer, R.A., Mann, G.J., Müller, S., Yang, J.Y.H. Determination of prognosis in metastatic melanoma through integration of clinic-pathologic, mutation, mRNA, microRNA, and protein information. Int*ernational Journal of Cancer* **2015***, 136*, 863-874.

Jones, R.G., Plas, D.R., Kubek, S., Buzzai, M., Mu, J., Xu, Y., Birnbaum, M.J., Thompson, C.B. AMP-activated protein kinase induces a p53-dependent metabolic checkpoint. *Molecular Cell* **2005**, *18*, 283-293.

Kallman, & K., Kazianis, S. The genus *Xiphophorus* in Mexico and Central America. *Zebrafish* **2006***, 3*, 271-285.

Kang, T.H., Reardon, J.T., Kemp, M., Sancar, A. Circadian oscillation of nucleotide excision repair in mammalian brain. *Proceedings National Academy of Science* **2009**, *8*, 2864-2867.

Kang, T.H., Reardon, J.T., Sancar, A. Regulation of nucleotide excision repair activity by transcriptional and post-transcriptional control of the XPA protein. *Nucleic Acids Research* **2010***,* 1-12.

Kazianis, S., Gimenez-Conti, I., Trono, D., Pedroza, A., Chovanec, L.B., Marizot, D.C., Nairn, R.S., Walter, R.B. Genetic analysis of neoplasia induced by N-nitroso-N-methylurea in *Xiphophorus* hybrid fish. *Marine Biotechnology* **2001a**, *3*, S37-43.

Kazianis, S., Gimenez-Conti, I., Setlow, R.B., Woodhead, A.D., Harshbarger, J.C., Trono, D., Ledesma, M., Nairn, R.S., Walter, R.B. MNU induction of neoplasia in a platyfish model. *Laboratory Investigation* **2001**, *81*, 1191-1198.

Kvam, V.M., Liu, P., Si, Y. A comparison of statistical methods for detecting differentially expressed genes from RNA-seq data. *American Journal of Botany* **2012**, *99*, 248-256.

Kielbassa, C., Roza, L., Epe, B. Wavelength dependence of oxidative DNA damage induced by UV and visible light. *Carcinogenesis* **1997**, *18,* 811–816.

Klein, S.L. The effects of hormones on sex differences in infection: from genes to behavior. *Neuroscience and Biobehavioral Reviews* **2000**, *24*, 627-638.

Kleitman, N. Biological Rhythms and Cycles. *Physiological Reviews* **1949**, *29*, 1–30.

Kohen, R., Nyska, A. Oxidation of biological systems: oxidative stress phenomena, antioxidants, redox reactions, and methods for their quantification. *Toxicologic Pathology* **2002**, *30*, 620-650.

Kondratov, R.V., Antoch, M.P. Circadian proteins in the regulation of cell cycle and genotoxic stress responses. *Trends in Cell Biology* **2007**, *17,* 311–317.

Korhonen, R., Kankaanranta, H., Lahti, A., Lähde, M., Knowles, R.G., Moilanen, E. Bi-directional effects of the elevation of intracellular calcium on the expression of inducible nitric oxide synthase in J774 macrophages exposed to low and to high concentrations of endotoxin. *Biochemical Journal* **2001**, *354*, 351-358.

Kosswig, C. Über Bastarde der *Teleostier Platypoecilus* und *Xiphophorus*. *Z Indukt Abstammungs-Vererbungsl*. **1928**, *44*, 150–158.

Krämer, A., Green, J., Pollard, J., Tugendreich, S. Causal analysis approaches in Ingenuity Pathway Analysis (IPA). *Bioinformatics* **2013**, 1-8.

Lee, J., Hong, F., Kwon, S., Kim, S.S., Kim, D.O., Kang, H.S., Lee, S.J., Ha, J., Kim, S.S. Activation of p38 MAPK induces cell cycle arrest via inhibition of Raf/ERK pathway during muscle differentiation. *Biochemical and Biophysical Research Communications* **2002**, *298*, 765-771.

Leech, D.A., Snyder, M.T., Wetzi, R.G. Natural organic matter and sunlight accelerate the degradation of 17β-estradiol in water. *Science of the Total Environment* **2009**, *407*, 2087-2092.

Lesser, M.P., Farrell, J.H., Walker, C.W. Oxidative stress, DNA damage and p53 expression in the larvae of atlantic cod (Gadus morhua) exposed to ultraviolet (290-400 nm) radiation. *The Journal of Experimental Biology* **2001**, *204*, 157–164.

Li, H., Handsaker, B., Wysoker, A., Fennell, T., Ruan, J., Homer, N., Marth, G., Abecasis, G., Durbin, R. The Sequence Alignment/Map format and SAMtools. *J. Gerontol*. **2009**, *25*, 2078–2079.

Li, J., Liu, Z., Tan, C., Guo, X., Wang, L., Sancar, A., & Zhong, D. Dynamics and mechanism of repair of ultraviolet-induced (6–4) photoproduct by photolyase. *Nature* **2010***, 466*, 887-890.

Li, Y. F., Heelis, P.F., Sancar, A. Active site of DNA photolyase: tryptophan-306 is the intrinsic hydrogen atom donor essential for flavin radical photoreduction and DNA repair in vitro. *Biochemistry* **1991**, *30,* 6322–6329.

Liu, E., Lee, A.Y., Chiba, T., Olson, E., Sun, P., Wu, X. The ATR-mediated S phase checkpoint prevents rereplication in mammalian cells when licensing control is disrupted. *Journal of Cell Biology* **2007**, *179,* 643–657.

Liu, S., Wang, F., Yan, Zhang, L., Song, Y., Xi, S., Jia, J, San, G. Oxidative stress and MAPK involved into ATF2 expression in immortalized human urothelial cells treated by arsenic. *Archives of Toxicology* **2013**, *87*, 981-989.

Lo, H.L., Nakajima, S., Ma. L., Walter, B., Yasui, A., Ethell, D.W., Owen, L.B. Differential biological effects of CPD and 6-4-PP UV-induced DNA damage on the induction of apoptosis and cell-cycle arrest. *BMC Cancer* **2005**, *5*, 1-9.

Lockwood, D.B., Wataha, J.C., Lewis, J.B., Tseng, W.Y., Messer, R.L. Hsu, S.D. Blue light generates reactive oxygen species (ROS) differentially in tumor vs. normal epithelial cells. *Dental Materials* **2005**, *21*, 683-688.

Lu, N.Z., Wardell, S.E., Burnstein, K.L., Defranco, D., Fuller, P.J., Giguere, V., Hochberg, R.B., McKay, L., Renoir, J.M., Weigel, N.L., Wilson, E.M., McDonnell, D.P., Cidlowski, J.A. The Pharmacology and classification of the nuclear receptor superfamilty: glucocorticoid, mineralcorticoid, progesterone, and androgen receptors. *Pharmacological Reviews* **2006**, *58*, 782-797.

Lucock, M., Yates, Z., Martin, C., Choi, J., Tang, B., Naumovski, N., ... Veysey, M. Vitamin D, folate, and potential early lifecycle environmental origin of significant adult phenotypes. *Evolution, Medicine, and Public Health* **2014***,* 69-91.

Luo, Y., Ishido, Y., Hiroi, N., Ishii, N., Suzuki, K. The emerging roles of thyroglobulin. *Advances in Endocrinology* **2014**, 4, 1-7.

Lyons, R.M., Moses, H.L. Transforming growth factors and the regulation of cell proliferation. *European Journal of Biochemistry* **1990**, *187*, 467-473.

Magoč, T., Salzberg, S.L. FLASH: fast length adjustment of short reads to improve genome assemblies. *J. Gerontol*. **2011**, *27*, 2957–2963.

Malewicz, M., Perlmann, T. Function of transcription factors at DNA lesions in DNA repair. *Experimental Cell Research* **2014**, *329,* 94–100.

Malloy, K.D., Holam. M.A., Mitchell, D., Detrich III, H.W. Solar UVB-induced DNA damage and photoenzymatic DNA repair in Antarctic zooplankton. *Proceedings of the National Academy of Sciences of the United States of America* **1997**, *94*, 1258-1263.

Maverakis, E., Miyamura, Y., Bowen, M., Correa, G., Ono, Y., & Goodarzi, H. Light, including ultraviolet. *Journal of Autoimmunity* **2010***, 34*, J247-J257.

McKenzie, R.L., Björn, L.O., Bais, A., Llyasd, M. Changes in biologically active ultraviolet radiation reaching the Earth's surface. *Photochemical & Photobiological Sciences* **2003***, 2*, 5-15.

Meador, J.A., Walter, R.B., Mitchell, D.L. Induction, distribution and repair of UV photodamage in the platyfish, *Xiphophorus signum. Photochemistry and Photobiology* **2000**, *71*, 260-266.

Meierjohann, S., Schartl, M., Volff, J.N. Genetic, biochemical and evolutionary facets of *Xmrk*-induced melanoma formation in the fish *Xiphophorus*. *Comparative Biochemistry and Physiology – C: Toxicology and Pharmacology* **2004**, *138*, 281-289.

Meierjohann, S., Schartl, M. From Mendelian to molecular genetics: the Xiphophorus melanoma model. *TRENDS in Genetics* **2006**, *22*, 654-661.

Mitani, H., Uchida, N., & Shima, A. Induction of Cyclobutane Pyrimidine Dimer Photolyase in Cultured Fish Cells by UVA and Blue Light. *Photochemistry and Photobiology* **1996***, 64*, 943-948.

Mitchell, D.L., Meador, J.A., Byrom, M., Walter, R.B. Resolution of UV-induced DNA damage in *Xiphophorus* fishes. *Marine Biotechnology* **2001**, *3*, S61-S71.

Mitchell, D., Paniker, L., & Douki, T. DNA Damage, Repair and Photoadaptation in a *Xiphophorus* Fish Hybrid. *Photochemistry and Photobiology* **2009**, *85*, 1384-1390.

Mitchell, D., Fernandez, A., Nairn, R., Garcia, R., Paniker, L., Trono, D., ... Gimenez-Conti, I. Ultraviolet A does not induce melanomas in a *Xiphophorus* hybrid fish model. *Proceedings of the National Academy of Sciences* **2010**, *107,* 9329-9334.

Moan, J., Dahlback, A., Setlow, R.B. Epidemiological support for an hypothesis for melanoma induction indicating a role for UVA radiation. *Photochemistry and Photobiology* **1999**, *70*, 243-247.

Moldovan, L., Moldovan, N.I., 2004. Oxygen free radicals and redox biology of organelles. *Histochemistry Cell Biology* **2004**, *122*, 395-412.

Nairn, R.S., Morizot, D.A., Kazianis, S., Woodhead, A.D., Setlow, R.B. Nonmammalian models for sunlight carcinogenesis: genetic analysis of melanoma formation in *Xiphophorus* hybrid fish. *Photochemistry and Photobiology* **1996a**, *64*, 440-448.

Nairn, R.S., Kazianis, S., McEntire, B.B., Coletta, L.D., Walter, R.B., Morizot, D.C. A CDKN2-like polymorphism in *Xiphophorus* LG V is associated with UV-B-induced melanoma formation in platyfish-swordtail hybrids. *Proceedings of the National Academy of Sciences of the United States of America* **1996b**, *93*, 13042-13047.

Nguyen, T., Nlol, P., Pickett, C.B. The Nrf2-antioxidant response element signaling pathway and its activation by oxidative stress. *The Journal of Biological Chemistry*, **2009**, *284*, 13291-13295.

Nho, R.S., Xia, H., Kahm, J., Kleidon, J., Diebold, D., Henke, C.A. Role of Integrin-linked Kinase in Regulating Phosphorylation of Akt and Fibroblast Survival in Type I Collagen Matrices through a β1 Integrin Viability Signaling Pathway. *The Journal of Biological Chemistry* **2005**, *280*, 26630-26639.

Paladini, R.D., Takahashi, K., Bravo, N.S., Coulombe, P.A. Onset of re-epithelialization after skin injury correlates with a reorganization of keratin filaments in wound edge keratinocytes: Defining a potential role for keratin 16. Journal of Cell Biology **1996**, *132*, 381–397.

Pergola, C., Dodt, G., Rossl, A., Neunhoeffer, E., Lawrenz, B., Northoff, H., Samuelsson, B., Rådmark, O., Sautebin, L., Werz, O. *PNAS* **2008**, *105*, 19881-19886.

Pfeifer, G.P., You, Y.H., Besaratinia, A. Mutations induced by ultraviolet light. *Fundamental and Molecular Mechanisms of Mutagenesis* **2005**, *571*, 19-31.

Ploth. D.W., Fitz, A., Schnetzler, D., Seidenfeld, J., Wilson, C.B. Thyroglobulin-anti-thyroglobulin immune complex glomerulonephritis complicating radioiodine therapy. *Clinical Immunology and Immunopathology* **1978**, *9*, 327-334.

Qian, Y., Zhong, X., Flynn, D.C., Zheng, J.Z., Qiao, M., Wu, C., Dedhar, S., Shi, X., Jiang, B.H. ILK mediates actin filament rearrangements and cell migration and invasion through PI3K/Akt/Rac1 signaling. *Oncogene* **2005**, *24*, 3154-3165.

Rastogi, R., Kumar, A., Tyagi, M., & Sinha, R. Molecular mechanisms of ultraviolet radiation-induced DNA damage and repair. *Journal of Nucleic Acids* **2010***,* 1-32.

Reed, K., Brewer, J., Lohse, C., Bringe, K., Pruitt, C., & Gibson, L. Increasing Incidence of Melanoma among Young Adults: An Epidemiological Study in Olmsted County, Minnesota. *Life Extension* **2013**, 328-334.

Reppert, S.M., Weaver, D.R. Coordination of circadian timing in mammals. *Nature* **2002**, *418,* 935–941.

Riehl, R., Schartl, M., & Kollinger, G. Comparative studies on the ultrastructure of malignant melanoma in fish and human by freeze-etching and transmission electron microscopy. *Journal of Cancer Research and Clinical Oncology* **1984**, *107*, 21-31.

Rinn, J.L., Snyder, M. Sexual dimorphism in mammalian gene expression. *Trends in Genetics* **2005**, *21*, 298-305.

Sancar, A., Lindsey-Boltz, L.A., Kang, T.H., Reardon, J.T., Lee, J.H., Ozturk, N. Circadian clock control of the cellular response to DNA damage. *FEBS letters* **2010**, *584*, 2618-2625.

Sangoram, A.M., Saez, L., Antoch, M.P., Gekakis, N., Staknis, D., Whiteley, A., Fruechte, E.M., Vitaterna, M.H., Shimomura, K., King, D.P., Young, M.W., Weltz, C.J., Takahashi, J.S. Mammalian circadian autoregulatory loop: A timeless ortholog and mPer1 interact and negatively regulate CLOCK-BMAL1-induced transcription. *Neuron* **1998**, *21,* 1101–1113.

Santin, A.P., Furlanetto, T.W. Role of estrogen in thyroid function and growth regulation. *Journal of Thyroid Research* **2011**, 1-7.

Santoro, M.G. Heat shock factors and the control of the stress response. *Biochemical Pharmacology* **2000**, *59,* 55–63.

Schuurs, A., Verheul, H. Effects of gender and sex steroids on the immune response. *Journal of Steroid Biochemistry* **1990**, *35*,157-172.

Sen, N., Satija, Y.K., Das, S. PGC-1α, a key modulator of p53, promotes cell survival upon metabolic stress. *Molecular Cell* **2011**, *44*, 621-634.

Siciliano, M.J., Perlmutter, A., Clark, E. Effect of sex on the development of melanoma in hybrid fish of the Genus *Xiphophorus*. *Cancer Research* **1971**, *31*, 725-729.

Setlow, R.B., Carrier, W.L. The disappearance of thymine dimers from DNA: an error-correcting mechanism. *Proceedings of National Academy of Science* **1964**, *51*, 226-231.

Setlow, R.B., Woodhead, A.D., Grist, E. Animal model for ultraviolet radiation-induced melanoma: Platyfish-swordtail hybrid. *Proceedings National Academic Science* **1989**, *86*, 8922-8926.

Setlow, R.B., Grist, E., Thompson, K., Woodhead, A.D. Wavelength effective in induction of malignant melanoma. *Proceedings National Academic Science* **1993**, *90*, 6666-6670.

Simon, H.U., Haj-Yehia, A., Levi-Schaffer, F. Role of reactive oxygen species (ROS) in apoptosis induction. *Apoptosis* **2000**, *5*, 415-418.

Shang, Y., Hu, X., DiRenzo, J., Lazar, M.A., Brown, M. Cofactor dyamics and sufficiency in estrogen receptor-regulated transcription. *Cell* **2000**, *103*, 843-852.

Shröder, M., Kaufman, R.J. The mammalian unfolded protein response. *Annual Review in Biochemistry* **2005**, *74*, 739-89.

Spelsberg, T.C., Subramaniam, M., Riggs, B.L., Khsla, S. The Actions and Interactions of Sex Steroids and Growth Factors/Cytokines on the Skeleton. *Molecular Endocrinology* **1999**, *13*, 819-828.

St Pierre, J., Buckingham, J.A., Roebuck, S.J., Brand, M.D. Topology of superoxide production from different sites in the mitochondrial electron transport chain. *The Journal of Biological Chemistry* **2002**, *277*, 44784-44790.

Strehlow, K., Rotter, S., Wassmann, S., Adam O., Grohe, C., Laufs, K., Böhm, M., Nickenig, G. Modulation of antioxidant enzyme expression and function by estrogen. *Circulation Research* **2003**, *93*, 170-177.

Solarczyk, K., Zarębski, M., Dobrucki, J. Inducing local DNA damage by visible light to study chromatin repair. *DNA Repair* **2012***, 11*, 996-1002.

Spector, A.A., Yorek, M.A. Membrane lipid Composition and cellular function. *Journal of Lipid Research* **1985**, *26*, 1015-1035.

Spitz, D.R., Azzam, E.I., Li, J.J., Gius, D. Metabolic oxidation/reduction reactions and cellular responses to ionizing radiation: a unifying concept in stress response biology. *Cancer and Metastasis Reviews* **2004**, *23*, 311-322.

Stockand, J.D., Meszaros, J.G. Aldosterone stimulates proliferation of cardiac fibroblasts by activating Ki-RasA and MAPK1/2 signaling. American *Journal of Physiology, Heart, and Circulatory Physiology* **2002**, *284*, H176-H184.

Suffredini, A.F., Fantuzzi, G., Badolato, R., Oppenheim, J.J., O'Grady, N.P. New insights into the biology of the acute phase response. *Journal of Clinical Immunology* **1999**, *19*, 203-214.

Swalwell, H., Latimer, J., Haywood, R.M., Birch-Machin, M.A. Investigating the role of melanin in UVA/UVB- and hydrogen peroxide-induced cellular and mitochondrial ROS production and mitochondrial DNA damage in human melanoma cells. *Free Radical Biology and Medicine* **2012**, *52,* 626–634.

Tang, D., Wu, D., Hirao, A., Lahti, J.M., Liu, L., Mazza, B., Kidd, V.J., Mak, T.W., Ingram, A.J. ERK Activation Mediates Cell Cycle Arrest and Apoptosis after DNA Damage Independently of p53. *The Journal of Biological Chemistry* **2002**, *277*, 12710-12717.

Taraviras, S., Monaghan, P., Schütz, G., Kelsey, G. Characterization of the mouse HNF-4 gene and its expression during mouse embryogenesis. *Mechanisms of Development* **1994**, *48*, 67-79.

Tarazona, S., García-Alcalde, F., Dopazo, J., Ferrer, A., Conesa, A. Differential expression in RNA-seq: a matter of depth. *Genome Research* **2011**, *21*, 2213-2223.

Thangaraju, M., Kaufmann, S.H., Couch, F.J. BRCA1 Facilitates Stress-induced Apoptosis in Breast and Ovarian Cancer Cell Lines. *The Journal of Biological Chemistry* **2000**, *275*, 33487-33496.

Theralight. How light penetrates the skin. http://theralightinc.com/how-light-penetrates-the-skin/ (accessed Apr 10, 2016).

Thomas-Ahner, J.M., Wulff, B.C., Tober, K.L., Kusewitt, D.F., Riggenbach, J.A., Oberyszyn, T.M. Gender differences in UVB-induced skin carcinogenesis, inflammation, and DNA damage. *Cancer Research* **2007**, *67*, 3468-3474.

Thompson, C.L., Sancar, A. Photolyase/cryptochrome blue-light photoreceptors use photon energy to repair DNA and reset the circadian clock. *Oncogene* **2002**, *21,* 9043–9056.

Thorpe, G.W., Fong, C.S., Allc, N., Higgins, V., Dawes, I.W. Cells have distinct mechanisms to maintain protection against different reactive oxygen species: oxidative-stress-response genes. *PNAS* **2004**, *101*, 6564-6569.

Tibbetts, R.S., Brumbaugh, K.M., Williams, J.M., Sarkaria, J.N., Cliby, W.A., Shieh, S.Y., Taya, Y., Prives, C., Abraham, R.T. A role for ATR in the DNA damage-induced phosphorylation of p53. *Genes and Development* **1999**, *13,* 152–157.

Tirona, R.G., Lee, W., Leake, B.F., Lan, L.B., Cline, C.B., Lamba, V., Parviz, F., Duncan, S.A., Inoue, Y., Gonzalez, F.J., Schuetz, E.G., Kim, R.B. The orphan nuclear receptor HNF4α determines PXR- and CAR-mediated zenobiotic induction of CYP3A4. *Nature Medicine* **2003**, *9*, 220-224.

Torsney, E., Charlton, R., Parums, D., Collis, M., Arthur, H.M. Inducible expression of human endoglin during inflammation and wound healing *in vivo*. *Inflammation Research* **2002**, *51*, 464-470.

Tzung, T.Y., Rünger, T.M. Assessment of DNA damage induced by broadband and narrowband UVB in cultured lymphoblasts and keratinocytes using the comet assay. *Photochemistry and Photobiology* **1998**, *67*, 647-650.

Vega-López, A., Galar-Martinez, M. Jimenez-Orozco, F.A., Garicia-Latorre, E., Dominguez-Lopez, M.L. Gender related differences in the oxidative stress response to PCB exposure in an endangered goodeid fish (*Girardinichthys viviparus*). *Comparative Biochemistry and Physiology Part A: Molecular & Integrative Physiology* **2007**, *146*, 672-678.

Verthelyl, D., Klinman, D.M. Sex hormone levels correlate with the activity of cytokine-secreting cells *in vivo*. *Immunology* **2000**, *100*, 384-390.

Vielkind, J., Vielkind, U., Anders, F. Melanotic and amlenotic melanomas in *Xiphophorin* fish. *Cancer Research* **1971**, *31*, 868-875.

Vielkind, J., Tron, V., Schmidt, B., Dougherty, G., Ho, V., Woolcock, B., Sadaghiani, B., & Smith, C. A monoclonal antibody derived from the melanoma gene in the Xiphophorus melanoma model. *American Journal of Pathology* **1993***, 143*, 656-662.

Vladutiu, A.O., Rose, N.R. Cellular basis of the genetic control of immune responsiveness to murine thyroglobulin in mice. *Cellular Immunology* **1975**, 17, 106-113.

Walter, R. & Kazianis, S. *Xiphophorus* Interspecies Hybrids as Genetic Models of Induced Neoplasia. *ILAR Journal* **2001***, 42*, 299-321.

Walter, R., Sung, H., Obermoeller, R., Mitchell, D., Intano, G., & Walter, C. Relative Base Excision Repair in Xiphophorus Fish Tissue Extracts. *Marine Biotechnology* **2001**, *3*, S050-S060.

Walter, D., Boswell, M., Volk de Garcia, S., Walter, S., Breitenfeldt, E., Boswell, W., Walter, R. Characterization and differential expression of CPD and 6-4 DNA photolyases in *Xiphophorus* species and interspecies hybrids. *Comparative Biochemistry and Physiology Part C: Toxicology and Pharmacology* **2014***, 163*, 77-85.

Walter, R.B., Walter, D.J., Boswell, W.T., Caballero, K.L., Boswell, M., Lu, Y., Chang, J., Savage, M.G. Gene Expression in *Xiphophorus* Skin Upon Exposure to Fluorescent Light Suggests Down Regulation of Mitotic Progression. *Comparative Biochemistry and Physiology Part - C: Toxicology and Pharmacology* **2015**, *178*, 93-103.

Wakamatsu, Y., Kawamura, S., & Yoshizawa, T. Light-induced pigment aggregation in cultrued fish melanophores: Spectral sensitivity and inhibitory effects of theophylline and cyclic adenosine-3',5'-monophosphate. *Journal Cell Science* **1980***, 41,* 65-74.

Wang, H., Kochevar, I.E. Involvement of UVB-induced reactive oxygen species in TGF-β biosynthesis and activation in keratinocytes. *Free Radical Biology and Medicine* **2005**, *38*, 890-897.

Wang, S., Setlow, R., Beriwkc, M., Polsky, D., Marghoob, A.A., Kopf, A.W., Bart, R.S. Ultraviolet A and melanoma: a review. *Journal of the American Academy of Dermatology* **2001**, *44*, 837-846.

Warnes GR, Bolker B, Bonebakker L, Gentleman R, Liaw WHA, Lumley, T., Maechler, M., Magnusson, A., Moeller, S., Schwartz, M., Venables, B., 2012. gplots: various R programming tools for plotting data. *http://CRAN.R-project.org/package=gplots*.

Webster, N.J., Green, S., Jin, J.R., Chambon, P. The hormone-binding domains of the estrogen and glucocorticoird receptors contain an inducible transcription activation function. *Cell* **1988**, *54*, 199-207.

Whitmore, D., Foulkes, N.S., Sassone-Corsi, P. Light acts directly on organs and cells in culture to set the vertebrate circadian clock. *Nature* **2000**, *404,* 87–91.

Wood, S., Berwick, M., Ley, R., Walter, R., Setlow, R., & Timmins, G. UV causation of melanoma in *Xiphophorus* is dominated by melanin photosensitized oxidant production. *Proceedings of the National Academy of Sciences* **2006***, 103*, 4111-4115.

Wu, T.D., Nacu, S. Fast and SNP-tolerant detection of complex variants and splicing in short reads. *J. Gerontol*. **2010**, *26*, 873–881.

Yang, K., Boswell, M., Walter, D., Downs, K., Gaston-Pravia, K., Garcia, T., ... Walter, R. UVB-induced gene expression in the skin of *Xiphophorus maculatus* Jp 163 B. *Comparative Biochemistry and Physiology Part C: Toxicology and Pharmacology* **2014***, 163*, 86-94.

You, Y.H., Lee, D.H., Yoon, J.H., Nakajima, S., Yasui, A., Pfeifer, G.P. Cyclobutane Pyrimidine Dimers Are Responsible for the Vast Majority of Mutations Induced by UVB Irradiation in Mammalian Cells. *Journal of Biological Chemistry* **2001**, *276*, 44688–44694.

Zhang, Z., Wang, Y., Wang, S., Liu, J., Warren, W., Mitreva, M., Walter, R.B. Transcriptome analysis of female and male Xiphophorus maculatus Jp 163 A. *PLOS One* **2011***, 6*, 1-6.